Abstract

Electron beam lithography (EBL) is expected to achieve the formation of very fine dot arrays for bit-patterned media applications due to its resolution capability and placement accuracy. However, the resolution-limiting factors of electron beam lithography (EBL) at the sub-10 nm length scale are not well understood, which has limited our ability to further improve its resolution. Therefore, using the simulation method to analyze the limiting factors of EBL for sub-10 nm patterning is necessary to be done.

In order to revealing the limiting factors of high resolution patterning, I focused my study on two main aspects. The first was evaluating the dependence of exposure conditions (such as incident beam energy, resist thickness, resist type, etc.) to reduce the electron beam scattering range. The second aspect was estimating resist profiles with solubility rates based on various developers to determine optimal development contrast. The details of the two aspects were described as follows.

The first aspect: Roughly evaluation of the resist profile estimated by critical energy deposition based on energy deposition distribution (EDD)

1) A home-made Monte Carlo simulation of electron-atom scattering was made.

2) The energy deposition distribution was calculated in thin resist layer on Si substrate.

3) The estimation of nano-sized dot arrays based on critical deposited energy in a parameter of incident electron energy, electron beam diameter, resist thickness and resist type were studied.

4) High incident energy beam, small sized Gaussian beam, thin resist film, negative resist were demonstrated that there are benefit to reduce electron beam scattering range and form very fine nano-sized pattern.

The second aspect: Precise estimation of HSQ resist profiles by using various developers with different contrast

1) A new development model of calculating resist profiles with solubility rates based on the three-dimensional EDD was proposed.

2) A sharpened nano-dot resist pattern was obtained by selecting a suitable EDD region.

3) The calculated resist profiles by using the new model agrees well with the experiment

results.

4) The effects of exposure dosage and solubility rate on contrast of developer were studied. The resist profiles with various contrast developers (γ from 12 to 1) were calculated. We demonstrated that small dosage interval (ΔEDD) is an important parameter to improve the resolution.

5) The suitable contrast of developers was determined by evaluating the predicted resist profiles. High contrast developer was effective to form very fine dot pattern with sufficient.

6) The exposure allowance for high contrast resist and low contrast resist was investigated. We demonstrated that high contrast resist has small exposure allowance. It indicted that we should control exposure dosage severely by using high contrast resist for high resolution patterning.

As described above, EB exposure and development calculation is demonstrated to obtain very fine resist profile using high energy electron high contrast developer and negative resist. This indicates that the optimal condition of EB lithography opens new era to control nanometer-sized structures.

要旨

電子線描画法は高分解能かつ位置精度が正確であるため、パターンドメディア技術のための微小ドット形成方法として有望視されている。しかし、sub-10 nm における電子線描画の解像度の限界について、現像プロセスまで含めた電子線描画法が殆ど研究されていないのが現状である。本研究においては、現像プロセスまで含めた電子線描画法をシミュレートすることにより、電子線描画法による微細化技術の限界を検討した。

本研究では、電子線描画法による微小パターン形成に与える要因を分析するため、以下の二つの研究を行った。一つは電子散乱領域を抑えるため、様々な露光条件の依存性（例：入射ビームのエネルギー、レジストの厚さ、レジストの種類など）について検討した。もう一つは、種々のコントラストを持つ現像液がパターンの形成に与える影響の分析である。これにより、各種コントラストを持つ現像液によるパターン形状の予測を行い、最適なコントラストを予測した。これら二つの研究の概要は以下の通りである。

１、3 次元エネルギー堆積密度（EDD）に基づき、閾値エネルギーによる、レジストプロファイルのラフな評価

１）ホームメード電子散乱のモンテカルロシミュレーションを構築した。

２）レジスト中で堆積したエネルギーの 3 次元密度分布を計算した。

３）上記エネルギー堆積密度に基づき、それぞれの露光条件（入射ビームのエネルギー、レジストの厚さ、レジストの種類など）において、形成されるナノドットの形状を予測した。

４）高エネルギー入射ビーム、微小ビーム径、薄膜レジスト、ネガティブレジストを用いることにより電子散乱領域を抑え、微小ナノドット列形成に有効であることを証明した。

２、各種コントラストの現像液における HSQ レジストプロファイルの正確な予測

１）実験の露光量と溶解速率に基づき、レジスト中の蓄積したエネルギーの分布により、レジストプロフアイルの計算ために新たな現像モデルを提案し、構築した。

２）最適なエネルギー領域を選択することにより、最適な微小ドットパターン（約 7nm 径）が形成できることが分かった。

3） 提案モデルで計算したレジストプロファイルは実験の結果と一致していることを示し、提案モデルがパターンプロフアイルの予測に有効であることを証明した。

4）露光量による溶解速度特性に基づいた 3 次元エネルギー蓄積分布と現像作用の関係を見出し、各種コントラストを持つ現像液がレジストプロファイルに与える影響を検討した。

5）計算したレジストプロファイルを評価することによって、微小パターンの形成には現像液の最適なコントラスト値を選択することが重要であることが分かった。コントラストが高い現像液は微小パターンの形成に有利であることが分かった。

6）コントラストが高い現像液は狭い露光許容量を持ち、反対にコントラストが低い場合は広い許容量がある。コントラストが高い現像液を用いる時には露光量を細かく制御する必要があることが分かった。

上記のように、電子線描画と現像過程のシミュレーションによって、高エネルギーの電子線、高コントラスト現像液、ネガティブレジストを用いることが、微小なパターンを形成するのに有効であることを明らかにした。実験において、電子線描画の最適な条件を見出すことにより、ナノメートル構造を制御することが可能になると予測される。

Table of Contents

List of Symbols

Z Atomic number of target atom, 23

e Electronic charge, 23

r_0 Screening radius, 23

a_0 Bohr's radius, 23

α Screening factor, 23

σ_e Rutherford cross section, 23

n Number of atoms in a unit volume, 24

N_A Avogadro's number, 24

ρ Density, 24

A Atomic weight, 24

E Energy of electron, 27

θ Scattering angle, 27

ϕ Scattering angle, 27

h Plack's constant, 27

p Electron momentum, 27

R Uniform random number between 0 and 1, 28

R_1 Uniform random number between 0 and 1, 28

R_2 Uniform random number between 0 and 1, 28

J_i Mean ionization energy of atom I, 28

S_n Step length between (n-1)th and nth scatterings, 28

$|dE/ds|_{E_n}$ Mean energy loss, 28

P_i Probability of scattering off an atom of the *i*-th element, 29

E_c Stopping energy, 31

ΔV The ring volume, 32

Δz Thickness of sub-layer, 32

Δr Increment in radius direction, 32

N_0 Total number of incident electron, 32

r Distance from a center of the beam, 50

σ Standard deviation, 50

P Uniform random number between 0 and 1, 50

$D(r,z)$ Energy deposition as a function of the radial distance r and vertical distance z, 67

v_r, v_z Solubility rates in the radial and vertical directions, respectively, 67

γ Contrast value, 68

R Experimental residual resist thickness, 68

R_0 Original resist thickness, 68

t Development time, 68

Δt Step time, 69

EB Electron beam, I

EBL Electron beam lithography, I

EDD Energy deposition distribution, I

BPM Bit pattern media, 2

FIB Focused ion beam lithography, 3

NIL Nano imprint lithography, 3

HSQ Hydrogen silseqioxene resist, 4

EID Energy intensity distribution, 5

PEB Post-exposure-bake, 11

PMMA Poly(methyl methacrylate), 16

PBS PolyButene-1-Sulfone, 16

EBR-9 A copolymer of trifluoroethyl a-chloroacrylate and tetrafluropropyl a-chloroacrylate, 16

ZEP A copolymer of chloromethacrylate and methylstyrene, 16

TMAH Tetramethylammonium hydroxide, 17

CMC6 p-chloromethyl-methoxy-calix[6]arene, 39

CMC4 p-chloromethyl- methoxy- calix[4]arene, 39

SEM Scanning electron microscope, 50

ΔEDD EDD interval between the initial EDD for minimum solubility rate and the full EDD for maximum solubility rate, 8

Acknowledgments

I would like to express my gratitude to my supervisor, Prof. S. Hosaka for giving me the opportunity to study in the Hosaka Laboratory of Guma University and for bringing me to get to know the EB-lithography for forming nano-scaled dot arrays. Your invaluable supervision and constant supports throughout the 3 years doctoral course of my study helped me to overcome difficulties and achieved the goals in my research works. Importantly, studying in your high quality and good environmental research group gives me a good opportunity to a professional career in the field of nanotechnology.

I would like to thank Assistant Prof. Y. Yin. He really supported me with patience and understanding during this experience. I would also like to thank all the members of our research group: Mr. T. Komori, Dr. T. Tamura, Dr. Z. Mohamad, Dr. M. Huda, and Ms. J. Liu. I especially would like to thank Mr. T. Komori for giving me the experimental results to support my simulation program which is one of the essential parts of the research. I also would like to acknowledge the Japanese Government (JASSO) for a financial support for my study.

Finally, I would like to thank my parents and my husband for their tireless support and encouragement from the beginning until the completion of my PhD program.

Chapter 1 Introduction

1.1 Background

Magnetic recording, invented over 100 years ago, has played a key role in the development of information storage technologies, including analog audio, video and digital data recording. Since the scale of the first magnetic hard disk drive by IBM in 1956, the capacity and storage density, i.e. the number of bits per square inch (bits/in.^{2}), have increased dramatically. The density will exceed 1 Tbit/in.^{2} with a couple of years (Fig. 1.1) [1-3].

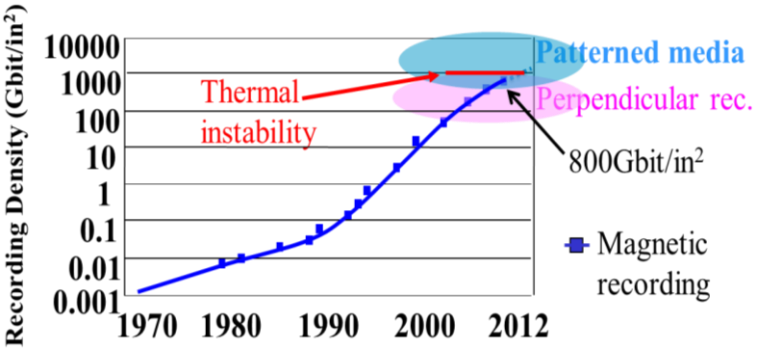

Fig.1.1 Trend of areal density of magnetic recording in production level.

Data is stored in circular tracks on a disk shown in Fig. 1.2 [4]. Within each track, a stream of data bits is recorded as regions of opposite magnetization. Each track consists of equally spaced bit cells, with a digital '1' being indicated by a boundary (called a magnetic transition) between regions of opposite magnetization within a bit cell, and a '0' being indicated by a continuous regions without such a boundary [4]. In each bit cell, there are many tiny magnetic grains. These grains are randomly created during the deposition of the magnetic film. Each grain behaves like an independent magnet whose magnetization can be flipped by the write head during the data writing process.

As the recording density increases, making smaller grains is necessary to be done to satisfy the progress of information technology. However, if the grain size becomes so small that further shrinkage would cause the magnetization of the individual grains to be unstable. The magnetic anisotropy energy of the grain becomes small compared to the thermal fluctuation energy at room temperature. [2] If the magnetic anisotropy falls below a certain value, the magnetization of the grain can flip spontaneously. If a significant fraction of the grains on the disk flip spontaneously, the data stored on the disk will erase itself. Thermal

fluctuation can be reduced by using material with high magnetic anisotropy energy. However, the reversal field becomes too high compared to the capability of current recording head material.

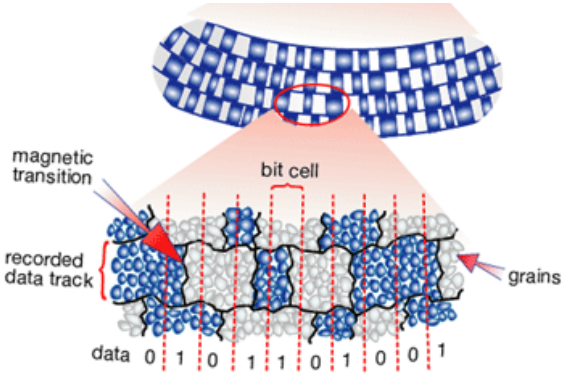

Fig.1.2 The schematic diagram of conventional media recording (HGST Corporation) [4].

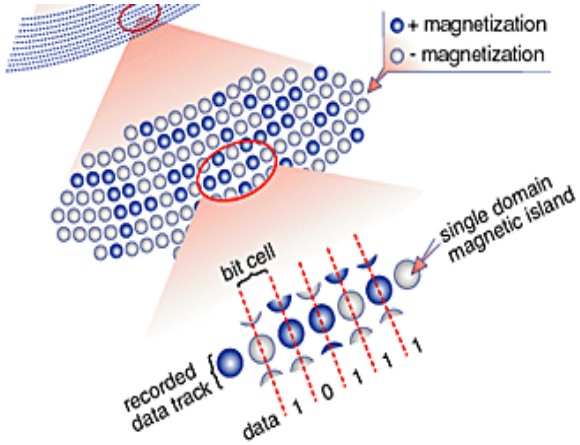

Fig.1.3 Schematic diagram of bit patterned media recording (HGST Corporation) [4].

Bit pattern media (BPM) as a promising approach has been proposed that it can overcome the problem of thermal instability [5-7]. With patterned media, the magnetic layer is created as an ordered array of highly uniform islands, each island capable of storing an individual bit as shown in Fig.1.3. Since each island is a single magnetic domain, patterned media is thermally stable, even at densities far higher than that can be achieved with conventional media. [4] There is a report that put forward by Hitachi Corporation [4] (shown in Fig. 1.4). If the recording density of 100 Gbit/in.^{2}, the islands need to have a center-to-center spacing of 86 nm. To move to 1 Tbit/in.^{2}, a spacing of 25 nm is needed. At 10 Tbit/in.^{2}, this spacing is just only 7.9 nm. Therefore, in order to utilize the patterned media technique to increase the data recording density, it is important to develop a way to form very fine patterns at first.

(a)

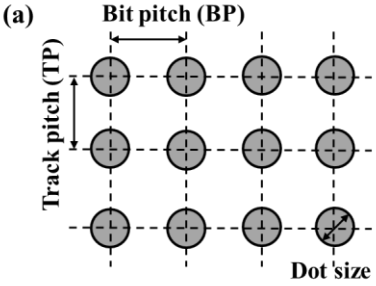

(b)

Areal Density (Tbit/in.^{2})	Pitch Size (nm)	Dot Size (nm)
0.1	86	43
1	25	12.5
3	15	7.5
10	7.9	3.9

Fig.1.4 Dimension requirements of the dot size, pitch size corresponding to the areal density with 0.1, 1, 3 and 10 Tbit/in^2.[4]

Electron beam lithography (EBL) [8], focused ion beam (FIB) lithography [9], and nano imprint lithography (NIL) [10] are currently the three most widely employed nano-lithography techniques. Unlike NIL, EBL can generate arbitrary patterns without the need of fabricating a mold first. Though not as versatile as FIB, which can do both lithography using a resist and milling, EBL is capable of drawing finely controlled pattern to resist without ion contamination [11]. Therefore, EBL is expected to allow the formation of very fine pitch or dot arrays with high resolution for patterned media with high density recording [12].

Using EBL, many researches of fabricating sub-10-nm dot arrays with various resists have been put forward. Calixarene has been studied as a candidate resist for fabricating very fine dot arrays with a 25 nm pitch using a 30 keV accelerating voltage. EB drawing using Calixarene resist promises to open the way toward ultrahigh-density recording at 1.6 Tbits/in.^{2} (corresponding to a dot array of 20-nm period) using very thin (less than 20 nm) film [10-11]. In recent, hydrogen silsesqioxene (HSQ) resist probably attracted more attention than other negative resists [12-13]. HSQ as an excellent inorganic EBL resist that has demonstrated the highest resolution of 9-nm period line array patterns due to its small molecular size [14]. Furthermore, many efforts have been made to improve the density of BPM by using new EBLs and new developments. For example, 12-nm-pitch HSQ dot arrays were fabricated by Yang et.al. [15] using 100 keV exposures combined with high concentration and high temperature development, and 9-nm-pitch HSQ nested “L” structures were fabricated by using a Raith 150 system at 30 keV combined with high contrast salty development [16]. However, the resolution limiting factors of EBL at the sub-10-nm scale are not well understood, which has limited our ability to further improve its resolution. Therefore, in order

to analyze the resolution-limiting factors, simulation becomes more and more necessary to be done.

Process simulation is a key tool for optimization of the experiments. For example, most EB-exposures are performed with high-energy electrons (between 50 and 100 keV) because they provide very high resolution [17]. Based on the analysis of trajectories of electron scattering, we can know that as the energy of incident electron increases, the range of trajectories become large [18]. Furthermore, many researches have focused on the effect of resist thickness on pattern resolution [18-21]. With calculating the energy deposition distribution in resist layer with various thicknesses, we can find that the standard deviation of EDD function in thin resist layer is smaller than in thick resist layer. A thinner resist film is advantageous to suppress the scattering of primary electrons in the resist film and to fabricate fine dot pattern. In addition, the simulation of research on the contrast of developer has been put forward for high resolution pattern fabrication with a dot size of <10 nm in these years [22-23].

1.2 The Purpose and Content of the Work

In this study, we try to use the simulation method to describe both the exposure process and development process. I tried to find the limitation factors of patterned resolution. I presented a general description of Monte Carlo simulation algorithm for modeling of exposure and development processes of EBL. In the exposure process, I established a home-made modeling of electron scattering with solid, and put forward a new modeling method of calculating energy deposition distribution (EDD) in resist layer. The EDD can instead of energy intensity distribution (EID) which can reflect on the energy deposition not only along the radius direction but also along depth direction. Based on it, I can calculate the energy deposition distribution for every depth of the resist. Furthermore, we calculated the trajectories of electrons at various incident beams and in different resists by using the home-made simulation. I demonstrated that thin resist, high incident beam, small electron beam size and negative resist can effectively make very fine dot arrays.

In the development calculation, Vutova and Koleva proposed a nonlinear model [23] using EID as a function of solubility rate to calculate the resist profile during development. However, the EID does not contain information about energy deposition distribution along the

depth-direction. The fundamental disadvantage of the nonlinear model is that the variation of the energy deposition along the depth direction is not considered in the simulation. Without the data of energy deposition in depth direction, it is difficult to reflect the change of solubility rates (development rate) with deposited energy variation in depth-direction. Even calculating the resist profile is impossible. However, the three-dimensional (3D) EDD can solve the problem of nonlinear model; it can reflect the energy deposition in depth-direction. Therefore, in this work, I proposed a new modeling for calculating the resist profile based on the 3D-EDD. The model, it is very important to determine the solubility rate based on the EDD for the development of latent patterns in the resist. By unifying solubility rate dependence of the exposure dose *D* (via experiment) and that of the EDD distributions (via calculations), I roughly calculated the solubility rates for 3D-EDDs by assuming that the EDD value is proportional to the exposure dose *D*. The development simulation was achieved by sequential calculation with solubility rates based on EDD, which was calculated by electron-atom scattering in Monte Carlo simulation. By determining a suitable EDD region (it is the same as selecting a suitable exposure dose in experiment) to make well patterning, I obtained a sharpened nano-dot pattern of resist. I demonstrated the results of the new model agree well with the experimental results. Moreover, based on the model, I changed the exposure conditions such as Gaussian beam size, incident energy and the development conditions such as using developers with various concentrations of NaCl to analyze the dependence. In addition, in order to study the effect of exposure dosage interval on the contrast of resist and the resolution of pattern, I tried to calculate HSQ resist developed profiles with various intervals of exposure dosage (ΔEDD). I demonstrated that the small dosage interval between the exposure dosages which correspond to maximum and minimum solubility rates is an important parameter for increasing the resolution of pattern. If a resist can form very fine pattern during a large range of exposure dosages, it can be demonstrated that the resist have good performance of exposure allowance. I selected two kinds of developers with high contrast and low contrast, respectively. Then I tried to observe that very fine dot arrays can be formed in which EDD region by selecting a series of EDD regions with ΔEDD of each developer. And I demonstrated that high contrast resist has the large exposure allowance and it is very useful for fabricating nano-sized dot arrays. I expect this study can

give us a deep understanding of improving the resolution of EBL by increasing the contrast of resist.

In summary, this thesis provides advances in EBL-based technological processes. In the exposure process, the electron-atom interaction in multi-layered solid thin film of resist by using Monte Carlo technique has been studied. Furthermore, a new method of calcualting the energy deposition distribution in the resist layer has been proposed, it is different as the energy intensity distribution. In addition, optimization of EBL has been accomplished by using proximity effect correction methods. In the development process, a new modeling method for calculationg developed profiles with a solubility rate based on EDD has been put forward. And the development behavior is studied for the different developers with various solubility rates. Moreover, the fundamental of increasing the contrast of resist has been discussed by change the interval of exposure dosage. The high contrast resist with the good performance in exposure allowance has also been demonstrated. Based on the analysis of simulation and experiment, I explore the possibility of resolution improvements in EBL.

1.3 The Outline of the Research

I divided the thesis into 7 parts as follows:

1. Chapter 1 briefly reports the nano-scale related aspects, needs for patterned media, fabrication methods for patterned media, the background of the research and the content of the work. This section aims to frame the contents of this thesis, coherently. It is intended to address the specific subjects under discussion or contained in the following chapters.
2. Chapter 2 briefly reviews the current development of electron beam lithography in nanofabrication, the fundamental of EBL, the electron-solid scattering process, different kinds of resists and the development process. From this section, we obtained a roughly understanding of the limiting factors of resolution in EBL such as resist material, the contrast of developer and so on.
3. Chapter 3 introduces the fundamental of the electron scattering process. In this study, I made home-made energy deposition distribution modeling and applied it to investigate under various conditions of electron traversing inside multi-layered thin

film of resist on Si. Using this simulation, the effects of incident energy, resist thickness and critical energy for development on nanometer sized pattern formation have been studied. The aim of the section is to investigate EB lithography using electron energy deposition distribution to ensure the higher resolution.

4. In Chapter 4, Gaussian beam instead of point beam shows in Chapter has been used to calculate the energy deposition distribution. The factors that determine the quantitative characteristics of the spatial distributions, such as beam voltage, beam sharp, beam size, beam distribution, resist material and film thickness etc. have been discussed.
5. In Chapter 5, a new development model of calculating the resist profile based on *EDD* with solubility rates has been proposed. The relationship between *EDD* and exposure dosage *D* has been estimated. And the *EDD* value is proportional to the exposure dosage *D* has been demonstrated. Using the relationship between D and *EDD*, I selected various *EDD* regions to evaluate the quality of resist profiles. And then, a suitable *EDD* region which can form a sharpened nano-dot pattern has been determined. The simulation results agree well with the experimental results by using high contrast developer with a combination of 2.3 wt% TMAH and 4 wt% NaCl developer. The effective of the new modeling for calculating resist profile has been demonstrated.
6. In Chapter 6, I investigated the factors that effect on the contrast of HSQ resist by using our proposed modeling method. I tried to calculate HSQ development profiles with different intervals of exposure dosage (ΔEDD). I demonstrated the ΔEDD is an indicator of contrast of resist and pattern resolution. In addition, I also demonstrated that high contrast developer as TMAH 2.3 wt% and NaCl 4 wt% developer has the small exposure interval, and the high contrast developer can provide high resolution patterning. Furthermore, I demonstrated that the high contrast developer has the good exposure allowance.
7. In Chapter 7, I gave the conclusion of the thesis and the future work.

References

1. Z. Mohamad, M. Shirai, H. Sone, S. Hosaka and M. Kodera, Nanotechnology **19** 025301 (2008).
2. A. Kikitsu, J. Mag. Mag. Mater., **321** 526 (2009).
3. R. Wood, J. Mag. Mag. Mater., **321** 555 (2009).
4. https://www1.hgst.com/hdd/research/storage/pm/index.html
5. W. Chang and J. R. Cruz, IEEE Trans. Magn. **46:11** 3899 (2010).
6. S. J. Greaves, H. Muraoka, and Y. Kanai, J. Magn. Magn. Mater., **324** 314 (2012).
7. F. Akagi, M. Mukoh, M. Mochizuki, J. Ushiyama, T. Matsumoto, and H. Miyamoto, J. Magn. Magn. Mater., **324** 309 (2012).
8. S. Ma, C. Con, M. Yavuz and B. Cui, Nanoscale Research Letters **6** 446 (2011).
9. H. Duan, D. Winston, J. K. W. Yang, B. M. Cord, V. R. Manfrinato, and K. K. Berggren, J. Vac. Sci. Technol. B **28(6)** C6C58 (2010).
10. S. Hosaka, H. Sano, K. Itoh, H. Sone, Microelectron Eng. **83** 792 (2006).
11. Z. Mohamad, M. Shirai, H. Sone, S. Hosaka, M. Kodera, Nanotechnology **19** 025301 (2008).
12. W. J. Word, I. Adesida, P. R. Berger, J. Vac. Sci. Technol. B **21(6)** 12 (2003).
13. S. Choi, M. J. Yan, L. Wang, I. Adesida, Microelectron Eng. **86** 12 (2003).
14. B. Cord, J. Yang, H. Duan, D. Joy, J. Klingfus, K. K. Berggren, J. Vac. Sci. Technol. B **27(6)** 2616 (2009).
15. X. M. Yang, S. Xiao, W. Wu, Y. Xu, K. Mountfield, R. Rottmayer, K. Lee, D. Kuo, and D. Weller, J. Vac. Sci. Technol. B **25** 2202 (2007).
16. J. K. W. Yang, B. Cord, H. G. Duan, K. K. Berggren, J. Klingfus, S. W. Nam, K. B. Kim, and M. J. Rooks, J. Vac. Sci. Technol. B **27** 2622 (2009).
17. K. Mitsuishi, Z. Q. Liu, M. Shimojo, M. Han, and K. Furuya, Ultramicroscopy **103** 17 (2005).
18. H. Zhang, T. Tamura, Y. Yin, and S. Hosaka, Key Eng. Mater. **497**, 127 (2012).
19. J. Fujita, Y. Ohnishi, S. Manako, Y. Ochiai, E. Nomura and S. Matsui, Microelectronic Eng. **42** 323 (1998).

20. V. Sidorkin, A. Grigorescu, H. Salemink, and E.V. D.Drift, Microelectronic Eng. **86** 749 (2009).
21. S. Hosaka, Y. Tanaka, M.Shirai, Z.Mohamad, and Y. Yin, Jpn. J. Appl. Phys., **49**, 046503 1-3 (2010).
22. J. K. W. Yang and K. K. Berggren, J. Vac. Sci. Technol. B **25(6)** 2025 (2007).
23. K. Vutova, E. Koleva, G. Mladenov, I. Kostic, T. Tanaka, Microelectronic Eng. **87** 1108 (2010).

Chapter 2 Electron Beam Lithography

2.1 Nanolithography

The main goal of lithography is to create a desired pattern in a resist layer and to subsequently transfer pattern into or onto the underlying layer or substrate [1]. The basic steps of a lithographic process are schematically illustrated in Fig.2.1.

First, the substrate (often silicon) is cleaned using chemical treatments or plasma procedures in order to remove contaminants which may lead to poor adhesion or defect formation in the resist layer. In the next step, a resist layer is spin-coated onto the substrate. Thinner resist layers can be obtained by using solutions with a higher dilution rate. After this, the sample is baked on a hotplate in order to remove the excess solvent from the resist and to thermally anneal residual stress in the resist layer. Next, the sample is e-beam-irradiated causing chemical changes in the exposed area during EBL. Following e-beam exposure, the sample is baked again to either thermally anneal the sample, in order to reduce unwanted chemical changes that might have been caused within the resist layer during the exposure, or to promote further chemical changes in the exposed or unexposed area. This step is referred as a post-exposure-bake (PEB). Subsequently, the sample is developed through spray, puddle or immersion method. A resist can have a negative or positive tone depending on whether the unexposed or the exposed regions are removed during the development process. Usually, the developed patterns are transferred into or onto the underlying layer or substrate by using techniques such as etching or lift-off. Finally, the resist structures are removed by a liquid stripping process or dry oxygen plasma etch. Lithography machines and resists play a crucial role in advanced nanolithography.

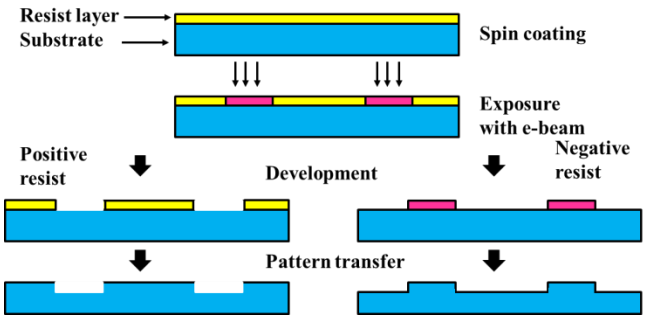

Fig.2.1 Schematic diagram of the basic steps of a lithographic process.

2.2 Electron Beam Lithography

EBL has been used in the IC industry since the 1960s. However, because of its very low throughput, its application is limited to small volume production such as fabrication of photo masks to be used for photolithography and in device prototyping [2]. The first EBL tool was built based on scanning electron microscope (SEM) [3-4]. In EBL tool, the electron beam is accelerated and focused onto a sample under a vacuum environment. While an SEM raster the beam on a sample to image the sample surface, an EBL tool finely focuses electron beam to any position of a sample for a particular duration and draws a shape by controlling the position, and blanking of the beam. Patterning requires a deflection and blanking systems which uses electrostatic or electromagnetic lenses to control the beam position, as shown schematically in Fig. 2.2. As an EBL tool can draw an arbitrary pattern, it is categorized as a mask less lithography.

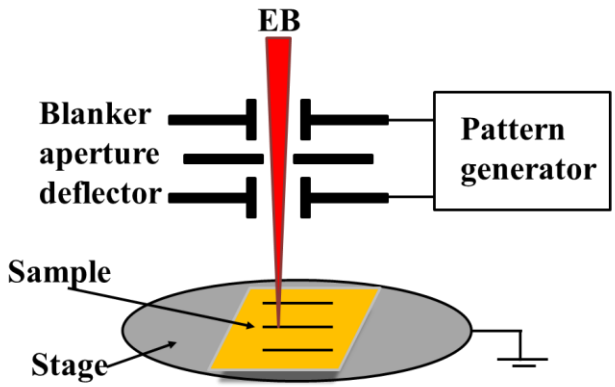

Fig.2.2 Schematic diagram of beam control elements in EBL.

EBL provides excellent resolution due to a small probe size [5-7]. In addition, EBL is a flexible patterning technique that can work with a variety of materials. There are two main EBL strategies, projection printing and EB drawing. In projection printing, a large EB mask pattern is projected onto a resist layer through the mask by using a high-precision lens system. In EB drawing, a small EB spot is moved on to the sample to draw figure with one by one pixel. Direct EB drawing can eliminate the expensive and time-consuming production of masks because the drawing can directly fabricate the resist pattern on the sample. Typically the drawing field, which is deflection range of the beam on the sample, is 10 micrometers to a few millimeters. Larger patterns require mechanical stage movements, which need to be very accurate in order to precisely stitch many drawing fields. The backscattered electrons from the substrate cause to expand the energy deposited areas, which is called by proximity effect. In

order to draw the pattern precisely, we correct the drawing pattern to eliminate the proximity effect. However, the proximity effect causes to deteriorate the patterning resolution. This cannot be corrected in practical EB drawing. In order to reduce the proximity effect, multi-resist method has been developed. Based on the discussion as above, in the next sections, we will use simulation to analyze the patterning resolution in EB drawing and to improve the pattern resolution for highly packed dot arrays.

2.3 Electron-Solid Interactions

Although the electron beam in EBL tools can be tightly focused to an extremely small beam diameter of less than few nanometers, it is also difficult to achieve a nanometer sized feature in a resist film. Electron–solid interactions [8] cause electron scattering in the resist film. When electrons inject into the resist, the energy deposits in the resist film due to electron scattering and inelastic energy loss. The energy deposition distribution provides a limitation of EB-drawing patterning. As primary electrons strike the resist, they experience two types of scattering events, forward scattering and backscattering, as shown in Fig.2.3. The forward scattering [9-10] causes incident electrons to change their direction by a small scattering angle, and to broaden the beam penetration area as electrons penetrate toward the bottom of the resist film. The backscattering occurs due to a large angle scattering event. It usually happens when primary electrons collide with an atom. Some backscattered electrons travel back to the sample surface through the resist at a range as far as micrometers away from the incident beam. These backscattered electrons cause the proximity effect. It causes that the feature connects with neighbor feature when they are located in a distance of less than 100 nm, or the feature size increases from the designed size (see Fig.2.3).

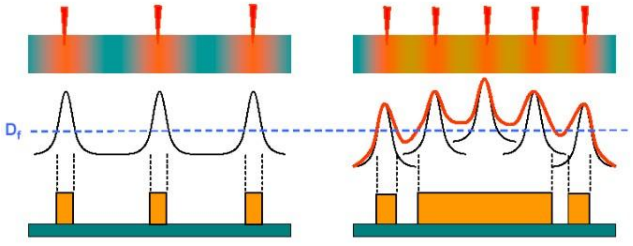

Fig.2.3 Representation of electron dose absorbed in the case of isolated (left) or areal (right) features.

Primary electrons can experience inelastic scattering events in the resist film and dissipate their energy to form pattern (see Fig. 2.4). The energy dissipation continues and

generates energy deposition along the scattering pathway of the primary electron until the primary electron loses all of its energy, initially between 5 and 50 keV in EBL. Secondary electrons with energies in a range of 2 to 50 eV are generated for the majority of resist exposure process. They are considered to cause additional beam diameter widening as they can travel a short distance, less than nanometers in the resist. This effect can be neglected because of extremely small range.

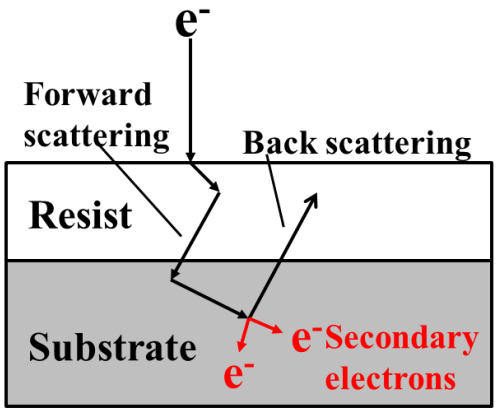

Fig.2.4 Schematic diagram of electron-solid interactions in resist and substrate.

The electron-solid interactions may cause that absorbed energy distribution confined to the zone where the electron has been traveled. The effective exposure in a point is influenced by others exposed at neighbor points based on reciprocity principle. The choice of system configuration or exposure conditions can minimize it, for example, the use of very thin resist layer or beam energy selection and also the design program can allow correcting the proximity effect.

2.4 Electron Beam Resist

Electron beam resists are sensitive to the energy of the electron beam. The chemistry of the resist defines the relationship of the absorbed energy to the change of the molecular weight of the resists. The resist solubility depends on the molecular weight or size in developer [11]. Typically in electron beam lithography, the energy of the primary electrons is 10–100 keV, but lower and higher energies also have been used. Since EBL is used for many different purposes, many properties of the resists have been developed. Usually, high resolution and high sensitivity are the most required properties of the resist. But when we want to transfer the resist pattern to the substrate, etching resistance of the material might be

more important together with above property.

The continuous researches on new resist materials and development chemistries have led to a wide variety of commercially available resists and developers. Resists are dissolved in a liquid solvent and they are spread on a substrate by spin coating in most cases. This is the most reproducible method. Other coating techniques such as spray, roll and dip coating are also used, but they produce less uniform layers. After spreading the resist the solvent is removed by soft bake (also called prebake). Soft bake affects the outcome of the exposure and development and therefore the baking should be done carefully, keeping the conditions and procedure constant. After electron beam exposure, the pattern in the resist is brought out in development. The resist is developed by immersion, spray or puddle method. Immersion development can be done simply in any chemical resistant vessel, but spray and puddle development methods require dedicated equipment. Since the latter two are automated processes, their reproducibility is better.

Resists are divided to two groups by their response to the energy of the electrons: those which are more soluble to the developer liquid after the irradiation are called positive and those which get less soluble are called negative. In general positive resists are used for making concave profiles and negative resists for making convex profiles. In this section, we introduce some positive resists and negative resists.

2.4.1 Positive resist

Poly(methyl methacrylate) (PMMA) is one of the early stage resists developed for EBL[12]. PMMA is typically used as a positive tone resist (Fig. 2.5), although it acts as a negative tone resist at very high dose, about two orders of magnitude greater than that used for the positive tone behavior. Upon EB irradiation, the polymer can undergo either bond breaking (chain scission) or radiation-induced bonding (crosslinking) simultaneously. Chain scission dominates in the positive tone mode of PMMA, leading to reduction of the molecular weight of the polymer, and thus enhancing solubility in particular developers. Crosslinking events forming a heavy molecular weight polymer, which becomes insoluble, dominate in the negative tone mode of PMMA.

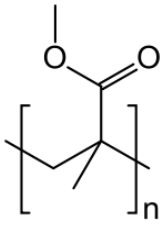

Fig. 2.5 Chemical structure of PMMA ($(C_5O_2H_8)_n$).

PMMA has a capability for high resolution, and its ultimate resolution has been demonstrated to be less than 10 nm [13]. The major problems of PMMA are its relatively poor sensitivity, poor dry etching resistance, and moderate thermal stability. Other important positive resists include PBS (PolyButene-1-Sulfone) and EBR-9 (a copolymer of trifluoroethyl a-chloroacrylate and tetrafluropropyl a-chloroacrylate) which have high sensitivity and ZEP (a copolymer of chloromethacrylate and methylstyrene) which has high-resolution. It is noted that the desired properties of a resist are high-resolution and high sensitivity (high speed). Unfortunately, the resist that have higher sensitivity, usually have lower resolution, especially compared to PMMA.

2.4.2 Negative resist

Negative resists tend to have less bias but they have problems with scum and swelling during development and bridging between features. Calixarene as one of popular negative resist is a cyclic oligomer containing repeating units of phenolic hydroxyl groups linked with methylene bridges (Fig. 2.6). Various calix[n]arene derivatives have been studied as the negative tone resists for EB lithography [14]. With molecular size of about 1 nm, the material has the potential for high resolution lithography. Sub-10 nm feature resolution was achieved in a film of p-methyl-acetoxycalix[6]arene.

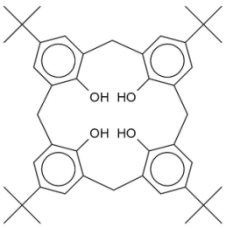

Fig. 2.6 Chemical structure of calix[4]arene with *para-tert*-butyl substituents ($C_{36}H_{36}O_4Cl_4$).

In the last decade, HSQ (Flowable Oxide, Fox-12 from Dow Corning) has become a serious candidate for a high-resolution e-beam resist because of its small line edge roughness,

high etching resistance and small molecular size [15] (Fig. 2.7). HSQ is also an excellent resist for testing EB machine resolution limits because HSQ lines on silicon can be imaged directly in a SEM without the need for gold evaporation for conduction or "lift-off" techniques [16]. Sub-10-nm isolated and dense features have been successfully fabricated using 100 keV EBL [17]. The properties of the resist (e.g. contrast, sensitivity, etching resistance) are influenced by numerous factors ranging from the manner of storage to the details of the development process.

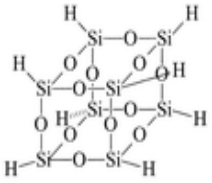

Fig. 2.7 Chemical structure of HSQ ($H_8Si_8O_{12}$).

2.5 Development Process

Besides the lithography tools and resist materials, the development process plays an important role in the EB patterning. Usually, HSQ is developed by manual immersion in aqueous solutions of different developers, tetramethylammonium hydroxide (TMAH) being one most frequently used [18]. Namatsu suggested that the development of HSQ in alkaline solutions is related to bond scission by ionization and that the dissolution rate strongly depends on the bond strength [15]. At low exposure doses, the dangling Si bonds are not stable and the unexposed and slight exposed areas close to the pattern are easily dissolved even when using a weak developer. At a high exposure dose, the Si bonds become more stable due to network formation and the dissolution rate of HSQ decreases remarkably. In this case, a strong developer is recommended because it might improve the dissolution rate due to its effectiveness in bond scission. That means that the optimum dose shifts to higher doses, improving the contrast but decreasing the sensitivity. The main risk of using a strong developer for nanostructures is that structures may be washed away and only highly exposed areas remain on the substrate [1]. While a low developer concentration is used, the sensitivity increases but the contrast is reduced because part of the slightly exposed area near the pattern remains on the substrate. In order to form pattern with fine resolution, the research on finding

suitable concentration of developer is very necessary to be done.

2.6 Conclusions

In this section, we briefly introduced electron beam lithography, several kinds of resists and the importance of the development process. I had obtained an understanding of that the performance of both the lithographic tool and the resist material can limit the resolution of resist-based EB lithography. In order to successfully form very fine nano dot arrays, I should study the various factors that limit the resolution, such as resist material, writing strategy, beam size, resist thickness and development process. In the next chapters, I will investigate these factors in exposure and development process to find the resolution limitation, and then to improve the resolution of patterns.

References

1. A. E. Grigorescu and C. W. Hagen, Nanotechnology, **20** 292001 (2009).
2. McCord, M. A., Rooks, M. J., Handbook of microlithography, micromachining, and microfabricaiton, **Vol. 1**, 144 (1997).
3. K. Mitsuishi, Z. Q. Liu, M. Shimojo, M. Han, and K. Furuya, Ultramicroscopy, **103** 17 (2005).
4. L. Li, S. B. Long, C. S. Wang, W. G. Wu, Y. L. Hao, M. Liu, Microelectronics Journal, **37** 317 (2006).
5. A. A. Tseng, K. Chen, C. D. Chen, and K. J. Ma, IEEE TRANSACTIONS ON ELECTRONICS PACKAGING MANUFACTURING, **26** 141 (2006).
6. S. Hosaka, H. Sano, M. Shirai, Y. Yin and H. Sone, Microelectronic Eng., **84** 802 (2007).
7. S. Manako, J. Fujita, Y. Ochiai, E. Nomura and S. Matsui, Jpn. J. Appl. Phys., **36** 7773 (1997).
8. H. S. Wong, N. R. Buenfeld, Cement and Concrete Research, **36** 1076 (2006).
9. R. Shimizu, Z. J. Ding, Rep. Prog. Phys., 487 (1992).
10. M. S. Son, B. H. Lee, M. R. Kim, S. D. Kim and J. K. Rhee, J. Korean Phys. Soc., **44** 408 (2004).
11. M. Kean, D. R., Schaedeli, U., M. Donald, S. A., J. Polym. Sci., Part A: Polym. Chem., **27**, 3927-3935 (1989).
12. M. Cord, M. A., Rooks, M. J., Handbook of microlithography, micromachining, and microfabricaiton, **1**, 205 (1997).
13. M. Khoury and D. K. Ferry, J. Vac. Sci. Technol. B, **14** 75 (1996).
14. S. Yasin, D.G. Hasko, H. Ahmed, Appl. Phys. Lett., **78**, 2760 (2001).
15. H. Namastu, Y. Takahashi, K. Yamaguchi, M. Nagase and K. Kurihara, J. Vac. Sci. Technol. B, **16** 69 (1998).
16. J. P. Weterings, A. K. van Langen-Suurling and H. Romijn, J. Vac. Sci. Technol. B, **18** 3419 (2000).
17. M. J. Word, I. Adesida and P. R. Berger, J. Vac. Sci. Technol. B, **21** L12 (2003).
18. A. E. Grigorescu, C. W. Hagen and P. Kruit, Microelectron. Eng., **84** 822 (2007).

Chapter 3 Monte Carlo Simulations of Electron Scattering in Solid for Electron Beam Lithography

The formation of high-density, nanometer-scale dot (nanodot) arrays is a challenging task. Such arrays are considered important not only for scientific study of the fundamental quantum-mechanical behavior of materials, but also for achieving a practical goal of ultrahigh-density data storage and electronic devices. In particular, methods for producing isolated high density magnetic nanodot arrays with a pitch of 20 nm or less have been extensively studied with the aim of fabricating the next generation of patterned magnetic media with a recording density of up to 1 terabit $inch^{-2}$. [1]

EBL with extremely high-resolution is as one of the most promising methods for fabricating the nano-scale structures [2]. However, charging-up and proximity effect can lead to poor pattern fabrication, especially it is very severe for high-density nanoscale features. Therefore, the understanding of electron beam interactions with samples and the physicochemical changes associated with these interactions are of vital importance to optimize the lithographic process for nanometer size-pattern. Based on the analysis of electron-atom interactions, correcting selection of the exposure and development conditions can ensure higher resolution and the desired resist profile and dimensions.

Monte Carlo EBL simulation technique has been already applied to single and multilayered samples of sub micron size to study electron beam interaction with atom [3-6]. In the calculation of the deposited energy in the resist layer, the EID function[7] was used. The EID function usually consists of two Gaussian functions with maximal values and dispersions. However, the EID function can reflect the energy deposition distribution in radial direction, we cannot get distribution of energy deposition in depth direction. In this study, we make our home-made EDD calculation program and apply it to investigate various conditions of electron traveling inside multi-layered thin film of resist on Si. Using this simulation, the effects of incident energy, resist thickness and critical energy for development on nanometer sized pattern formation have been studied. Our aim is to investigate EB lithography using electron energy deposition distribution to ensure the higher resolution and we also want to use

the results of the simulation to improve the results in experiments.

3.1 Elastic Scattering

3.1.1 Basics

Elastic scattering results from the interaction between incident electrons and the electrostatic field of an atomic nucleus as screened i.e. reduced in range and magnitude, by the atomic electrons. Because the large mass of the nucleus compared to that of the electron the average energy lost by the incident electron in such an interaction is very small and usually neglected. Therefore the incident electron is considered to change its direction without losing energy. This interaction is dominant and mainly occurs in the spatial distribution around the electron incident direction in the solid.

In general, we can write the differential cross section for elastic scattering $\mathrm{d}\sigma/\mathrm{d}\Omega$, which represents the probability of an incident electron being scattering per unit solid angle Ω by the atom, as a function of complex scattering amplitude or scattering factor *f*, i.e.:

$$\frac{d\sigma}{d\Omega} = |f(\theta)|^2 \tag{3.1}$$

where f is a function of the scattering angle θ.

Within the first Born approximation f is proportional to the Fourier transform of the atomic potential $V(r)$ with r the distance from the nucleus. By choosing a suitable expression for $V(r)$ we can obtain an expression for the differential cross section for elastic scattering.

3.1.2 Rutherford cross section

The earliest and simplest model for elastic scattering of charged particles is based on the unscreened electrostatic field of a nucleus and was first used by Rutherford to study the scattering of alpha particles. A simple way to account for screening is given by using a so-called Wentzel potential in which the nuclear potential is attenuated exponentially as a function of the distance *r* as follow:

$$V(r) = -\frac{Ze^2}{r} exp\left(-\frac{r}{r_0}\right) \tag{3.2}$$

$$r_0 = a_0 Z^{-\frac{1}{3}} \tag{3.3}$$

where Z the atomic number of the target atom, e is the electronic charge, r_0 is the screening radius and a_0 is Bohr's radius.

The exponentially decaying function is a rough approximation of the screening of the nucleus by its atomic number. Using such a potential leads to following expression for the differential elastic scattering cross section [8]:

$$\frac{d\sigma}{d\Omega} = \frac{Z^2 e^4}{4E^2} \frac{1}{(1-cos\theta+\alpha)^2} \tag{3.4}$$

with α being the so-called screening factor and defined as:

$$\alpha = \frac{1}{2E^2 {r_0}^2} = \frac{m_e e^4 \pi^2}{h^2} \frac{Z^{\frac{2}{3}}}{E} \tag{3.5}$$

In the special case of no-screening (i.e. $\alpha = 0$) we obtain the well-known Rutherford formula:

$$\frac{d\sigma}{d\Omega} = \frac{Z^2 e^4}{4E^2} \frac{1}{(1-cos\theta)^2} \tag{3.6}$$

The total elastic Rutherford cross section σ_e is obtained by integrating Eq.3.6 over all possible scattering angles:

$$\sigma_e = \int \left(\frac{d\sigma}{d\Omega}\right) d\Omega = \int_0^{\pi} 2\pi \sin\theta \left(\frac{d\sigma}{d\Omega}\right) d\theta \tag{3.7}$$

3.1.3 Mott cross section

The screened Rutherford cross section is only valid for incident electrons with sufficiently high energy (a few keV) and for atoms with intermediate atomic number *Z*. For lower energies and heavy elements it does not correctly describe elastic scattering since in the derivation of the differential cross section we have ignored the spin of the incident particle and subsequent spin polarization effects. Also, the simplistic exponentially decaying atomic potential *V(r)* we have used should be replaced by a more realistic one. A differential cross section which incorporates all these factors in detail is the Mott cross section [9-12]. According to Mott (Mott,1929), by solving Dirac equation a relativistic representation of the differential elastic scattering cross section is given by

$$\frac{d\sigma_e}{d\Omega} = |f(\theta)|^2 + |g(\theta)|^2 \tag{3.8}$$

where the scattering amplitudes is derived by a partial wave expansion method [10-12] (Mott & Massey, 1965):

$$f(\theta) = \frac{1}{2ik}\sum_{l=0}^{\infty}\left[(l+1)\left(e^{i2\delta_l^+} - 1\right) + l\left(e^{i2\delta_l^-} - 1\right)\right] P_l(cos\theta) \tag{3.9}$$

$$g(\theta) = \frac{1}{2ik}\sum_{l=1}^{\infty}\left[-e^{i2\delta_l^+} + e^{i2\delta_l^-}\right] P_l^1(cos\theta) \tag{3.10}$$

where $\hbar k$ is the electron momentum, $P_l(cos\theta)$ and $P_l^1(cos\theta)$ are Legendre and the first order associated Legendre functions, δ_l^+ and δ_l^- are the phase shifts of the *l* th partial wave for spin up and spin down electrons, respectively.

The total elastic cross section σ_e can be obtained by integrating the differential elastic scattering cross section over whole solid angles,

$$\sigma_e = \int \frac{d\sigma_e}{d\Omega} d\Omega = 2\pi \int_0^{\pi} sin\theta\{|f(\theta)|^2 + |g(\theta)|^2\}\, d\theta \tag{3.11}$$

which is related to elastic scattering mean free path in solid via

$$\lambda_e = (n\sigma_e)^{-1} \tag{3.12}$$

where $n = N_A\rho/A$ is the number of atoms in a unit volume, N_A is Avogadro's number, ρ is the density and *A* is the atomic weight.

The elastic scattering mean free path is the average distance between two successive elastic collisions between a moving electron and solid atoms, which is the basic information requested in the MC simulation for electron transport in solids.

3.2 Inelastic Scattering

The inelastic electron-atom collisions result in electron energy loss due to such effects as generation of secondary electrons, bremsstrahlung emission, or Plasmon excitation. A single stopping power (i.e. energy loss per unit electron path length) is used to model electron energy loss due to all possible inelastic scattering events between two subsequent elastic scatterings. The commonly used electron stopping power is that defined by the Bethe law.

$$-\frac{dE}{ds} = \frac{2\pi e^4}{E} nZ\, ln\frac{1.166E}{J} \tag{3.13}$$

where *n* is the number of atoms in a unit volume. *J* is an adjustable parameter called mean ionization potential and defined empirically as a function of the atomic number. Another issue of using Eq. (3.13) is that it gives a negative value on the right hand for electron energies smaller than *J*/1.166.

In place of Eq.3.13, there has been reported the use of a relativistic expression of the

Bethe law [13-14] that should be more adequate for high (50-100 keV) energetic electrons. In compact form, the relativistic Bethe formula can be written as

$$-\frac{dE}{ds} = \frac{2\pi e^4}{mv^2} nZ \left[ln \frac{mv^2 E}{2J^2\gamma^2} - (2\gamma - \gamma^2) ln2 + \gamma^2 + \frac{1}{8}(1-\gamma)^2 \right] \quad (3.14)$$

where v is the relativistic electron velocity, which relates to the given kinetic energy $E = mc^2(\gamma^{-1} - 1)$ via relativistic correction factor $\gamma = \sqrt{1 - (v/c)^2}$. m is the electron rest mass. As for the value of J, it was calculated according to Berger and Seltzer similar to the case of the usual Bethe formula above.

One of the commonly used expressions for the stopping power is given by the modified Bethe relationship, which is expressed as [15]

$$-\frac{dE}{ds} = 78500 \frac{z\rho}{AE} ln\left(\frac{1.166(E+0.85J)}{J}\right) \quad (3.15)$$

Here J, the mean ionization potential, is assumed to be available from the experiments. The shortcomings of the Bethe relationship is that it incorrectly represents the stopping power at low electron energies (i.e., <1 keV). The experimental data demonstrated a wider range of application in various electron energies, and they can be easily incorporated in a Monte Carlo Method (MCM) which further improves the accuracy of MCM results.

3.3 Monte Carlo Modeling

Various models for Monte Carlo simulation, which have been widely used since the start of this approach in the 1960s, are briefly explained below.

3.3.1 Multiple scattering model

This model, initiated by Berger (1963)[16] for practical Monte Carlo calculations of penetration of charged particles in matter, was based on the use of the Bethe's stopping power equation describing energy loss and angular distributions for electron scattering, which is derived for a certain electron path, s, from the transport equation

$$f(\theta) = (4\pi)^{-1} \sum_{t=0}^{\infty} (2l+1) P_l\,(cos\theta) exp - \int_0^s K_l ds \quad (3.16)$$

where

$$K_l = 2\pi N \int_0^x \sigma(\theta)\,[1 - P_l(cos\theta)] sin\theta d\theta \quad (3.17)$$

with $P_l(cos\theta)$ is the Legendre polynomial, and $\sigma(\theta)$ is the screened-type Rutherford scattering cross-section. For applications of this type of Monte Carlo calculation as applied to EPMA the reader may find the work by Heinrich (1968) [17] very useful and instructive. This model was superseded by the single scattering model.

3.3.2 Single Scattering Model

This model [18], which is still widely used, adopts the screened Rutherford scattering cross-section $\sigma_R(\theta)$ in place of the angular distribution $f(\theta)$ represented by Eq. (3.16) while the energy loss calculated by Bethe's stopping power equation as in the multiple scattering model. Wider applications of this model will be mentioned in section 3.4.

3.3.3 Hybrid model

In this model each individual inner-shell ionization was simulated according to Gryzinski's formula [19]. The energy loss due to valence electron excitations was imposed on each step length between two individual scattering events in the so-called continuous slowing down approximation, being assessed directly by

$$\Delta E = \int_0^s \left(-\frac{dE}{ds}\right)_{valence} ds \tag{3.18}$$

where the stopping power of valence electrons was estimated by the difference of Bethe's stopping power and the stopping power of the inner-shell electrons, $\sum_n(-dE\ /\ ds)_n$,

$$\left(-\frac{dE}{ds}\right)_{valence} = \left(-\frac{dE}{ds}\right)_{Bethe} - \sum_n \left(-\frac{dE}{ds}\right)_n \tag{3.19}$$

where, according to Gryzinski,

$$\left(-\frac{dE}{ds}\right)_n = N \int_{E_n}^{E} (\Delta E) \frac{d\sigma_n}{d(\Delta E)} d(\Delta E)$$

$$= \pi e^4 N z_n \frac{1}{E} \left(\frac{E - E_n}{E + E_n}\right)^{\frac{3}{2}}$$

$$\times \left[ln\left(\frac{E}{E_n}\right) + \frac{4}{3} ln\left(2.7 + \sqrt{\frac{E}{E_n} - 1}\right)\right] \tag{3.20}$$

This hybrid model, initially proposed by Schneider and Cormack (1959) for the discrete and continuous energy loss processes, has been further developed by some authors (e.g. Berger 1963, Shimizu *et a1* 1972, Reimer and Krefting 1976, Shimizu 1977, Shimizu and

Everhart 1978, Ich'mura and Shimizu 1981, Murata *et* af 1981, Reimer and Stelter 1986), and has done much to extend Monte Carlo calculations to alloys and compound materials including secondary electron generation.

3.4 Modeling of Electron Scattering Process

When a beam of high energy electrons hits a solid target, the electrons will interact with the electrical fields of the target's atoms and undergo elastic and inelastic scattering events. In elastic scattering, the incident electron is deflected with no energy loss. In this study, for the treatment of electron elastic scattering, we considered the incident electron energy of 10 keV-30 keV, while the Mott scattering model was just used for the low energy. Here, we selected the screened Rutherford scattering model [20-21] as the elastic model:

$$\frac{d\sigma_i}{d\Omega} = \frac{e^4 Z_i(Z_i+1)}{4E^2(1-cos\theta+2\beta)} \tag{3.21}$$

where β is the screening parameter which is given by

$$\beta = \frac{1}{4}\left(\frac{1.12\lambda_0 h}{2\pi p}\right) \tag{3.22}$$

$$\lambda_0 = Z^{\frac{1}{3}}/0.885a_0 \tag{3.23}$$

where *e* is the electronic charge, *Z* is the atomic number of the material, *E* is the energy of electrons, θ is the scattering angle, a_0 is the Bohr radius, *h* is the Planck's constant and *p* is the electron momentum.

The scattering step length of electron with energy *E* is derived from the following formula:

$$S = -\frac{A}{N\rho\sigma} \cdot \ln R \tag{3.24}$$

where σ is the total cross section calculated from differential scattering cross section, *N* is the Avogadro's number, *A* is the atomic weight and ρ is the mass density, *R* is a uniform random number between 0 and 1.

Scattering angle θ and azimuthal angle ϕ can be obtained using the following equations:

$$\theta = cos^{-1}\left(1 - \frac{2\beta R_1}{1-\beta-R_1}\right) \tag{3.25}$$

$$\phi = 2\pi R_2 \tag{3.26}$$

where the R_1 and the R_2 are independent equidistributed random number between 0 and 1.

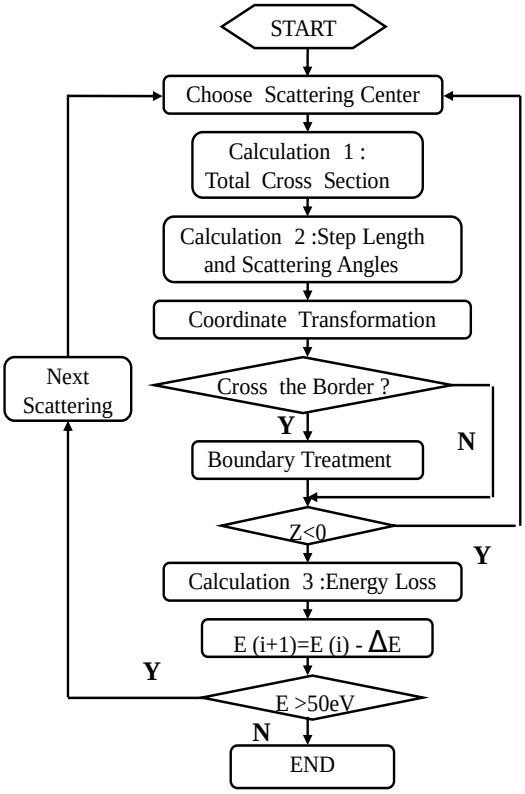

Fig.3.1 Flow chart of the home-made Monte Carlo simulation program.

Since the electron suffers scattering to make its trajectory, it continuously loses its kinetic energy to make its trajectory. Figure 3.1 shows the flow chart of the Monte Carlo simulation program. In the simulation, incident electron is slowing down following Bethe's formula, which is a good empirical method of calculating this energy loss in electron-atom interaction. The Bethe's approximation [20] is given by

$$-\frac{dE}{ds} = \frac{2\pi e^4}{E}\sum_i n_i Z_i \ln\left(\frac{1.166E}{J_i}\right) \tag{3.27}$$

where the n_i is the number of atoms in a unit volume, the J_i is mean ionization energy of atom i .

The energy just before the nth scattering is:

$$E_{n+1} = E_n - |dE/ds|_{E_n} \cdot S_n \tag{3.28}$$

where the E_n is the energy of the (n-1)th scattering, the S_n is step length between (n-1)th and n^{th} scatterings, and the $|dE/ds|_{E_n}$ is the mean energy loss rate which can be obtained from Eq.(3.27).

3.4.1 Determination of scattering center in polybasic material

When we select the polybasic material as the resist, for each scattering of electron in simulation, it must be determined by random sampling which element atom will act as the scattering center, then the scattering step length, scattering angle and energy loss are calculated.

Based on the Rutherford-Bethe model, the formula $\sum_{i=0}^{k-1} P_i < R \leq \sum_{i=0}^{k} P_i$ $(k = 1,2,\ldots,N)$ is used to determine whether the *k*-th element atom acts as the scattering center in the medium with *N* kinds of elements, here P_i denotes the probability of scattering off an atom of the *i*-th element and *R* is a uniform random number distributed between 0 and 1.

3.4.2 Multilayer system

For a multilayer system, i.e. a sandwich-like sample, special attention should be paid to the existence of an interface between two layers, in regard to the various possibilities of the location of path over different layers that possess unequal mean free paths for electron travel.

When there is a large difference in atomic number between a film and a substrate, boundary treatment is significant for electrons crossing the interface as shown in Fig. 3.2.

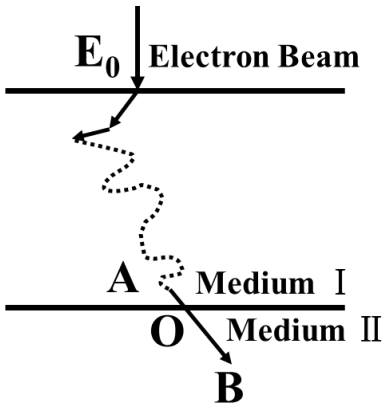

Fig.3.2 Sketch of the electron path crossing the boundary.

The boundary treatment equation is

$$S - \overline{AO} - \overline{OB} \cdot \lambda_1/\lambda_2 = 0 \tag{3.29}$$

where *S* is step length starting at Point A before correction, λ_1 and λ_2 are respectively the mean free paths in the two kinds of mediums Ⅰ and Ⅱ of electrons with energy E_A. If $S > \overline{AO}$, the corrected $\overline{OB}$ should be calculated, it can be obtained from Eq (3.29) is the scattering length of electron in medium Ⅱ. Thus, the real step length after correction of the step length S is $S' = \overline{AO} + \overline{OB}'$.

3.4.3 Calculation of trajectories of primary electron in scattering process

The electron goes forward one step, and its position at the next scattering point is given by the equation

$$\begin{pmatrix} x_{n+1} \\ y_{n+1} \\ z_{n+1} \end{pmatrix} = \begin{pmatrix} x_n \\ y_n \\ z_n \end{pmatrix} + s_n \begin{pmatrix} sin\theta_n cos\phi_n \\ sin\theta_n sin\phi_n \\ cos\theta_n \end{pmatrix} \tag{3.30}$$

where the angles (θ_n, ϕ_n) in the sample coordinate system are related to $(\theta_{n-1}, \phi_{n-1})$ in the coordinate system moving with the electron by the transformation relations:

$$\begin{aligned} \cos\theta_n &= cos\theta_{n-1} cos\vartheta - sin\theta_{n-1} sin\vartheta cos\varphi \\ \sin(\phi_n - \phi_{n-1}) &= sin\vartheta sin\varphi / sin\theta_n \\ \cos(\phi_n - \phi_{n-1}) &= (cos\vartheta - cos\theta_{n-1} cos\theta_n)/(sin\theta_{n-1} sin\theta_n) \end{aligned} \tag{3.31}$$

We have made an assumption in the simulation that an electron transverses the first step, without scattering at the sample-vacuum interface, as shown in Fig 3.3.

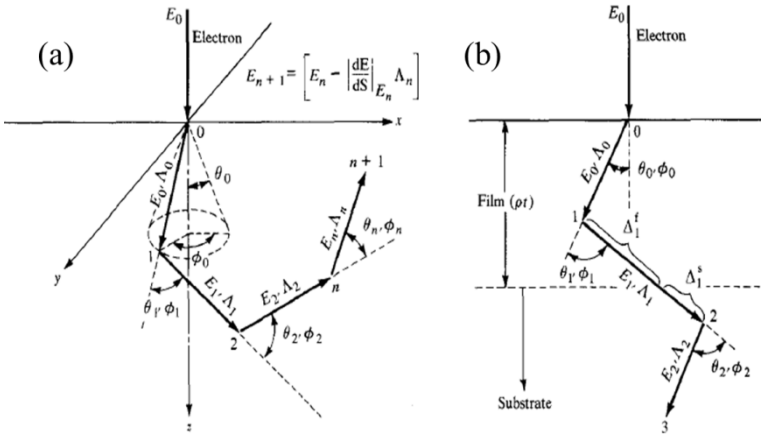

Fig.3.3 Primary electron trajectories in steps of electron scattering and energy loss, (a) in a thick target and (b) in a thin film on a thick substrate.

This is necessary to achieve a reasonable backscattering yield. The collision point of the first flight is defined as first scattering point (x_1, y_1, z_1). Tracing back the procedures described by equations (3.21)-(3.28), we can then derive the second scattering position, and repeat this process forms an electron trajectory which is terminated only after (for a bulk sample there is no penetrating case) its kinetic energy falls below a cut-off energy, E_c. In the calculation, the E_c was 50 eV. When the energy of electron slows down to 50 eV, it has not enough energy to make the trajectory. The scattering process will be stopped.

3.4.4 Calculation of Electron Deposition Distribution in resist film

Energy deposition density is an important parameter in consideration of EBL. In order to calculate the energy deposition distribution in resist, we used cylindrical coordination system and proposed a new algorithm to calculate the energy distribution in every sub-layer. We divided the resist layer along z-axis into several thin sub-layers. The EDD was calculated in a radius-depth coordination system, assuming that the scattering to azimuth direction is in symmetry. This means that the resist layer was divided into many concentric rings. The simulation was executed to calculate the total energies $E(r,z)$ in every unit ring for EDD function. The ring volume ΔV is given by following equation,

$$\Delta V = (\pi(r+\Delta r)^2 - \pi r^2)\cdot \Delta z \tag{3.32}$$

where the Δz is the thickness of sub-layer and the Δr is increment in radius direction. From the volume, the *EDD* function is given by following equation,

$$EDD(r,z) = E(r,z)/(\Delta V \cdot N_0) \tag{3.33}$$

where the N_0 is total number of incident electron.

3.5 Application of Monte Carlo simulation

3.5.1 Positive resist (PMMA resist)

PMMA $(C_5H_8O_2)$ [21] is a compound of carbon (C), hydrogen (H) and oxygen (O) having average density 1.23 g/cm^3 and average atomic weight 100.067. Here, I present Monte Carlo simulation results of energetic electrons impinging in thin film of Si with resist PMMA based on the model and method that I explained in the previous sections. The parameters are shown in the Table 3-1.

Resist	PMMA ($C_5H_8O_2$)
Density	1.23 g/cm^3
Average atom weight	100.067
Incident energy	30 keV/ 10 keV
Resist thickness	100 nm
Number of electrons	30000

Table 3-1 The parameters used in the calculation.

3.5.1.1 Description of electron scattering trajectories

In the simulation, it was assumed that the electron suffers first scattering at the sample surface $(x_0 = 0, y_0 = 0, z_0 = 0)$ and starts traveling into depth-direction suffering electron-atoms scattering. By generating uniform random numbers between 0 and 1, the scattering angles θ and ϕ can be calculated by using Eqs.(3.25) and (3.26), respectively. Using Eqs.(3.27) and (3.28), we can calculate the energy loss ΔE due to scattering of the electrons with atoms in the sample to make its trajectory. The trajectory of the electron was traced till its energy slowed down to 50 eV. We used random sampling method to determine the scattering center, the step length and a new coordinate conversion method for calculating the trajectories of electrons. The initial energies of the incident electrons were taken to be 30 keV and 10 keV. The scattering trajectories of electrons with various incident electron energies in the PMMA resist layer on Si target were shown in Figs. (3.4)-(3.7). In the simulation, the thickness of the resist layer of 100 nm and the number of incident electrons of 500 was used. With incident energy of 30 keV, penetration depth was about 3.5 μm and lateral range was about 1.5 μm in Si (Fig.3.4). In the resist layer, the electron scattering was expanded only to about 20 nm in radius direction (Fig.3.5). We found that the depth (about 0.6 μm) of penetration was small by using 10 keV incident electrons; however, the scattering range (about 50 nm) in the resist layer is larger than that using high incident energy (Fig.3.7). It indicated that as the energy decreases, the electrons scattering range is expanded in the thin resist layer.

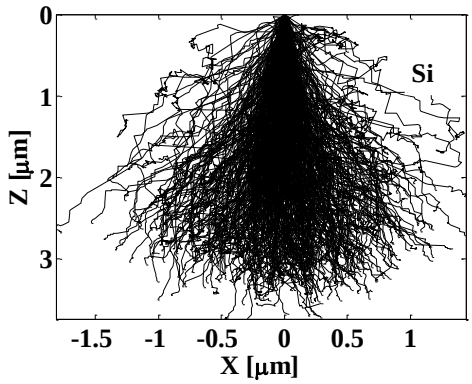

Fig.3.4 Electron scattering trajectories in Si at incident energy of 30 keV.

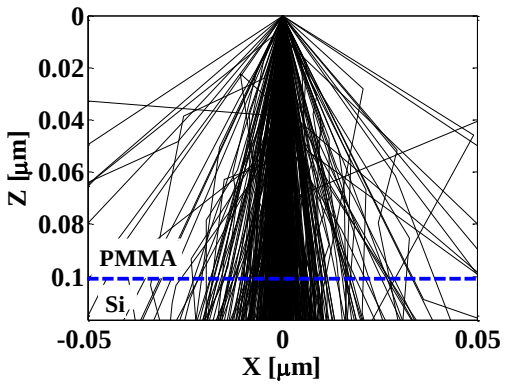

Fig.3.5 Trajectories of incident electrons in 100 nm-thick resist on Si substrate at incident energy of 30 keV.

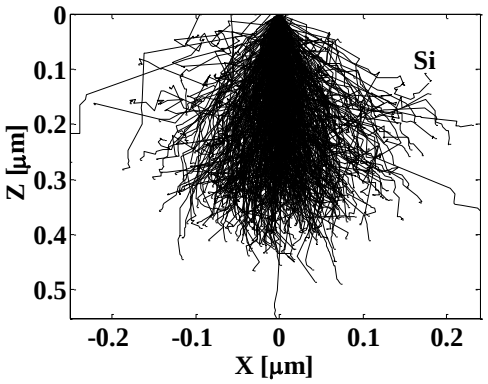

Fig.3.6 Electron scattering trajectories in Si at incident energy of 10 keV.

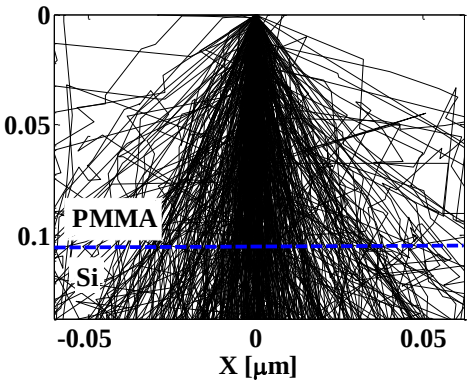

Fig. 3.7 Trajectories of electrons in 100 nm-thick resist at incident energy of 10 keV.

3.5.1.2 Energy deposition distribution (EDD)

The EDD at various depths in the thin resist was calculated. The thickness of the resist was 100 nm, the incident energy was 30 keV. The Δz and Δr were 2nm, the number of incident electrons was 30000. Figure 3.8 shows the EDD in the resist layer of different depths 10 nm, 50 nm and 100 nm. It can be clearly seen that the shallower the depth from the resist

surface, the narrower and the shaper the distribution. Figure 3.9 shows the relationship between resist depth and standard deviation σ of the *EDD* assuming that the *EDD* is approximated by Gauss distribution.

$$EDD(r) = \frac{1}{\sqrt{2\pi}} \cdot \frac{1}{\sigma} exp\left(-\frac{(r-r_0)^2}{2\sigma^2}\right) \tag{3.34}$$

It indicates that small pattern could be produced by using thin resist. It can effectively reduce proximity effects and thus greatly improve resolution.

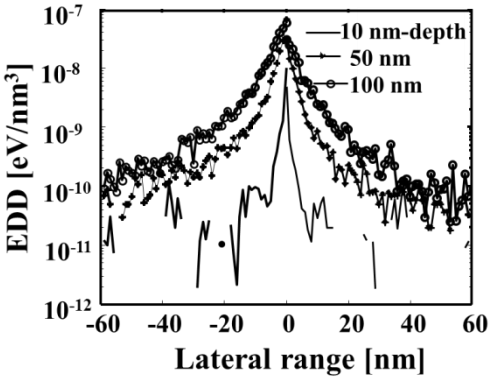

Fig.3.8 Energy deposition distribution of different depths of resist.

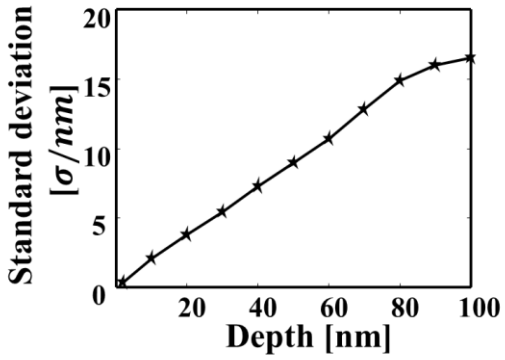

Fig.3.9 Relationship between resist depth and width (σ) of dots using 100 nm-thick PMMA resist with incident electron energy of 30 keV.

3.5.1.3 Consideration for resist development based on the EDD

In this study, resist development is defined as the resist molecule is solved and linked at various critical energy densities in positive and negative resists, respectively. Figures 3.10 (a)-(e) show the area over the critical energy density of 28.125-0.5 keV/cm^3. It is clear that small pattern formation is possible by selecting the critical energy density, which corresponds to exposure dosage in experiment. In the positive resist, however, it is very important to solve

the top layer at first. When the critical energy is between 28.125 keV/cm^3 and 6.25 keV/cm^3 in Fig.3.10 (a)-(d), the top layer cannot be solved. As a result, it is estimated that no patterning occurs in the energy region as shown in Fig.3.10 (f)-(i). When the critical energy density is less than 0.5 keV/cm^3, the hole pattern appears as Fig.3.10 (j). The hole diameter increases with the depth in the resist layer. In the experiment, however, the small diameter of about 4 nm is difficult to be existed [22]. This may be caused by capillary force. The minimum diameter of about 7 nm was obtained in the experiment using ZEP520 positive resist [23].

On the other hand, Figs.3.10 (k)-(o) show the developed resist profiles at various critical energy densities in negative resist. According to the negative resist development mechanism, the linked molecule is remained on the substrate. Although the height of the resist pattern is not complete and short, nanometer-sized patterns are formed as shown in Fig.3.10 (k). When the critical energy density at 28 keV/cm^3, the pattern of 4 nm can be formed. It is clear that the smaller pattern size is obtained by selecting the higher critical energy density, but the height of the resist pattern decreases as the critical energy density increases. Therefore, negative resist is very suitable to form nanometer-sized pattern.

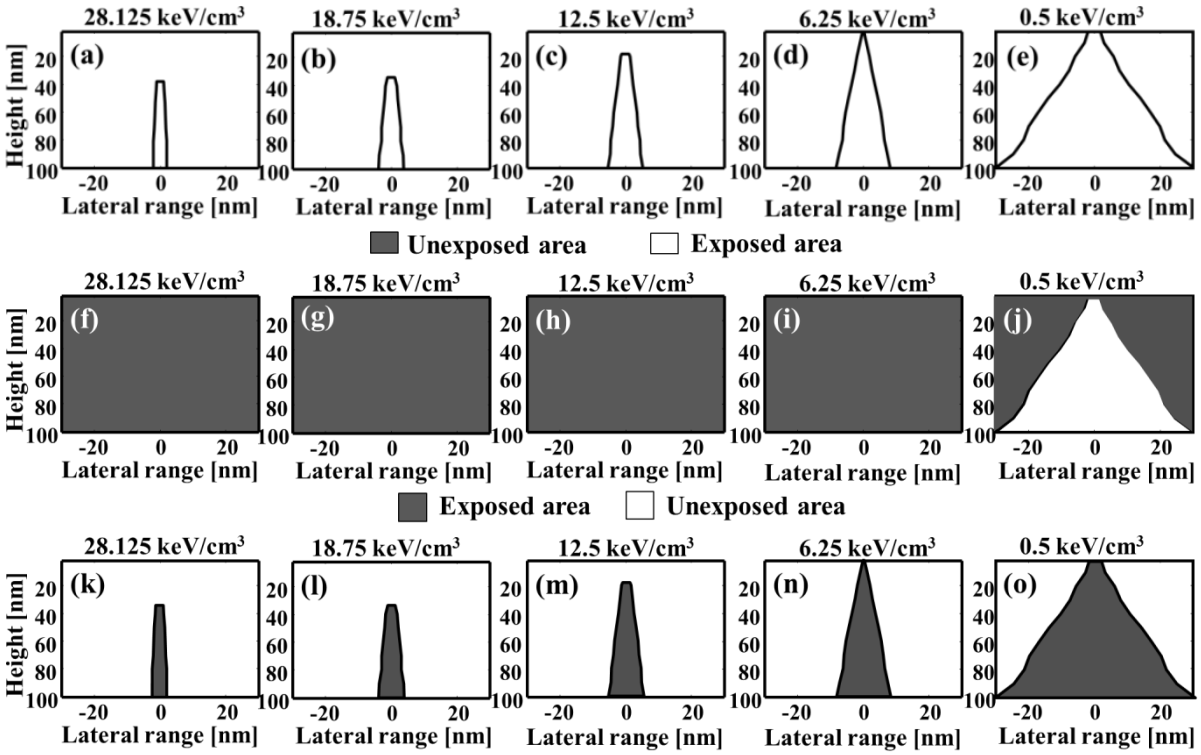

Fig.3.10 Simulated resist profiles at various critical energies.(f)-(g) Positive resist;(k)-(o)Negative resist.

3.5.2 Negative resist (Calixarene resist)

Advances in nanometer-scale device fabrication have increased the demand to form very fine pattern. In EBL, ultra-fine resolution EB resists must be used. Calixarene [24], which is a cyclic oligomer synthesized from phenols and aldehydes, is one of these high-resolution negative resist candidates. EBL using p-methyl-methylacetoxy-calix[6]arene was first reported in 1996. In the work, 10-nm-line patterning was demonstrated [25]. The subsequent reports on p-chloromethyl-methoxy-calix[6]arene (CMC6) resist achieved a ten times higher sensitivity and 12-nm-line patterning [26-27]. The properties of p-chloromethyl-methoxy-calix[4]arene (CMC4) as a high resolution EB resist have been put forward in 2003.[28]

3.5.2.1 Electron scattering trajectories in thin Calixarene resist

As the same simulation conditions as in PMMA resist, here, the initial energies of the incident electrons were 30 keV and 10 keV. The trajectories of electrons with some incident electron energies in 100 nm-thick Calixarene resist layer on Si substrate were shown in Figs.3.11-3.12. In the simulation, the thickness of the resist layer of 100 nm, Gaussian beam diameter of 2 nm, and the number of incident electrons of 500 were used. The parameters in the calculation are shown in Table 3-2.

Resist	Calixarene ($C_{36}H_{36}O_4Cl_4$)
Density	1.09 g/cm^3
Gaussian beam size	2 nm
Incident energy	30 keV/ 10 keV
Resist thickness	100 nm
Number of electrons	30000

Table 3-2 The parameters used in the calculation by using calixarene resist.

With incident energy of 30 keV, penetration depth was about 4 μm and lateral range was about 1.5 μm in Si (Fig.3.11 (a)). In the resist layer, the electron scattering was expanded only to about 20 nm in radius direction (Fig.3.11 (b)). Although 10 keV incident electrons can diffuse as deep as 0.6 μm into the sample, lateral range was expanded to be about 40 nm in the resist layer which is larger than that of 30 keV (Fig.3.12 (a) and Fig. 3.12 (b)). It indicated that as the energy decreases, the electrons scattering range is expanded in the thin resist layer.

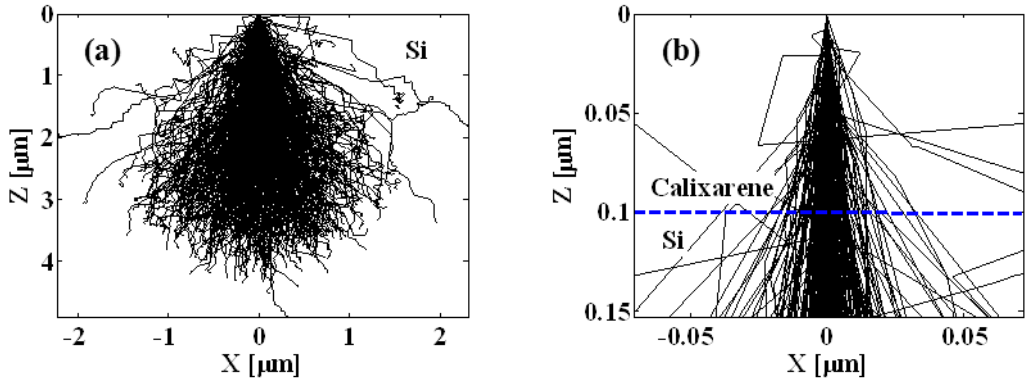

Fig.3.11 Simulated trajectories of electron scattering. (a) electron trajectories in Si with incident energy of 30 keV and (b) trajectories in Calixarene resist (thickness 100nm) with incident energy of 30keV.

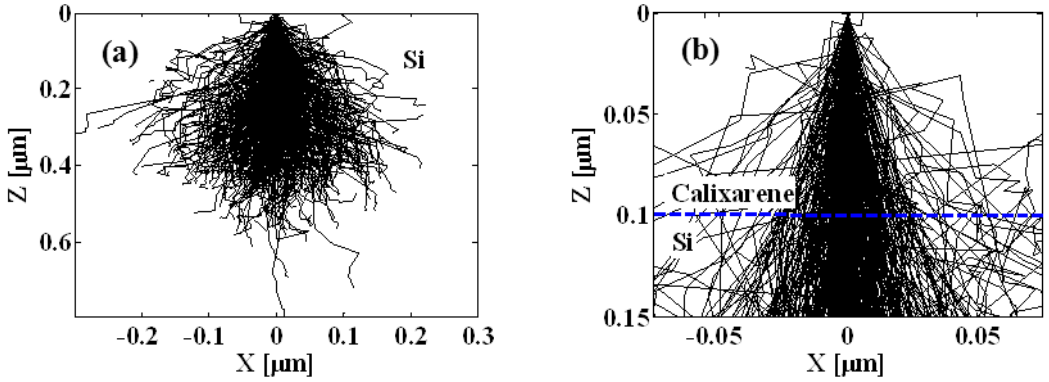

Fig.3.12 Simulated trajectories of electron scattering. (a) electron trajectories in Si with incident energy of 10 keV and (b) trajectories in Calixarene resist (thickness 100 nm) with incident energy of 10 keV.

3.5.2.2 Energy deposition distribution in Calixarene resist

The spatial distribution of the deposited energy density in the resist is the most important value that determines the characteristics of the obtained latent image during the electron beam exposure process. Here, in order to evaluate the dependence of resist thickness on the formation of very fine dot arrays using electron energy of 30 keV, the EDD at various depths in thin Calixarene resist film was calculated. Figure 3.13 shows the radial distribution of the EDD in the Calixarene resist layer of various depths of 10 nm, 50 nm and 100 nm. It can be clearly seen that the shallower the depth from the surface of the resist, the narrower and the sharper the distribution. Therefore, the resist film is used must be as thin as possible for very fine dot array formation.

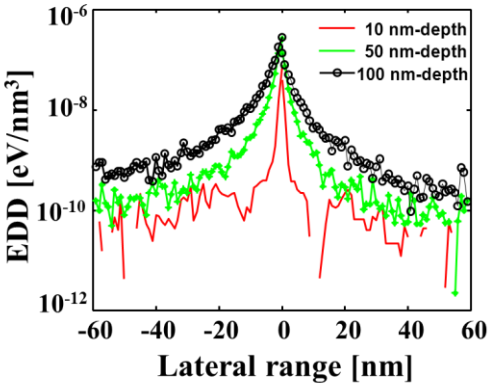

Fig.3.13 EDD of various depths of Calixarene resist film at electron energy of 30 keV.

3.5.3 Comparison of Calixarene and ZEP520 resists using their EDD

Calixarene resist dot arrays with 20 nm pitch with very thin resist layer were demonstrated by Hosaka et al. at a 30 kV in accelerating voltage [29]. ZEP520 and PMMA resists with high resolution has been reported by D. M. Tanenbaum by using a low accelerating voltage [30]. Although there are great efforts in enhancing the resolution of EBL in experiments, analyzing the resolution limitation of different resists is very necessary for the further development. So far, the calculation of nano-patterning using EB drawing with calixarene and ZEP520 resists has not been done yet to analyze the resolution-limiting factors of EBL in the sub-10-nm range. Therefore, in this work, I try to calculate EDD and resist profile after development to analyze the mechanism of dot array formation in resist layer and reveal the limiting factors of these two resists.

3.5.3.1 Energy deposition distribution in Calixarene and ZEP520 resists

The spatial distribution of the EDD in the resist is the most important value that determines the characteristics of the obtained latent image formed by the EB exposure process. In order to evaluate the dependence of resist material on the formation of very fine dot arrays, the EDDs at various depths in thin calixarene and ZEP520 resists were calculated. In the simulation, the incident energy is 30 keV, Gaussian beam size is 2 nm and the number of incident electrons is 30000. Figure 3.14 shows the EDDs at a depth of 50 nm of calixarene

and ZEP520 resists. I can assume that the EDD is approximated by a Gaussian distribution function as shown in Eq.(3.35).

$$EDD(r) = \frac{1}{\sqrt{2\pi}\sigma} e^{-\frac{r^2}{2\sigma^2}} \tag{3.35}$$

Using the Gaussian function, I can calculate the sizes $(2\sigma_1, 2\sigma_2)$ of the EDD in calixarene and ZEP520 resists, respectively. I obtained the size of about 5.4 nm in calixarene resist which is smaller than that of 6.8 nm in ZEP520 resist. Since the deposited energy is more centralized in calixarene resist, it means that calixarene resist has the possibility to form smaller pattern than ZEP520 resist.

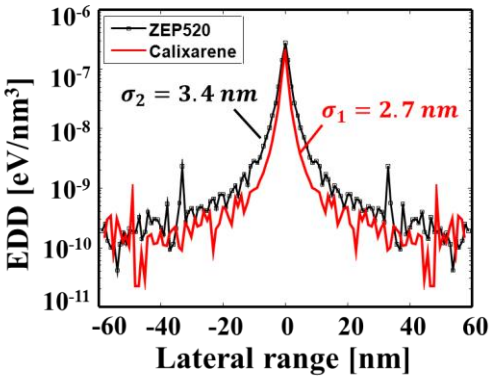

Fig.3.14 EDD in the depth of 50 nm of calixarene and ZEP520 resist at electron energy of 30 keV.

3.5.3.2 Relationship between dot size and critical energy for development

In this section, we define the critical energies whether the resist dot pattern is formed or not to determine the dot size of the resist dots after development process. Here, I considered EB formed dot size at the critical energy density range between of $6.25 - 156.25$ keV$/cm^3$. Figure 3.15 shows that the dot size of calixarene resist is smaller than that of the ZEP520 resist, when I compared them at the same critical energy density. As the critical energy increases, the dot size becomes smaller. This is the same as experimental results in previous research [21,31]. We can consider that the critical energy corresponds to inverse of EB exposure dosage necessary to form the dot after development. It is indicated that it is suitable to form small dot arrays using calixarene resist with high critical energy. It is clear that not only resist thickness but also critical energy (exposure dosage) controls making the dot diameter small.

Small pattern formation is possible by selecting the resist requires the higher critical energy density, which corresponds to exposure dosage in experiment.

Furthermore, considering the capillary force in ZEP520, EBL using ZEP520 is not suitable for formation of the small dot arrays. This tendency agrees well with experimental results. Hosaka et.al reported that minimum dot sizes of using Calixarene and ZEP520 are 13 nm and 20 nm, as shown in Fig.3.16 and Fig.3.17, respectively [21].

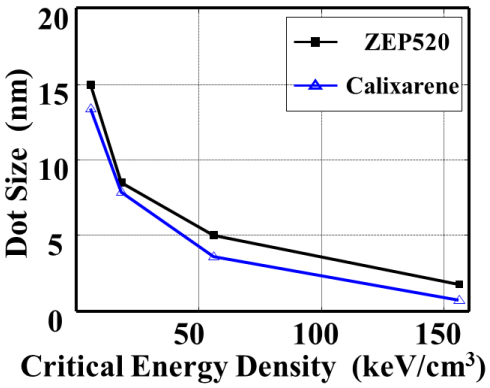

Fig.3.15 Relationship between dot size and critical energyin ZEP520 and Calixarene resists.

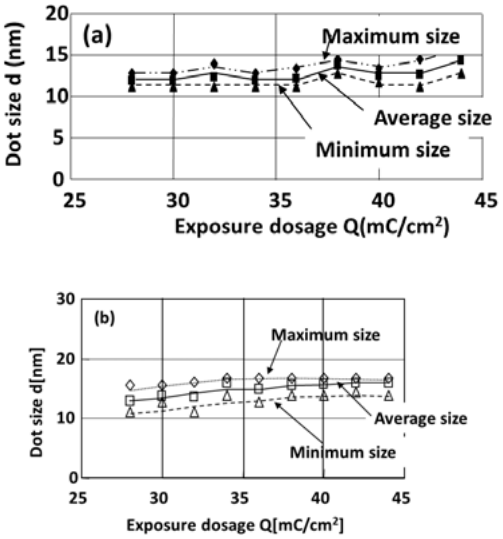

Fig. 3.16 Variations of the calixarene dot size in ultra-high-packed dot arrays. (a) a pitch of 30 nm×30 nm, (b) 25 nm × 25 nm.

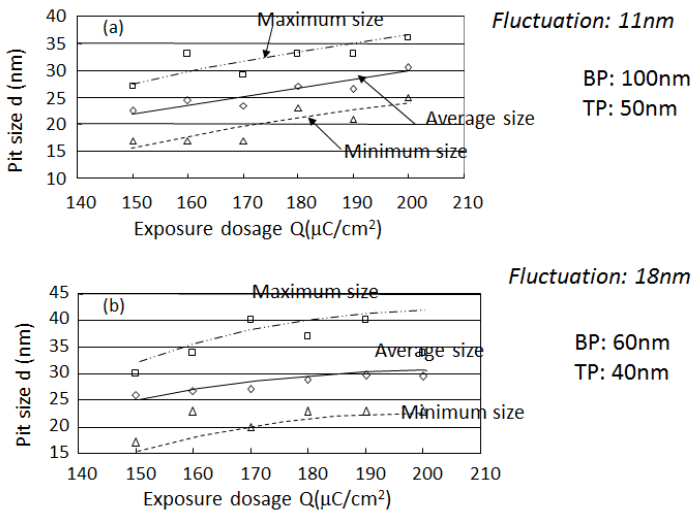

Fig. 3.17 Variations of ZEP520 resist pit width in ultrahigh packed pit arrays (a) with a pitch of 100 nm × 50 nm and (b) 60 nm × 40 nm for exposure dosage at 30 kV.

3.5.3.3 Consideration for resist development based on the EDD

The aim of the simulation is to predict the resist profile formed by EB drawing and development process. I suppose that the resist molecule will be linked in negative resist and be solved in positive resist when the deposited energy is larger than the critical energy density. For evaluation of the dot size, calculations in a wide range of critical energy densities were executed. In previous research, I have calculated the resist profile for the case of single incident beam. Here, in order to consider the dot arrays, I calculate for the case of three incident beams to evaluate the profile at various critical energy densities of $156 - 6\,\mathrm{keV}/cm^3$ in calixarene and ZEP520 resist using the same development manner as described above.

According to the negative resist development mechanism, the exposed resist portions remain on the substrate. Although the height of the resist pattern after development is not large enough, it is estimated that when the critical energy density of $156\,\mathrm{keV}/cm^3$, the dot pattern with 2 nm in diameter can be formed as shown in Fig.3.18 (a). It is clear that the smaller pattern size is obtained by selecting the higher critical energy density, but the height of the resist pattern decreases as the critical energy density increases. In experiments, we cannot observe such a small dot pattern. We think that the dot is collapsed due to too sharp dot like a needle. As the critical energy decreases, the dot pattern becomes complete and large.

When the critical energy less than 18 keV/cm^3, the proximity effect will occur due to the energy superposition caused by exposing neighbor dots. Because of this, the bottom of the resist cannot dissolve but link with each other.

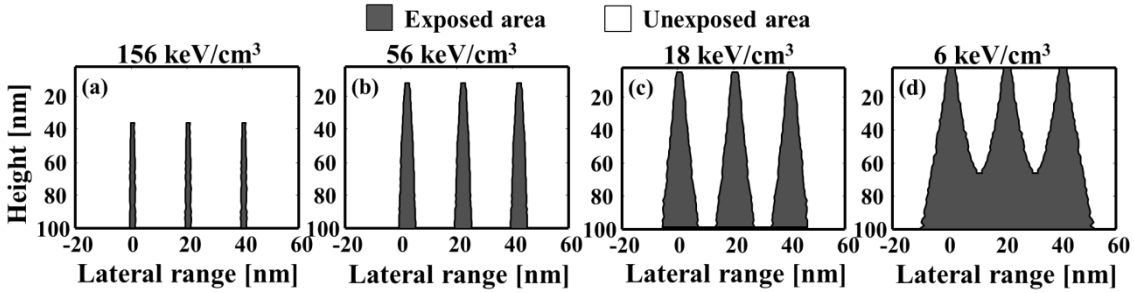

Fig.3.18 Simulated resist profiles for the negative resist (calixarene) at various critical energies. Critical energy at (a) 156 keV/cm^3; (b) 56 keV/cm^3; (c) 18 keV/cm^3; (d) 6 keV/cm^3.

In the positive resist, the exposed resist portions are weakened and become more soluble in the developing solution because many chemical bonds in the portions are broken by the deposited energy. Furthermore, in order to form pattern in the positive resist, it is very important to dissolve the top layer at first. When the critical energy is larger than 15 keV/cm^3, the energy densities of the top layer do not reach to the critical energy density. As a result, no patterning occurs in the exposed region as shown in Fig.3.19 (a). When the critical energy density is less than 15 keV/cm^3, the exposed region of top layer becomes soluble. As the hole size is about 2 nm in Fig.3.19 (b), however, the hole pattern cannot be formed as shown in Fig.3.19 (b) because of the capillary force. As the critical energy decreases, the hole diameter increases, but it also cannot form the hole pattern with pitch size of 20 nm because of the proximity effect as shown in Fig.3.19 (c). In order to form the isolate pit arrays in ZEP520, it necessary to increase the pitch size to 50 nm at least and use the low critical energy of 6 keV/cm^3 as shown in Fig.3.19 (d). The isolate pit size about 24 nm can be formed by ZEP520. It indicates that the pit arrays pattern with pitch of 50 nm is the limit for ZEP520. The experimental results supported this result as shown in Fig.3.20. [31]

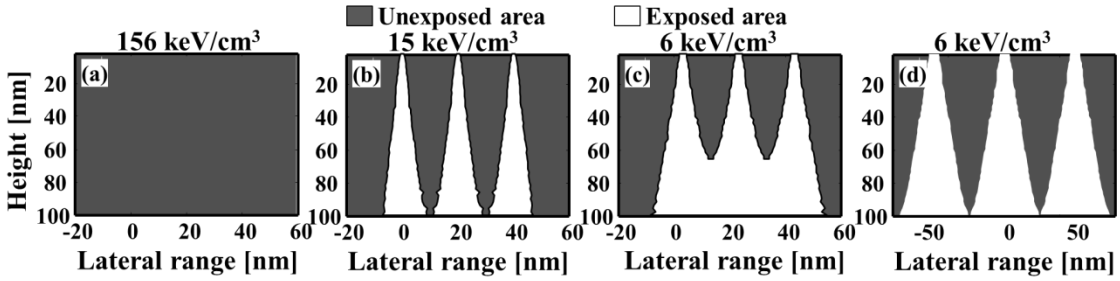

Fig.3.19 Simulated resist profiles for the positive resist (ZEP520) at various critical energies. Critical energy at (a) 18 keV/cm^3; (b) 15 keV/cm^3; (c) 6 keV/cm^3 with 20 nm pitch; (d) 6 keV/cm^3 with 50 nm pitch.

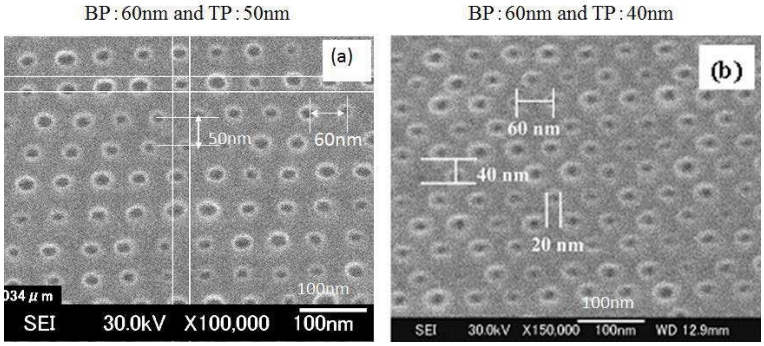

Fig.3.20. SEM images of ultrahigh packed pit resist pattern using ZEP520 (180 C/cm^2, 30 kV), (a) pitch of 60 nm×of 50 nm, (b) 60 nm×40 nm.[31]

3.5.3.4 Consideration of the different limitations in ZEP520 and Calixarene resists

The difference between the limitations of ZEP520 and Calixarene resists using EBL has been investigated by Monte Carlo simulation in previous sections. In the experiment, we demonstrated that calixarene negative resist is more suitable to form very fine dot arrays than ZEP520 positive resist. This may be due to the molecular size, structure of ZEP520 resist and capillary force in the development. The size of ZEP520 is a few nm assuming to be spherical. Sometimes, ZEP520 may be in a chain structure when the molecule is not solved after EB exposure. This comparison indicates that the smallest pattern in EB writing may be determined by the resist's molecular size, structure and resist type.

3.6 Conclusions

In this work, we briefly reviewed the Monte Carlo technique in electron beam lithography and apply the method to investigate various properties of electron traversing inside multilayered thin film of PMMA, calixarene and ZEP520 resists. The energy deposition distributions have been calculated by our home-made Monte Carlo simulations. As results using both positive and negative resists with thin thickness, the following conclusions can be obtained.

1. Thin resist thickness can be provided to make smaller pattern.
2. High critical energy density for resist pattern formation is suitable to smaller dot or pit arrays pattern.
3. Increase of incident electron energy has the same effect for making smaller pattern as thinning of the resist.
4. The simulation shows that the EDD profile seems to be cone shape, which is very suitable for formation of nanometer-sized dots using negative resist, while it is not suitable in a case of using positive resist.
5. These results agree well with experiment results using EB drawing.
6. It is estimated that fine dot arrays with a dot size of less than 10 nm and a pitch size of 20 nm can be formed by using Calixarene negative resist, however, it is impossible that the small pit arrays pattern can be formed by using EB-drawing with ZEP520 resist because of the capillary force.
7. In the experiment, the minimum dot or pit size was about 10 nm. The simulation results which mean that it is necessary that too sharp dot or pit should be considered deeply due to collapse and capillary force.

References

1. B. D. Terris, T. Thomson, J. Phys. D, Appl. Phys., **38**, 199 (2005).
2. H. G. Duan, D. Winston, J. K. W. Wang, J. Vac. Sci. Technol. B, **28**(6), C6C58 (2010).
3. M. S. Son, B. H. Lee, M. R. Kim, S. D. Kim, and J. K. Rhee, J. Korean Phys. Soc., **44**, 408 (2004).
4. B. H. Lee, S. D. Kim, and J. K. Rhee, J. Korean Phys. Soc., **43**, 427 (2003).
5. H. H. Kim, B. O. Lim, S. C. Kim, S. D. Lee, D. H. Shin, and J. K. Rhee, Microelectronics, **63**, 417 (2002).
6. S. C. Kim, B. O. Lim, H. S. Lee, D. H. Shin, S. K. Kim, H. C. Park, and J. K. Rhee, *Materials Science in Semiconductor Processing* (2004).
7. G. M. Mladenov, K. J. Vutova, E. G. Koleva, Physics and Chemistry of Solid State, **10(3)**, 707 (2009).
8. K. Murata, D. F. Kyser, Adv. Electron. Electron Phys., **69**, 175 (1987).
9. R. Shimizu, D. Ze-Jun, Rep. Prog. Phys., 487 (1992).
10. D. Gregory, M. Fink, At. Data Nucl. Data Tables, **14**, 39 (1974).
11. M. Fink, J. Ingram, At. Data, **4** 129 (1972).
12. L. Reimer, B. Lodding, Scanning, **6** 128 (1984).
13. A. Antolak, W. Williamson, J. Appl. Phys., **58**, 526 (1985).
14. Z. J. Ding, R. Shimizu, K. Obori, J. Appl. Phys., **76**, 7180 (1994).
15. D. C. Joy. Monte Carlo modeling for electron microscopy and microanalysis. New York: Oxford University Press, (1995).
16. M. J. Berger, In methods in computational physics., Statistical Physics, **Vol.1**135 (1963).
17. K. F. J. Heinrich, NBS Special Publication 298 (Washington, DC: National Bureau of Standards), (1968).
18. N. Aizaki, Jpn. J. Appl. Phys., **18** 319-325 (1978).
19. M. Gryzinski, Phys. Rev., **138**, A305 (1965).
20. K. Murata, T. Matsukawa, and R. Shimizu, Jpn. J. Appl. Phys., **10** 677-686 (1971).
21. M. S. Sigh, R. K. B. Singh, R. Khatri and B. I. Sharma, Adv. Sci. Lett., **3** 57 (2010).
22. S. Hosaka, Recent Advances in Nanofabrication Techniques and Applications,

978-953-307-602-7, (2011).

23. S. Hosaka, H. Sano, Appl. Phys. Lett., **89** 223131 (2006).
24. J. Fujita, Y. Ohnishi, S. Manako, Y. Ochiai, E. Nomura and S. Matsui, Microelectron. Eng., **41** 323 (1998).
25. Z. B. Mohamad, M. Shirai, H. Sone, S. Hosaka and M. Kodera, Nanotechnology, **19** 025301 (2008).
26. J. Fujita, Y. Ohnishi, S. Manako, Y. Ochiai, E. Nomura, T. Sakamoto and S. Matsui, Jpn. J. Appl. Phys., **36** 7769 (1997).
27. T. Sakamoto, S. Manako, J. Fujita, Y. Ochiai, E. Nomura, T. Sakamoto and S. Teshima, Jpn. J. Appl. Phys., **77** 301 (2000).
28. M. Ishida, J. Fujita, T. Ogurai, Y. Ohshima and J. Momoda, Jpn. J. Appl. Phys., **42** 3913 (2003).
29. S. Hosaka, H. Sano, M. Shirai, H. Sone, Appl. Phys. Lett., **89** 223131 (2006).
30. D. M. Tanenbaum, C. W. Lo, M. Isaacson, and H. G. Craighead, J. Vac. Sci. Technol. B, **14(6)** 3829 (1996).
31. S. Hosaka, H. Sano, K. Itoh, and H. Sone, Microelectronic Eng., **83** 792 (2006).

Chapter 4 Dependence of Electron Beam Diameter, Electron Energy, Resist Thickness and Resist Type for Forming Nano-sized Dot Arrays in EB Lithography

Regarding very fine pattern formation using EBL, there are many works to challenge to form nanometer sized pattern. For example, 10-nm wide line patterning by using p-methy1-methy-lacetoxy-calix[6]arene was reported firstly by Fujita et al [1]. Calixarene resist dot arrays with 20-nm pitch were demonstrated by Hosaka et al. by using a 30 keV accelerating voltage [2]. However, the formation of high-density nano-scale dots is still one of challenging works because the exposure dosage cannot be controlled due to the charging-up [3] and proximity effects [4]. So far, the calculation of exposure and development processes by using EB drawing with Calixarene resist has not been done yet to analyze the resolution-limiting factors of EBL in the sub-10-nm range, which has limited our ability to further improve its resolution. Therefore, we try to explore the dependence of electron beam diameter, electron energy, resist thickness and resist type for forming nano-sized dot arrays in Calixarene resist and find the suitable conditions to improve the resolution of pattern.

In this paper, I briefly described Monte Carlo simulation for the scattering model using a Gaussian beam as an incident electron beam with various diameters from 2 nm to 8 nm to investigate the electron scattering trajectories and energy deposition distribution (EDD) in thin Calixarene resist. From the trajectories and EDD, it is obvious that the high resolution incident beam should be adopted for formation of very fine dots. The analysis of relationship between thickness and dot diameter based on critical energy densities shows that resist of less than 20 nm is potential to form sub-10 nm-diameter dot arrays. In addition, high critical energy densities are benefit to form small dot arrays. Furthermore, I demonstrated that Calixarene resist is more suitable than PMMA positive resist by comparing some parameters of the two resists.

4.1 Beam Diameter Dependence

4.1.1 The modeling of Gaussian beam

In EBL, the EB drawing system uses a finely focused Gaussian electron beam for formation of fine pattern. We have to consider the Gaussian beam profile as an incident electron beam in the simulation. Intensity of Gaussian electron beam can be represented in one dimension by the function [5]:

$$I(r) = \frac{1}{\sqrt{2\pi}\sigma} e^{-\frac{r^2}{2\sigma^2}} \tag{4.1}$$

where *r* is the distance from a center of the beam, and σ is the standard deviation.

For the miniaturization of the dot size, fine electron beam with small σ value is required. The σ value has to be 1 nm because the advanced scanning electron microscope (SEM) has very fine beam with a resolution of about 2 nm [6]. I can determine the incident position of primary electron in Gaussian beam using Monte Carlo simulation. Using the probability *P* and Eq.(4.1), the position *r* is determined by following equations,

$$\mathrm{V}(r) = \int_0^r I(r) \cdot 2\pi r dr \tag{4.2}$$

$$P = \frac{V(r)}{\int_0^\infty V(r) dr} \tag{4.3}$$

where *P* is a uniform random number between 0 and 1.

I prepared to make a data table consists with *r* and probability *P* (Eq.4.3) by every increment of *r* of 0.2 nm in a range of the *r* from 0 to 5σ. The normalized $V(r)$ corresponds to the probability *P*. Then I used Monte Carlo random generator to generate a random data P' between 0 and 1. By comparing the P' with each *P* of data table, I can find the position of the new P' in the data table. And I can use the linear interpolation method to calculate the *r*.

4.1.2 Effect of beam diameter on nano-sized-formation

Beam diameter is one of the major characteristics that affects the accuracy and resolution of EBL. Our electron beam writing system can provide us high probe current up to > 2 nA at small probe diameter of <10 nm. Therefore, in this section, I used the Gaussian beam with various beam sizes of less than 10 nm to calculate the trajectories and EDD in resist layer and investigate the effect of beam diameter.

In order to study the effect of the Gaussian beam diameter, I simulated the electron trajectories in Calixarene resist and EDD when σ was from 1 nm to 4 nm, which means the beam resolution was from 2 nm to 8 nm. In this simulation, the incident energy was 30 keV, the thickness of resist was 100 nm. From the Fig.4.1, I can see that when the beam had a very small diameter about 2 nm, the scattering area is very narrow that is about 20 nm in resist. When σ increases from 1 nm to 4 nm, the scattering area becomes larger as the beam probe diameter increases. I can get that beam diameter has a directly effect on the performance of EBL system. Fig.4.5 and Fig.4.6 show the EDDs when beam diameter increases from 2 nm to 8 nm at 10 nm and 30 nm depth of resist, respectively. It indicated that the smaller the beam diameter, the smaller the energy deposition distribution. High resolution of probe beam can effectively to form very fine dot pattern.

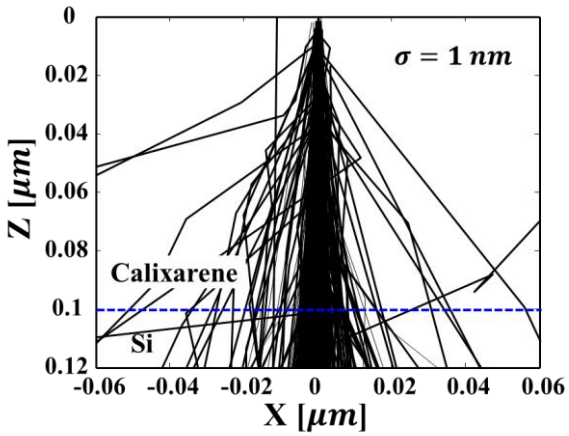

Fig.4.1 Electron scattering trajectories at 30 keV in resist (thickness 100 nm) when electron beam radius σ is 1 nm.

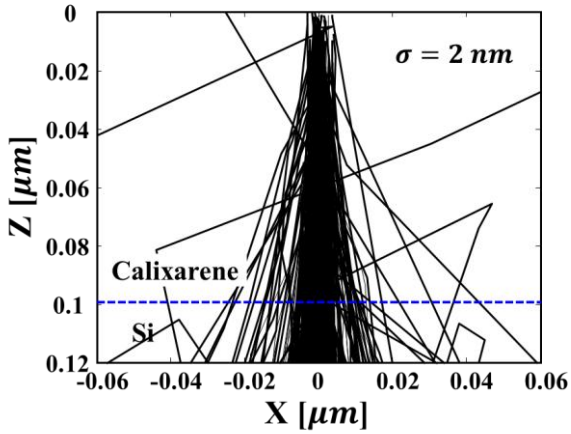

Fig.4.2 Electron scattering trajectories at 30 keV in resist (thickness 100 nm) when electron beam radius σ is 2 nm.

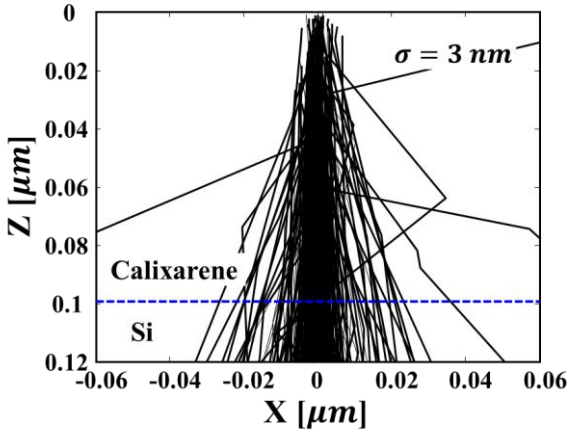

Fig.4.3 Electron scattering trajectories at 30 keV in resist (thickness 100 nm) when electron beam radius σ is 3 nm.

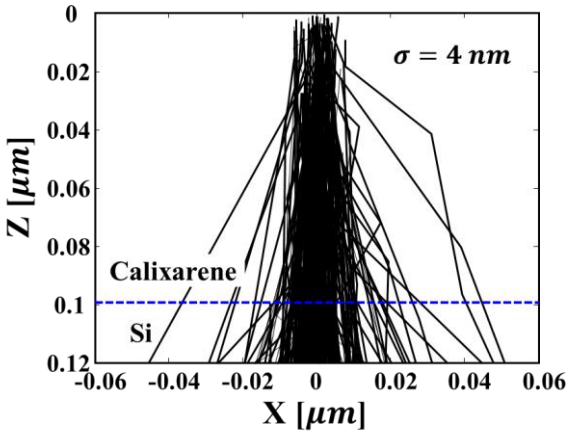

Fig.4.4 Electron scattering trajectories at 30 keV in resist (thickness 100 nm) when electron beam radius σ is 4 nm.

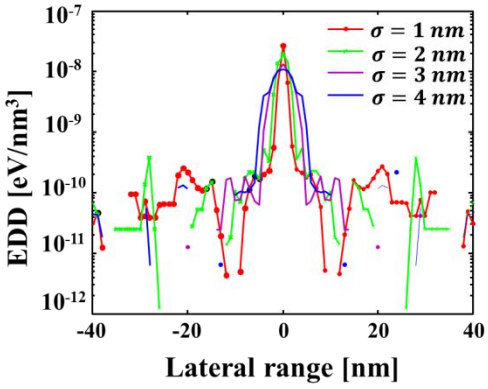

Fig.4.5 EDD with various beam diameters in 10-nm-thick resist layer.

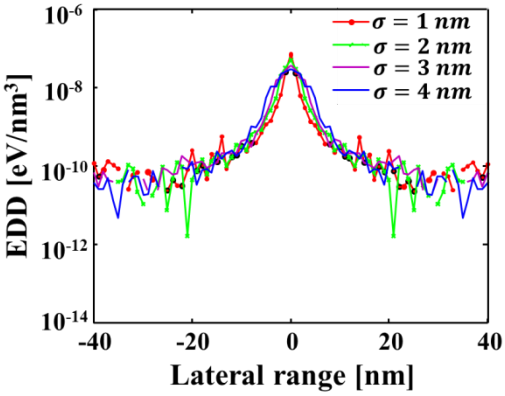

Fig.4.6 EDD with various beam diameters in 30-nm-thick resist layer.

4.2 The Dependence of Incident Electron Energy

The initial energies of the incident electrons were 100 keV, 30 keV and 10 keV. The scattering trajectories of electrons with different incident beam energies in the Calixarene-Si target are simulated as shown in Figs.4.7-4.9. In the simulation, the thickness of the resist layer of 100 nm, Gaussian beam diameter of 2 nm and the number of incident electrons of 500 were used.

Using an incident energy of 100 keV, electrons penetrated very deeply into the Si substrate about 35 μm. In the resist layer, the electron scattering in lateral-direction was only 20 nm. With an incident energy of 30 keV, penetration depth was about 4 μm and lateral range was about 1.5 μm in Si (Fig.4.8 (a)). In the resist layer, the electron scattering was expanded only about 40 nm in lateral direction (Fig.4.8 (b)). Using 10 keV incident electrons, it can just diffuse only 0.6 μm into the sample (Fig.4.9 (a)), however, the lateral range was expanded to be about 60 nm in the resist layer which is larger than that of 30 keV and 100 keV (Fig.4.9 (b)). It indicated that as the energy decreases, the electrons scattering range is expanded in the thin resist layer.

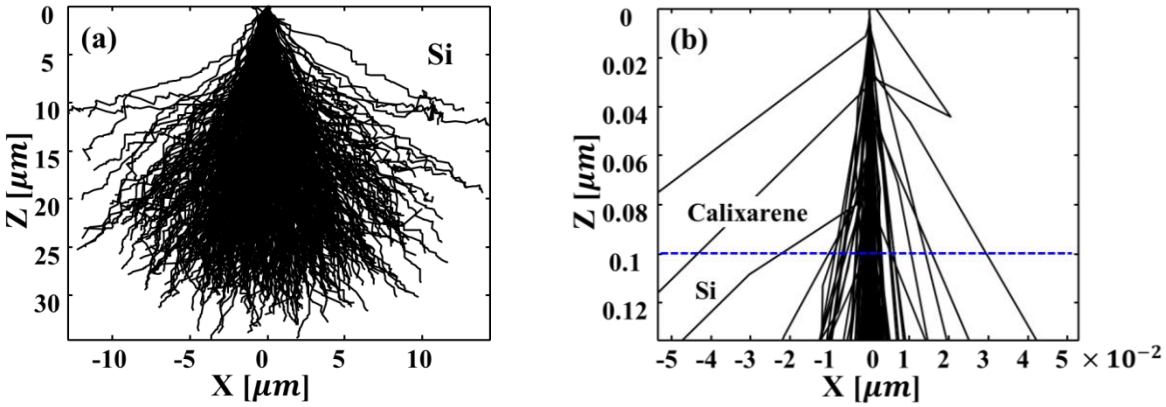

Fig.4.7 Electron scattering trajectories with incident energy of 100 keV in Monte Carlo simulation, (a) electron scattering trajectories in overall; (b) enlarged trajectories in the 100 nm-thick- resist layer.

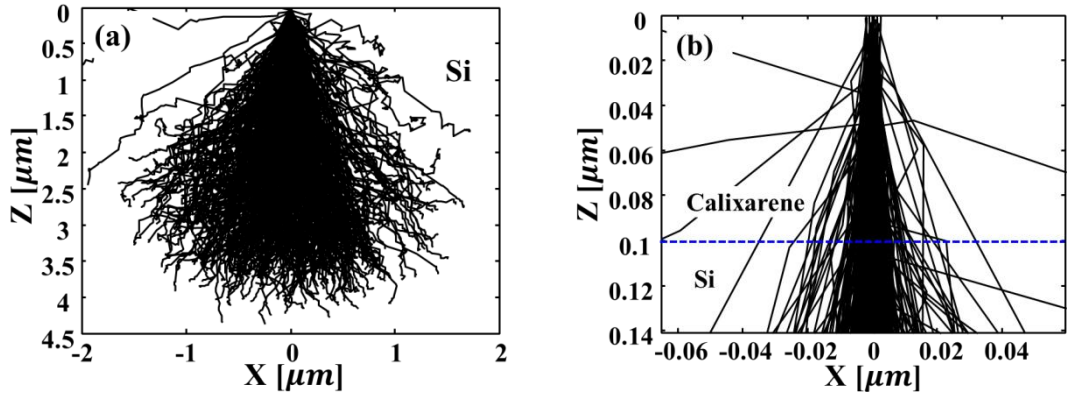

Fig.4.8 Electron scattering trajectories with incident energy of 30 keV in Monte Carlo simulation, (a) electron scattering trajectories in overall; (b) enlarged trajectories in the 100 nm-thick- resist layer.

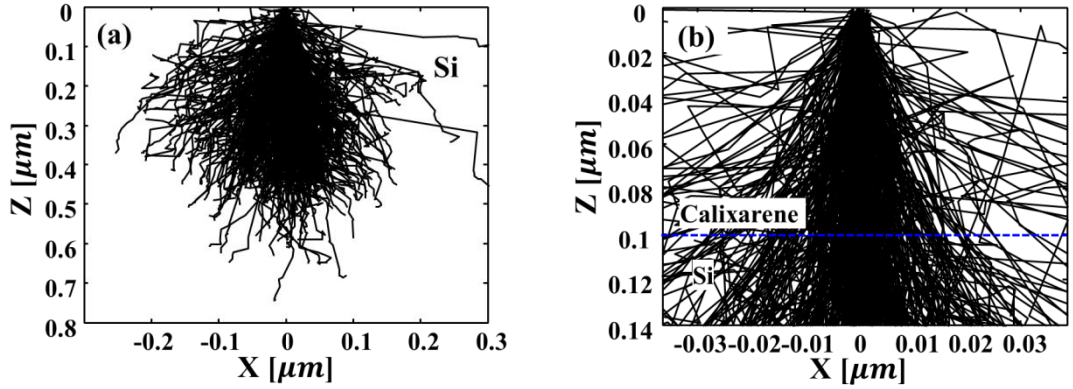

Fig.4.9 Electron scattering trajectories with incident energy of 10 keV in Monte Carlo simulation, (a) electron scattering trajectories in overall; (b) enlarged trajectories in the 100 nm-thick- resist layer.

4.3 Dependence of Thickness of Resist

The spatial distribution of the deposited energy density in the resist is the most important value that determines energy deposited latent image during the EB-drawing [7]. Here, in order to evaluate the dependence of resist thickness on the formation of very fine dot arrays using

30 keV EB drawing, the EDD at various depths in thin Calixarene resist layer was calculated. Figure 4.10 (a) shows the radial distribution of the electron energy deposition at various depths of 10 nm, 50 nm and 100 nm in the resist layer in the case of negative resist Calixarene on Si substrate. The EDD is obtained by 30000 electrons with a Gaussian beam with a probe diameter of 2 nm. It can be seen clearly that the shallower the depth from the surface of the resist layer, the narrower and the sharper the distribution. From the EDDs, we can obtain the relationship between thickness of resist and the dot diameter in various critical energies, as shown in Fig.4.10 (b). The figure shows that the resist thickness of less than 30 nm can form the sub-10 nm dot pattern, especially, the thickness of less than 20 nm can provide to form very fine dot with a size of 5 nm. Therefore, the resist film should be used as thin as possible for very fine dot array formation.

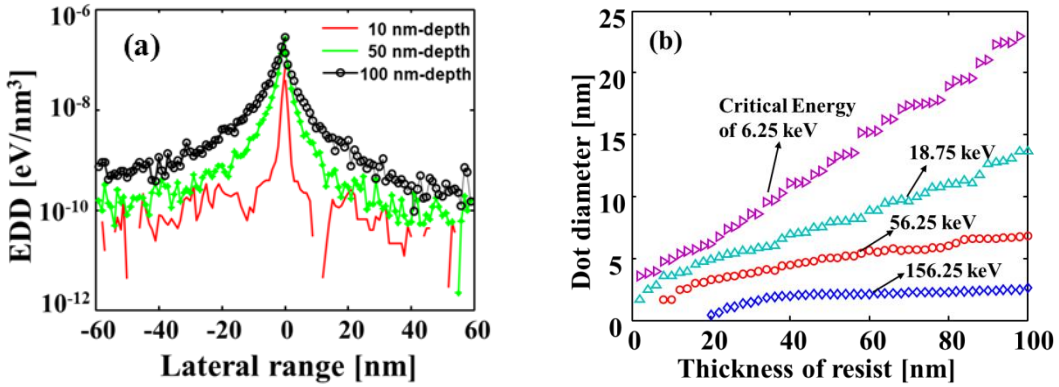

Fig.4.10 (a) EDDs at various depths of resist and (b) relationship between the resist thickness and dot diameter at various critical energies.

In experiment, Hosaka et al. [8] have formed the very fine pitched dot arrays by 30 keV EB lithography at a dosage of 16 mC/cm^2 with various resist thickness of 16.1 nm, 14.7 nm, 13.1 nm and 11.8 nm. Figures 4.11 (a) and (b) show many defects such as the dots combined with neighbor dots. And the number of defect decreases as the thickness becomes thinner. At the resist thickness of 13.1 nm, the 20 nm×20 nm pitched dot array have completely been drawn as shown in Fig.4.11 (c). Furthermore, using further thin resist film, the dot arrays appear unclearly (Fig.4.11 (d)) because the SEM contrast becomes poor due to thin thickness. Therefore, the resist thickness of about 13 nm is very suitable for forming very fine pitch dot arrays with 20 nm×20 nm. Using thin resist is very useful for forming nano-scale dot arrays.

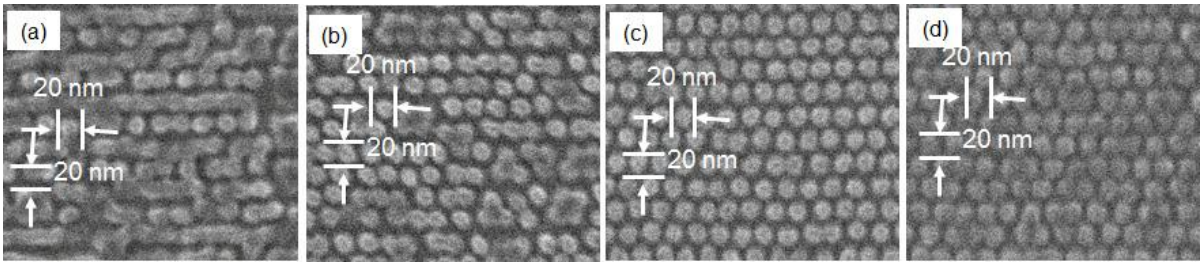

Fig.4.11 SEM images of 20 nm×20 nm fine pitch dot arrays formed by 30 keV EB lithography at a dosage of 16 mC/cm^2, (a) with a resist thickness of 16.1 nm, (b) 14.7 nm, (c) 13.1 nm and (d) 11.8 nm.[8]

From Fig.4.11, the variations of average calixarene dot size for various thickness and exposure dosages were obtained as shown in Fig.4.12. The figure shows that the dot diameter decreases with not only thickness but also exposure dosage. Although the diameter variation with exposure dosage means that proximity effect occurs, the thin resist layer contributes to suppress the proximity effect as same as using high electron energy. The tendency agrees with the simulation results. From Fig.4.12, it can see that in order to draw the 20 nm×20 nm pitch dot arrays pattern, we need a dot size of 15 nm at least. It is necessary to choose an exposure dosage of <16 mC/cm^2 and a resist thickness of <13 nm for the fine pitch arrays formation. While, in the simulation results (Fig.4.10 (b)), it is possible to form the 15 nm dot arrays using a resist thickness of 10 nm and a critical energy >56.25 keV. In the consideration, the critical energy in simulation is opposite to the exposure dosage in experiment.

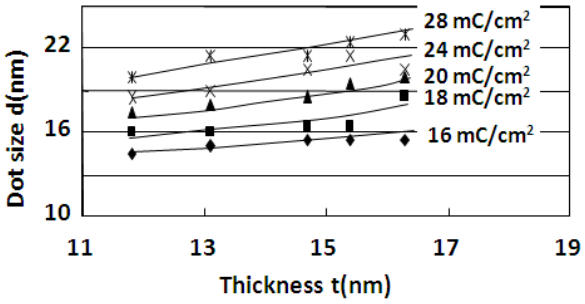

Fig.4.12 Variations of average calixarene dot size with thicknesses for various exposure dosages [8].

4.4 Dependence of Critical Energy

The goal of the simulation of the processes in EBL is the prediction of the resist profile of the developed exposed microstructure. Resist development is defined as the resist molecule is solved and linked at critical energy density in positive and negative resists, respectively. For

the evaluation of the dot size in resist profile, calculations in a wide range of critical energy densities were executed. Figure 4.13 (a)-(d) show the developed resist profiles at various critical energy densities of $156.25\ \text{keV}/cm^3 - 6.25\ \text{keV}/cm^3$ in Calixarene resist. It is clear that the dot diameter decreases with critical energy increasing. Small pattern formation is possible by selecting the higher critical energy density, which corresponds to selecting low exposure dosage in experiment.

According to the negative resist development mechanism, the exposed resist portions are remained on the substrate. Although the height of the resist pattern is not complete and short, when the critical energy density is $156.25\ \text{keV}/cm^3$, the dot height of 3 nm can be formed as shown in Fig.4.13 (a). It is clear that the smaller dot size is obtained by selecting the higher critical energy density, but the height of the resist pattern decreases as the critical energy density increases. In practice, the sharp and small dots cannot have been observed in the experiments yet. This is caused by the collapse of dots in development process or some mistakes in the simulation for development.

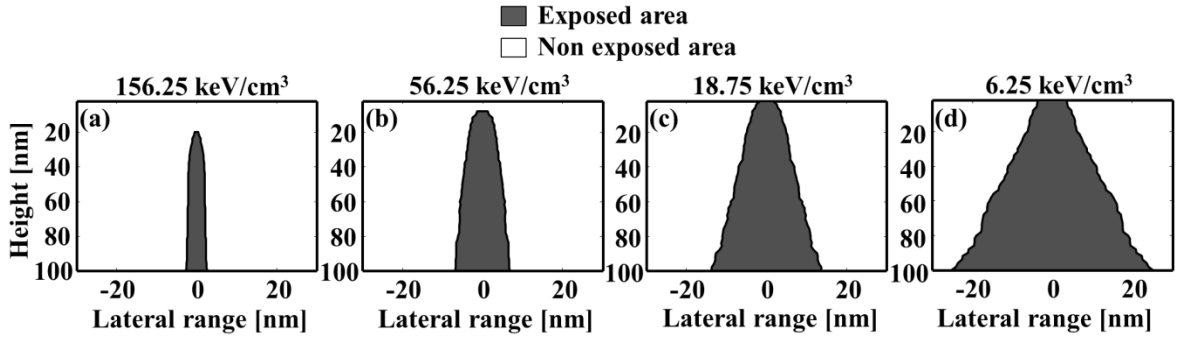

Fig.4.13 Simulated resist profiles at various critical energies, (a) critical energy of $156.25\ \text{keV}/cm^3$, (b) $56.25\ \text{keV}/cm^3$, (c) $18.75\ \text{keV}/cm^3$, and (d) $6.25\ \text{keV}/cm^3$.

In experiment, Hosaka et al. [9] have formed the 20 nm×20 nm pitch dot arrays patterns drawing with a thickness of 11.8-14.7 nm at some exposure dosages (Fig. 4.14). The exposure dosages were 14 mC/cm^2, 16 mC/cm^2 and 18 mC/cm^2. At a dosage of 14 mC/cm^2, there are some vacancies as defects. It may be caused for the reason that the dosage is not enough to make the resist molecular link. When using commercial developer, the insufficient exposed resist part was solved so that the completed dots could not be formed. The result agrees with the result of critical energy with 156.25 keV/cm^3. At a dosage of 16 mC/cm^2, it is enough to makes complete dots. In a case of a dosage of 18 mC/cm^2, the dot was combining together

with neighbor dots. The simulation and experimental results demonstrated that 30 keV EB drawing can form 20 nm×20 nm very fine pitch dot arrays pattern using optimal resist thickness and exposure dosage. The next, let's consider compare the experiment and simulation.

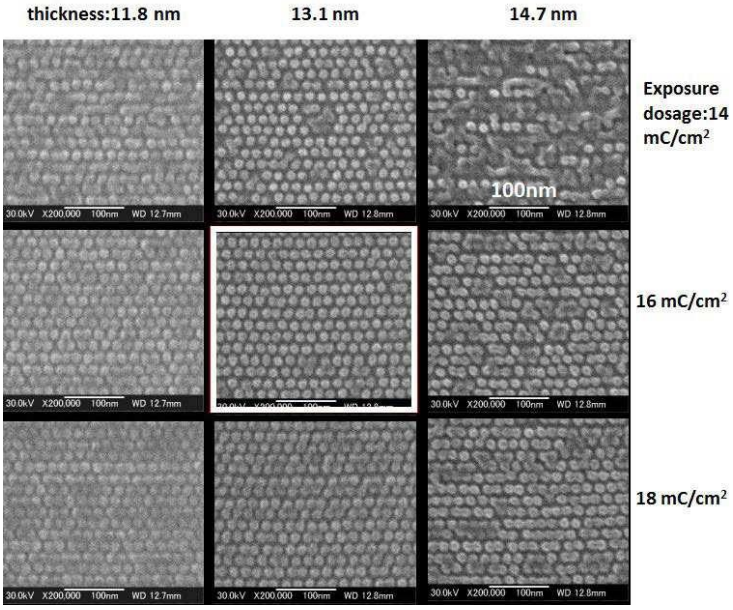

Fig. 4.14 SEM images of 20 nm ×20 nm pitched calixarene resist dot arrays formed by 30 keV EB drawing on Si substrate (1.6 Tb/in.^{2}) in 9 shots/dot drawing [9].

4.5 Comparison of Calixarene Resist with PMMA Resist

PMMA ($(C_5H_8O_2)_n$) [10] as a positive resist is a compound of carbon (C), hydrogen (H), and oxygen (O) with a molecular weight of 100.067 having average density 1.19 g/cm^3, however, Calixarene ($C_{36}H_{36}O_4Cl_4$) is roughly a ring-shaped molecule with a diameter of less than 1nm and thus is mono-dispersed with a molecular weight of 674 and having density 1.09 g/cm^3. [11-12] I use the random number method to select the scattering atom, and get that the total cross section in PMMA is larger than that in Calixarene (see Table. 4.1). Consequently, the scattering lateral range of about 40 nm in PMMA resist is larger than that about 20 nm in Calixarene resist by using 30 keV in incident energy. Furthermore, because the basic component of Calixarene is a phenol derivative from the strong chemical coupling of the benzene ring, which seems Calixarene has high durability and stability. Therefore, Calixarene negative resist is very suitable to form nanometer-sized dot.

	Calixarene	PMMA
Molecular weight	674	100.067
Density	1.09 g/cm^3	1.19 g/cm^3
Total cross section	3.35×10^{-2} nm	7.53×10^{-2} nm
Scattering range of lateral component	20 nm	40 nm

Table 4.1 Comparison of parameters of calixarene and PMMA resists.

4.6 Conclusions

Using the home-made Monte Carlo simulation program with Gaussian electron beam and calixarene negative resist, I calculated electron interactions in sample at various conditions. In the simulation, I calculated energy deposition distributions due to 30 keV incident electrons in the sample of 100-nm-thick calixarene resist layer on silicon substrate. The evaluation of resist dot size and its profile was studied as a function of incident energy, Gaussian beam diameter and resist thickness, theoretically. As a result, the followings conclusions can be obtained:

(1) It is necessary to use the thinner resist film for the formation of very fine dots using Gaussian beam with fine probe diameter of 2 nm.

(2) It is potential to form sub-10 nm-diameter dot when the resist thickness is less than 20 nm using negative resist calixarene by the simulation.

(3) High critical energy density is suitable to form very fine dot pattern.

(4) Increasing of incident electron energy can also make it easy to form smaller pattern by comparison of EDDs with 10 keV and 30 keV electron energy.

(5) Calixarene negative resist has an ability to make smaller pattern comparing with PMMA positive resist.

(6) The EB drawing with thin calixarene resist promises to open the way toward ultrahigh-density recording at >1 Tb/in.^{2} and the quantum devices.

References

1. J. Fujita, Y. Ohnishi, Y. Ochiai, and S. Matsui: Appl. Phys. Lett., **68** 1297 (1996).
2. S. Hosaka, Y. Tanaka, and M. Shieai: Jpn. J. Appl. Phys., **49**, 046503 (2010).
3. M. Kotera, S. Yamaguchi, S. Umegaki, and H. Suga: Jpn. J. Appl. Phys., **33** 7144 (1994).
4. H. G. Duan, D. Winston, J. K. W. Yang, and B. M. Cord: J. Vac. Sci. Technol., **28** C6C58 (2010).
5. T. H. P. Chang: J. Vac. Sci. Technol., **12** 1271-1275 (1975).
6. S. Hosaka, H. Sano, and K. Itoh, Microelectron. Eng., **83** 792 (2006).
7. K. Vutova, G. Mladenov, and I. Raptis: J. Mater. Process. Technol., **184**, 305-311 (2007).
8. Z. B. Mohamad, M. Shirai, H. Sone, S. Hosaka and M. Kodera, Nanotechnology **19** 025301 (2008).
9. S. Hosaka, Y. Tanaka, M. Shirai, Z. Mohamad and Y. Yin, Jpn. J. Appl. Phys. **49**, 046503 (2010).
10. M. S. Singh, R. K. B. Singh, R. Khatri., and B. I. Sharma: Adv. Sci. Lett., **3** 57-61 (2010).
11. M. Ishida, J. I. Fujita, and T. Ogura: Jpn. J. Appl. Phys., **42**, 3913-3916 (2003).
12. P. Jedrasik, M. Hanson, and B. Nilsson: Microelectron. Eng., **53** 497-500 (2000).

Chapter 5 New Simulation Model for Developing Resist Pattern Based on EDD in EBL

EBL is a powerful method for forming very fine patterns that are used for the fabrication of ultrahigh packed magnetic storages, quantum devices, etc.[1–4] The resolution in EBL can be improved by increasing the contrast (the γ-value for development) of the resist.[5–7] There are many efforts for development with EBL. 4.5 nm-half-pitch line patterns were formed using a hydrogen silsesquioxane (HSQ) resist with 2.4% tetramethylammonium hydroxide (TMAH) as the developer.[8] Further, 7 nm half-pitch nested "L" structures were fabricated using a combination of 1 wt% NaOH and 4 wt% NaCl as the developer.[9] Many experimental efforts have been made toward advancing the resolution of the patterns by increasing the contrast of the resist with various developers.[10–12] However, a simulation method for calculating the resist profile based on various solubility rates is also a key tool for improving the resolution of EBL.[13–15]

Recently, Vutova et.al have proposed a nonlinear model[16] with a delay effect that depends on the energy intensity distribution for development in EBL. The EID is defined by a combination of two Gaussian distributions that indicate the average exposure dosage per area.[4,17,18] However, the EID does not contain information about the energy deposition along the depth direction. The fundamental disadvantage of the nonlinear model is that the variation of the energy deposition along the depth direction is not considered in the results. If a Monte Carlo simulation is used, the three-dimensional (3D) EDD can reflect the energy deposition distribution in both lateral and depth directions. Without the 3D EDD, it is difficult to determine the change of the solubility rate (development rate) with EDD variation in depth-direction. Therefore, simulation for development should be considered with 3D EDD.

This paper proposes a simulation model that calculates the resist profile based on the 3D EDD for the development of EB-drawn patterns.[19] The 3D EDD can reflect 3D energy deposition of the resist in both the depth and the radial directions. The model

is composed of three parts. The first part is the EDD calculation program by electron scattering. The second is the unification of the exposure dose *D* dependence (in experiment) and EDD dependence (in calculation) of solubility rate. I roughly calculate various solubility rates for 3D EDD. The third is the development program for simulation of resist profile with solubility rate. I demonstrate that the new simulation model agrees with experimental results. The simulation is useful for studying high-resolution patterning via EB drawing. I describe a detail of the model, simulation and evaluation as follows.

5.1 Modeling of Resist Development in EB Drawing

5.1.1 EDD calculation

EDD is an important parameter in consideration of EBL. Here, I used Monte Carlo simulation based on a single scattering model[20] which used Rutherford elastic scattering and Bethe energy losses.[21] For calculating the EDD in the resist, I used a cylindrical coordination system. I divided the resist layer along the z-axis into several thin sub-layers. The EDD was calculated by a Monte Carlo simulation of electron scattering in a radius-depth coordination system, meaning that the resist layer was divided into concentric rings. The simulation was executed to calculate the total deposited energy, $E(r,z)$, in each unit ring as a function of EDD. The ring volume ΔV is given by following equation:

$$\Delta V = (\pi(r+\Delta r)^2 - \pi r^2)\cdot \Delta z \tag{5.1}$$

where Δz is the thickness of the sub-layer and Δr is the radial increment.

From the volume, the EDD is given by the following equation, where N_0 is the total number of incident electrons:

$$EDD(r,z) = E(r,z)/(\Delta V \cdot N_0) \tag{5.2}$$

In order to unify the calculation with experiments, I used the same exposure conditions in both the calculation and the experiments. In the simulation, the dot arrays pattern with 15 nm in pitch was used. Each dot consisted of 4 shots with a pitch

of 2 nm, as shown in Fig.5.1. The resist was HSQ, whose chemical composition and density are $H_8Si_8O_{12}$ and 1.3 g/cm^3, respectively. A 12 nm thick Si substrate was coated with the resist. The Gaussian beam was used with a radius of 0.4 nm which corresponded to our EB drawing condition.[22,23] The incident beam energy was 30 keV, and the number of incident electrons was 10^6. The increments Δr and Δz were 2 nm each. In particular, I calculated the profiles of an EB-drawn 3-dot pattern with a pitch of 15 nm as shown in the top panel of Fig.5.1. The EDDs at various depths in the HSQ resist layer were calculated via a cylindrical coordinate system, as shown in Fig.5.2.

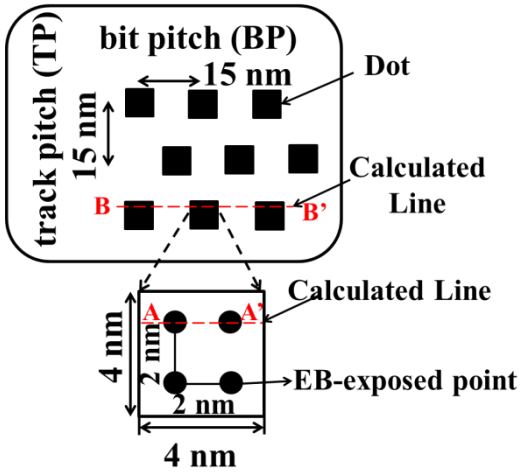

Fig.5.1 The schematic diagram of dot arrays arrangement.

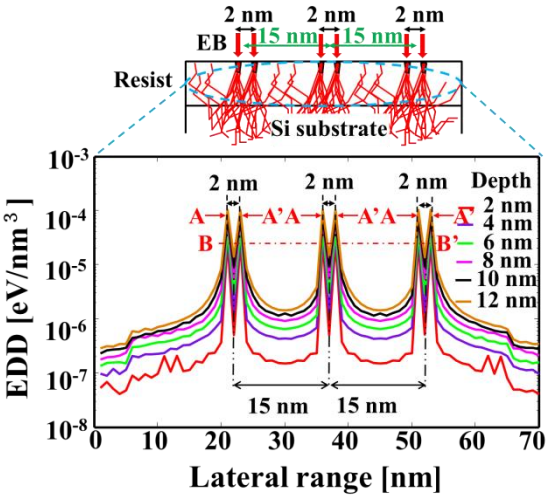

Fig.5.2 Energy deposition distributions of different depths of resist.

5.1.2 Resist development model

Resist development[24] was simulated using the local solubility rate *v*, which was determined by the exposure dosage *D* of experimental data. Assuming that *v* is proportional to *D*, the following can be obtained:

$$v_r(\mathrm{r},\mathrm{z}) = -cos\theta \cdot K \cdot D(r,z)^{-1} \tag{5.3}$$

$$v_z(r,z) = -sin\theta \cdot K \cdot D(r,z)^{-1} \tag{5.4}$$

where θ is the angle between the direction of solubility and the direction of the resist surface. When the resist surface is flat, the development advances in a perpendicular direction to the sample surface; therefore, the solubility direction is opposite to the horizontal direction (see Fig.5.3). $D(r,z)$ is the energy deposition as a function of the radial distance r and vertical distance z. v_r and v_z are the solubility rates in the radial and vertical directions, respectively. K is the coefficient of exposure dosage region. The difference of resist thickness between exposed areas and unexposed areas with development time can provide the experimental development rate for a particular exposure dosage. However, the experimental rate is in only two dimensions, without the depth component. The EDD of the Monte Carlo simulation can reflect the energy deposition along the depth-direction. Therefore, in order to make the EDD instead of *D*, the relationship between the expose dose *D* and EDD should be considered at first. Their dimensions are $[\frac{C}{m^2}]$ and $[\frac{J}{m^3}]$, respectively. I can represent the EDD with an equation of $\left[\frac{\mathrm{J}}{m^3}\right] = \left[\frac{\mathrm{C}}{m^2}\right] \cdot \frac{\bar{V}}{m} = D \cdot \left[\frac{\bar{V}}{m}\right]$, where $\left[\frac{\bar{V}}{m}\right]$ is the electric field. When the resist is thin, $\frac{\bar{V}}{m}$ is constant. Define the $\frac{\bar{V}}{m}$ as k, we can find the EDD is only roughly proportional to *D*.

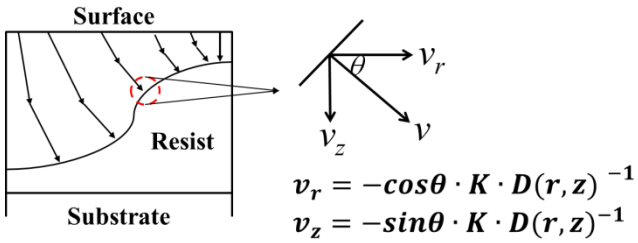

Fig.5.3 The schematic diagram of resist development from the surface of resist with the solubility rate *v*.

In this study, a combination of 2.3 wt% TMAH and 4 wt% NaCl as the developer with a γ value of 8.1 was used to determine the development rates as a function of

exposure dosage. Figure 5.4 (a) shows the experimental residual resist thickness *R* for various exposure dosages. From Fig.5.4 (a), the average development rate, graphically shown in Fig.5.4 (b), was estimated using $(R_0 - R)/t$, where R_0 is the original resist thickness and the *t* is the development time.

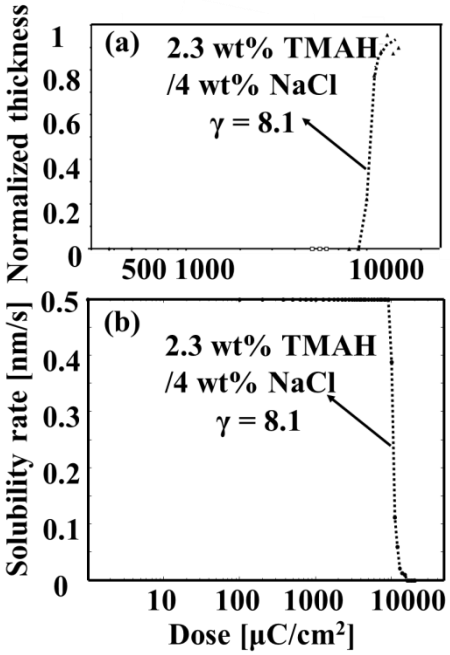

Fig.5.4 (a) Remained HSQ resist thickness for exposure dosage using TMAH 2.3 wt%/NaCl 4 wt% developer and (b) the solubility rate for the exposure dose at TMAH 2.3 wt%/NaCl 4 wt% developer, which derived from Fig.5.4 (a).

I determined the solubility rates of v_1, v_2, ..., v_n for the exposure dosages of D_1, D_2, ..., D_n, respectively from Fig.5.4 (b). Using the above-explained relationship between EDD and *D*, the equation can be given by $EDD = k \cdot D$; here, k is a proportional coefficient. Therefore, *v* can be determined by the following calculation flow:

[1] If $EDD_{(i,j)} \leq kD_1$, the resist will be dissolved at a rate of v_1;

[2] If $kD_1 < EDD_{(i,j)} \leq kD_2$, the resist will be dissolved at a rate of v_2;

…

[n-1] If $kD_{n-1} < EDD_{(i,j)} \leq kD_n$, the resist will be dissolved at a rate of v_n; and

[n] If $EDD_{(i,j)} > kD_n$, the resist will not be dissolved and the rate is 0.

where the *i* and *j* correspond to r and z, respectively.

By comparing the EDD with exposure dosage D, I calculated the resist profile with a time step of Δt using a sequential method, as shown in Fig.5.5. The positions (r_{i+1}, z_{i+1}) of the resist profile can be given as follows:

$$r_{i+1} = r_i + v_r \cdot \Delta t \tag{5.5}$$

$$z_{i+1} = z_i + v_z \cdot \Delta t \tag{5.6}$$

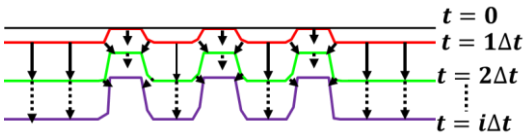

Fig.5.5 The schematic diagram of calculation for development process (arrow is vector of solubility rate).

The flow chart of resist development calculation can be concluded as Fig.5.6.

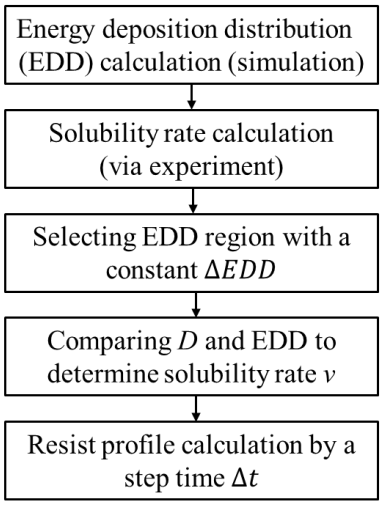

Fig.5.6 The flow chart of resist profile calculation program.

5.2 Verification of the New Model

In order to obtain a fine resist profile, it is important to select an optimal EDD region that corresponds to a region of exposure dosage in the experiments. In our experiment, a suitable exposure dosage was determined by evaluating a scanning electron microscopy (SEM) image of the resist pattern[25-27]. In the simulation, an ideal EDD region was determined by evaluating the calculated resist profile as described above. The properties of the residual resist after exposure dosage were used for the calculation when using the combination of 2.3 wt% TMAH and 4 wt% NaCl as the developer. In our experiments, we measured the solubility rates of the HSQ resist by

measuring the residual resist thickness in an exposure dosage region of $9000 - 15000\ \mu C/cm^2$, as shown in Fig.5.4 (b). As described above, the relationship between *D* and the EDD is given as follows:

$$EDD = k \cdot D \tag{5.7}$$

Using an exposure dosage region between D_A and D_B with a changeable solubility (development) rate, I can consider an energy deposition region between EDD_A and EDD_B. EDD_A and EDD_B are given by follow equations,

$$\mathrm{EDD_A} = \mathrm{k} \cdot \mathrm{D_A} \tag{5.8}$$

$$EDD_B = k \cdot D_B \tag{5.9}$$

Taking the logarithm of both sides of the equations, the following are obtained:

$$logEDD_A = logk + logD_A \tag{5.10}$$

$$logEDD_B = logk + logD_B \tag{5.11}$$

This allows definition of ΔD and ΔEDD, which are given as $\log D_A - logD_B$ and $\log EDD_A - logEDD_B$, respectively. From the above equations, we can easily derive the following relationship between the EDD and *D*:

$$\Delta D = log\frac{D_A}{D_B} = log\frac{EDD_A}{EDD_B} = \Delta EDD \tag{5.12}$$

D_A and D_B are $15000\ \mu C/cm^2$ and $9000\ \mu C/cm^2$, respectively, as shown in Fig.5.4 (b). I can easily obtain the ΔEDD by

$$log\frac{EDD_A}{EDD_B} = log\frac{5}{3} \tag{5.13}$$

Much more information about the EDD regions can be obtained using ΔEDD. In the experiments, the optimal exposure dosage was evaluated by evaluating SEM images of the EB-drawn resist patterns at different exposure dosages. In the simulation, the optimal energy deposition was calculated by varying the EDD region with a constant ΔEDD and evaluating the simulated resist profile via the same method as in the experiments. I selected some EDD regions with ΔEDD from 10^{-5} to 10^{-8} (eV/nm^3), as shown in Fig.5.7. By the simulation, I obtained the resist profiles shown in Fig.5.8. Evaluation of the EDD range of 10^{-5} to 10^{-6} (eV/nm^3) in region A in Fig.5.7 revealed that any dots pattern is not formed. That means the most of resist molecular may be dissolved by the developer. On the other hand, in the EDD range of

10^{-8} to 10^{-9} (eV/nm^3) in region B, non-isolated connected dots pattern is formed because there are so much remained resist. Therefore, I can consider that the optimal EDD is existed in the range of 10^{-6} to 10^{-8} (eV/nm^3). I chose three exposure regions (regions 1, 2, and 3) from much EDD regions in the range of 10^{-6} to 10^{-8} (eV/nm^3) as shown in Fig.5.7.

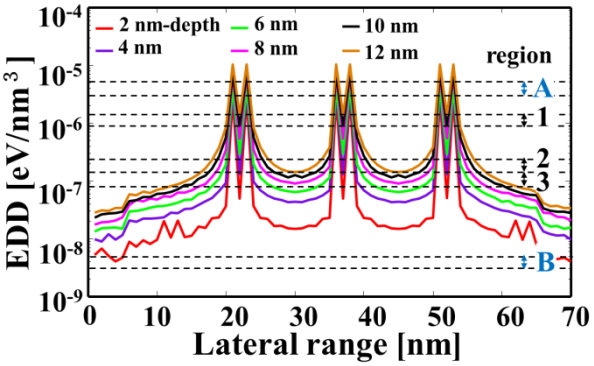

Fig.5.7 Energy deposition distribution at various depths in resist layer when using 30 keV electron beam and 5 regions for the simulation.

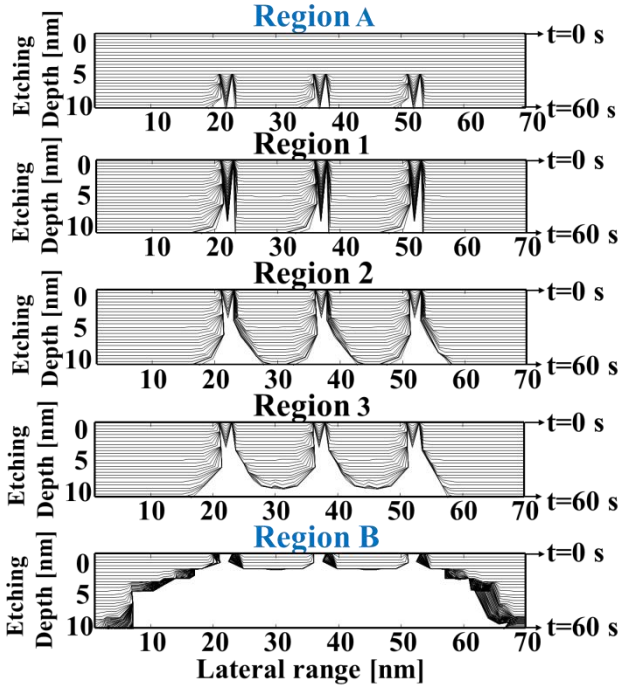

Fig. 5.8 Simulated resist profiles using TMAH 2.3 wt%/NaCl 4 wt% developer when selecting 5 EDD regions (as shown in Fig.5.7).

In region 1 in Fig.5.7, too sharp dots are formed only in the center of the exposure regions. These dots are very small; their diameters are about 3 nm. The heights are 12 nm. In practice, the dots may be collapsed. After development, the dots are not remained. Using region 3, formation of isolated resist dots was not favored,

because of the insufficient development of the space between the dots.[28-30] In region 2, small resist dots are formed completely to solve the resist in the space. However, the dots have neck part. The part causes to collapse upper part as the sharp and slender needle during development. Consequently, the dot height becomes lower. It may be about 7 nm. The shape of the cross section is like a triangle. As described above, I determined the suitable EDD regions by evaluating calculated resist profiles.

Before the calculations, I decided a step time Δt for the development simulation by evaluation of the simulated resist profiles of each EDD region using various time steps, Δt of 5, 2, 1, and 0.1 s. I found that the resist profile did not vary significantly with the time steps. Consequently, I selected the step time of 1 s and a development time of 60 s in the simulation.

In experiment, Komori et al.[23] have demonstrated that dot arrays with an average dot diameter of 9.8 nm can be obtained using a combination of 2.3 wt% TMAH/4 wt% NaCl as the developer at an exposure dosage of 58 mC/cm^2, as shown in Fig.5.9. The diameter agrees with the predicted one of 7 nm from the simulation closely. Furthermore, under changing exposure dosage from 34 to 70 mC/cm^2 in the experiments, the sharpest dot arrays were formed at the exposure dosage of 58 mC/cm^2. As the dosage decreased to 34 mC/cm^2, it is difficult to form the complete and clear dots, it agrees with the region A in Fig.5.8. As the dosage increased to 66 mC/cm^2, the dots become less sharp. Comparison of the SEM image (Fig.5.8 (d)) at this dosage with the resist profile in region 3 in Fig.5.8 reveals that the resist profile contains small and unclear dot arrays. When the dosage increased to 70 mC/cm^2, the bottom of resist connects to each other as a line because of the proximity

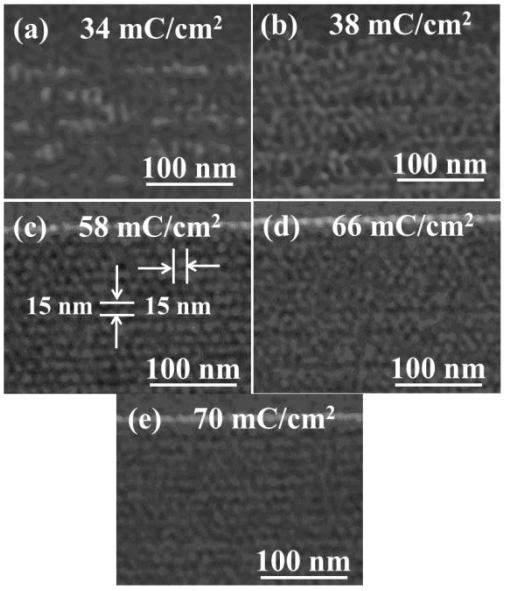

Fig.5.9. SEM images of 15 × 15 pitched HSQ resist dot arrays formed by 30-keV EB drawing developed in 2.3 wt% TMAH and 4 wt% NaCl developer at various exposure dosages.

effect, it is the same as resist profile shown in region B of Fig.5.8. This tendency agrees with the simulation results. This demonstrates that the simulation model of resist development is useful in the calculation of the resist profile formed by EB drawing.

5.3 Conclusions

I proposed a new simulation model based on EDD for the development of EB-drawn patterns. By unifying the exposure dose (via experiment) and the EDD distributions (via calculations), we roughly calculated solubility rates for three-dimensional EDDs, and established the proposed model. The development simulation was achieved by sequential calculation by solubility rates based on EDD, which was calculated by Monte Carlo simulation. By determining a suitable EDD region as exposure dose to make well patterning, we obtained a sharpened nanodot pattern of the resist. This simulation result agrees well with the experimental results obtained by using a combination of 2.3 wt% TMAH and 4 wt% NaCl developer. Using the model, I demonstrated that it is very useful to simulate fine patterns formation. I obtained conclusion as follows:

1) In new model, the simulation can be performed by assuming that the EDD is proportional to exposure dosage *D*.
2) The suitable region of EDD can be obtained for sharp dot pattern by controlling the region.
3) It is estimated that the dot size of sub-7 nm with pitch size 15 nm can be formed by using the developer with combination of TMAH 2.3 wt% and NaCl 4 wt% when the range of EDD are between 93.75-156.25 kV/cm^3 (region 2). This estimated size almost agrees with that in the experiments.
4) The new model can provide us a good prediction of resist dot profile based on the solubility rate in the future work.

References

1. J. Lohau, A. Moser, C. T. Rettner, M. E. Best, and B. D. Terris: IEEE Trans. Magn., **37** (2001) 1652.
2. Y. Kamata, A. Kikitsu, N. Kihara, S. Morita, K. Kimura, and H. Izumi: IEEE Trans. Magn., **47** (2011) 51.
3. H. Wang, M. T. Rahman, H. Zhao, Y. Isowaki, Y. Kamata, A. Kikitsu, and J. Wang: J. Appl. Phys., **109** (2011) 07B754.
4. S. Hosaka, H. Sano, and M. Shirai: Microelectron. Eng., **84** (2007) 802.
5. K. Vutova and E. Koleva: Microelectron. Eng., **86** (2009) 714.
6. J. K. W. Yang and K. Berggren: J. Vac. Sci. Technol. B, **25** (2007) 2025.
7. X. Yang, S. Xiao, W. Wu, Y. Xu, K. Mountfield, R. Rottmayer, K. Lee, D. Kuo, and D. Weller: J. Vac. Sci. Technol. B, **25** (2007) 2202.
8. S. Ma, C. Con, and M. Yavuz: Nanoscale. Res. Lett., **6** (2011) 446.
9. J. Yang, B. Cord, and H. Duan: J. Vac. Sci. Technol. B, **27** (2009) 2622.
10. T. Okada, J. Fujimori, M. Aida, M. Fujimura, T. Yoshizawa, M. Katsumura, and T. Iida: J. Vac. Sci. Technol. B, **29** (2011) 021604.
11. S. Strobel, K. J. Harry, H. Duan, J. K. W. Yang, V. R. Manfrinato, and K. K. Berggren: Nanotechnology, **22** (2011) 375301.
12. K. J. Harry, S. Strobel, J. K. W. Yang, H. G. Duan, and K. K. Berggren: J. Vac. Sci. Technol. B, **29(6)** (2011) 06FJ01-1.
13. E. Koleva and G. Mladenov: Vacuum, **77** (2005) 361.
14. X. G. Tang, X. Y. Yang, F. H. Gao, and Y. K. Guo: Microelectron. Eng., **84** (2007) 1100.
15. Q. Dai, S.-Y. Lee, S. H. Lee, B.-G. Kim, and H.-K. Cho: Microelectron. Eng., **88** (2011) 902.
16. K. Vutova and E. Koleva: Microelectron. Eng., **87** (2010) 1108.
17. K. Vutova, E. Koleva, and G. Mladenov: J. Vac. Sci. Technol. B, **27** (2009) 52.
18. I. Raptis, N. Glezos, E. Valamontes, E. Zervas, and P. Argitis: Vacuum, **62** (2001) 263.

19. H. Zhang, T. Tamura, Y. Yin, and S. Hosaka: Key Eng. Mater., **497** (2012) 127.
20. K. Murata, T. Mastukawa, and R. Shimizu: Jpn. J. Appl. Phys., **10(6)** (1971) 678.
21. M. S. Singh, R. K. B. Singh, R. Khatri, and B. I. Sharma, Adv. Sci. Lett., **3** (2010) 57.
22. Z. B. Mohamad, M. Shirai, and H. Sone: Nanotechnology, **19** (2008) 025301.
23. T. Komori, H. Zhang, T. Akahane, Z. Mohamad, Y. Yin and S. Hosaka: Jpn. J. Appl. Phys., **51** (2012) 06FB02.
24. Y. S. Jun, B. Lee, and G. A. Waychunas: Environ. Sci. Technol., **44(21)** (2010) 8182-9.
25. S. Hosaka, Y. Tanaka, M. Shirai, Z. Mohamad and Y. Yin: Jpn. J. Appl. Phys., **49** (2010) 046503.
26. S. Hosaka, H. Sano, K. Itoh, and H. Sone: Microelectronic Eng., **83** (2006) 792.
27. S. Hosaka, Z. B. Mohamad, M. Shirai and H. Sano: Appl. Phys. Express, **1** (2008) 027003.
28. W. Zhang, A. Potts, D. M. Bagnall, and B. R. Davidson: Thin Solid Films, **515** (2007) 3714.
29. R. Wuest: Photonic Nanostruct., **7** (2009) 212.
30. S. Hosaka, H. Sano, M. Shirai, and H. Sone, Appl. Phys. Lett., **89** (2006) 223131.

Chapter 6 Estimation of HSQ Resist Profile by Enhancing Contrast for High Resolution Lithography

In EBL, patterning resolution can be improved by (1) reducing the lateral spread of electron scattering in resist in EB drawing and (2) increasing the resist contrast in developing process [1]. The electron beam lateral spread can be limited by the substrate and incident electron energy. For instance, the small lateral spread can be achieved by patterning on thin membrane substrates and using high electron beam acceleration voltages. The fabrication of densely packed sub-20 nm pitch HSQ structures has been achieved with extremely thin resist film (10 nm) and high electron-beam acceleration voltages (100 kV) [2].

Increasing the developer contrast as another effective method to improve the patterning resolution has been putforward these years [3-6]. For instance, improving the contrast by adding concentrated alkalis [7-9] and elevating development temperatures has been demonstrated when using HSQ resist [10-11]. In particular, J. Kim *et al.* have reported that the addition of NaCl into TMAH developer could significantly increase the contrast of the HSQ resist [12]. However, the simulation method to analyze the effects of different contrast developers on pattern resolution has not been studied yet. In order to investigate the effect of contrast, we should understand that which factors effect on the contrast at first.

In the previous chapter, I have demonstrated that the performance of development is related to the solubility rate, EDD and exposure dosage [13]. In order to observe the effect of EDD interval on the contrast of resist and the final resolution of pattern, in this study, I try to calculate developed HSQ dot profiles with various intervals of EDD (ΔEDD) using my home-made development model. I try to estimate that high contrast developer for fabrication of nano-sized dot arrays has small EDD interval ΔEDD. The ΔEDD is defined by the EDD interval between the initial EDD for minimum solubility rate and the full EDD for maximum solubility rate. It might be an important parameter to increase the resolution of nano-patterning. Furthermore, I

can study allowance of fabrication of nano patterning with high contrast developer. I demonstrate that high contrast resist has the small exposure allowance. It is very useful for fabricating nano-sized dot arrays. These considerations are provided to investigate the development and contrast of HSQ in TMAH developers with varying concentrations of salts. In addition, I study the possibility to form high resolution resist pattern in a regard to high contrast developing comparing with simulation and experimental results. In this chapter, I study to make it clear that how contrast is needed for high resolution nano-patterning and its allowance using the simulation.

6.1 High Contrast of Developers for Nano-sized Patterning

6.1.1 Definition of contrast parameter in developing

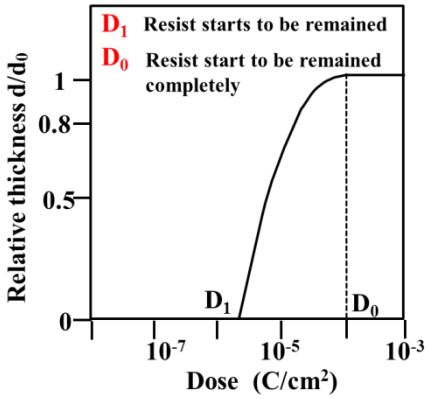

Fig.6.1 Dependence of the relative thickness d/d_0 vs. the exposure dose using a positive-tone resist in development.

One can evaluate the contrast of the resist pattern using the experimental change of the resist thickness *d(D)* at development time *t*. The *d(D)* started to decrease from a given initial thickness d_0 . This change occurs by the dissolution removal of the exposed or the un-exposed area in positive or negative resist, respectively. Variable value is the dose *D* at chosen energy E of the electrons as well as at constant development conditions (developer type, time and temperature of development) [14]. An example of such curve *d(D)* is given in Fig.6.1.

The contrast parameter γ is defined by the dose interval between the initial exposure dose D_1 (at which the resist starts to dissolve in developer) and the full dose D_0 (at which the resist starts completely to dissolve). The value of the contrast

parameter γ for the positive-tone resists can be calculated by Eq.(6.1):

$$\gamma = [log(D_1/D_0)]^{-1} \quad (6.1)$$

when the removed normalized thickness (namely the ratio $\Delta d/d_0$, where Δd is the removed resist thickness) is equal to 1. In the case of negative-tone resists, γ is given by:

$$\gamma = [log(D_0/D_1)]^{-1} \quad (6.2)$$

where D_1 and D_0 are the initial exposure dose at a start of the dissolubleness and the full dose at an end of complete dissolubleness, respectively. [14]

6.1.2 Relationship between exposure dose D and EDD

Based on the definition of the contrast parameter γ, I propose a relationship between exposure dose interval and contrast. The contrast parameter γ defines exposure dose interval between D_0 and D_1. However, in order to use the simulation method to analyze the effect of the γ value on the contrast of resist pattern, I should consider the relationship between the expose dose *D* and *EDD* at first. In our previous work, we established new development simulation model based on the EDD. Furthermore, we defined the relationship between EDD (via simulation) and *D* (via experiment) as described in chapter 5:

$$EDD = k \cdot D \quad (6.3)$$

Using an exposure dose region between D_0 and D_1, the energy depositions of EDD_0 and EDD_1 are given as follows:

$$EDD_0 = k \cdot D_0 \quad (6.4)$$

$$EDD_1 = k \cdot D_1 \quad (6.5)$$

Taking the logarithm of both sides of the equations, the following are obtained:

$$\log EDD_0 = logk + logD_0 \quad (6.6)$$

$$\log EDD_1 = logk + logD_1 \quad (6.7)$$

EDD_0 is the energy that the resist begins to be unsolved, and EDD_1 is the energy that the resist stops solving in a case of a negative resist.

When I define the ΔD and ΔEDD as $logD_0 - logD_1$ and $logEDD_0 - logE\mathrm{DD}_1$, respectively, I can easily derive the following relationship between the

ΔEDD and ΔD:

$$\Delta D = log(\frac{D_0}{D_1}) \tag{6.8}$$

$$\Delta EDD = log\left(\frac{D_0}{D_1}\right) \tag{6.9}$$

$$\Delta EDD = \Delta D \tag{6.10}$$

$$\gamma = \frac{1}{log\left(\frac{D_0}{D_1}\right)} = \frac{1}{\Delta D} = \frac{1}{\Delta EDD} \tag{6.11}$$

Therefore, I can use ΔEDD instead of ΔD in simulation. Furthermore, the ΔEDD is a parameter related with the γ.

6.1.3 The ΔEDD used in the simulation

In this section, I change the data of ΔEDD and calculate the resist profiles with each ΔEDD. I put forward a hypothesis of that the developer with small ΔEDD has the high contrast and high resolution. Here, I changed the ΔEDD from the small one of log(1.1) to the large one of log(9), and calculated the resist profiles. I made various properties of solubility rate vs. exposure dose based on the property with a developer 2.3 wt% TMAH and 4 wt% NaCl as shown in Fig. 6.2. I obtained the property of EP-DATA using the developer that the property corresponds to $\Delta D = \Delta EDD$ of log(1.7). Here, the maximum solubility rate of 0.5 nm/s was fixed and the energy deposition interval ΔEDD was only changed in the following calculations.

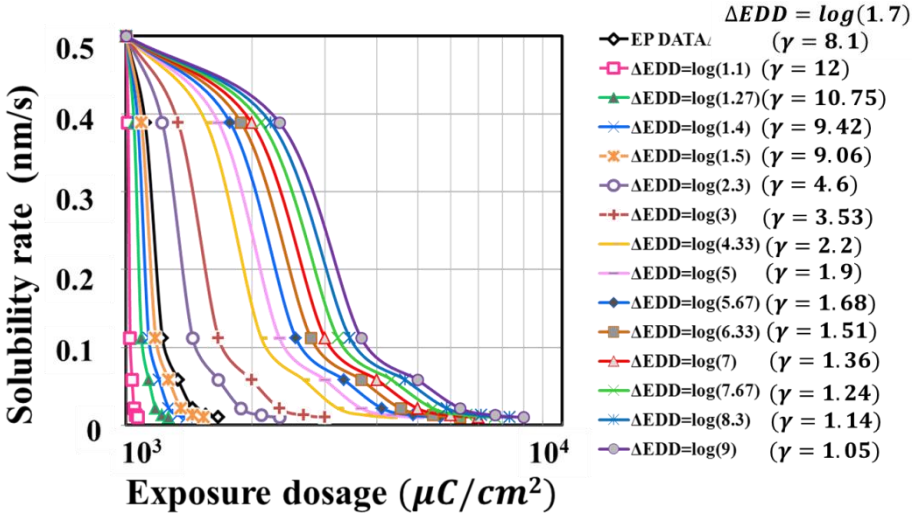

Fig.6.2 Plots of solubility rates vs. exposure dose with various ΔEDD.

6.1.4 Calculating optimal resist profile based on EDD

In order to calculate the optimal resist profile with various ΔEDD, I used EDD and solubility rates as described in chapter 5. For the simulation, I used pattern data of dot arrays with a 15 nm pitch. Each dot consisted of 4 shots as shown in Fig.6.3. The resist was HSQ, whose chemical composition and density are $H_8Si_8O_{12}$ and 1.3 g/cm^3, respectively. A 12 nm-thick resist was coated on Si substrate. The 30 keV-Gaussian electron beam had a radius of 0.4 nm. The number of incident electrons was 10^6. The increments of Δr and Δz were 2 nm each for calculation of EDD. In particular, I calculated the profiles of an EB-drawn 3-dot pattern with a pitch of 15 nm as shown in Fig.6.3. The EDDs at various depths in the HSQ resist layer were calculated with a cylindrical coordinate system as shown in Fig.6.4.

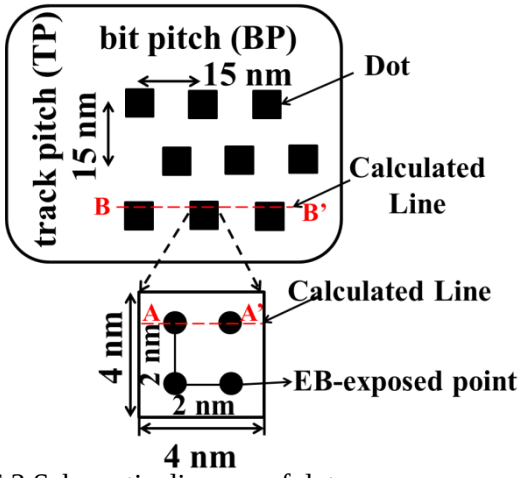

Fig.6.3 Schematic diagram of dot array arrangement.

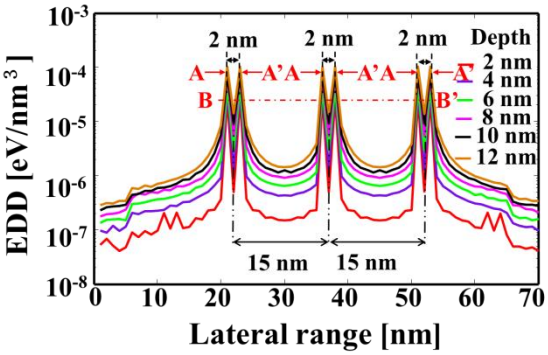

Fig.6.4 Calculation of EDDs for different depths of HSQ resist at 30 keV-incident beam.

Then, I studied the optimal resist profile in the range of 10^{-4}-10^{-8} (eV/nm^3) with ΔEDD using the same method as previous chapter. Here, I used the ΔEDD of $\log(1.7)$ as an example to explain the calculation process.

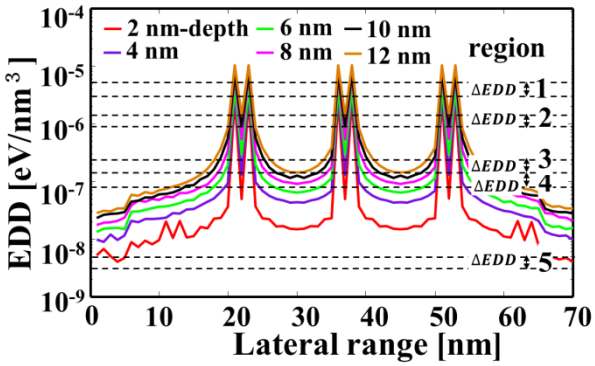

Fig.6.5 Many exposure regions using EDD for the development simulation.

With constant ΔEDD, much more information about the EDD regions can be obtained. We can find the optimal EDD region in the EDD range from 10^{-4} to 10^{-8} (eV/nm^3) (see Fig.6.5) by evaluation of the simulated resist profile. It is the same as manner in experiment that the optimal exposure dosage was determined by evaluating SEM images of the EB-drawn resist patterns at various exposure dosages. The optimal resist profiles using various developers with each ΔEDD have been calculated as shown in Fig.6.6.

From Fig.6.6, the profiles have a sharp and slim part in the upper of the dot. These slim parts will be collapsed in the practical development. Consequently, as the EDD increases, the height of dot becomes small. Sufficient height of dot is obtained in a range of less than $\log(3)$ in ΔEDD. When the ΔEDD over $\log(4.3)$, the height is insufficient. In order to obtain high resolution pattern by EB drawing, ΔEDD of $\log(1.1)$ to $\log(3)$ should be used.

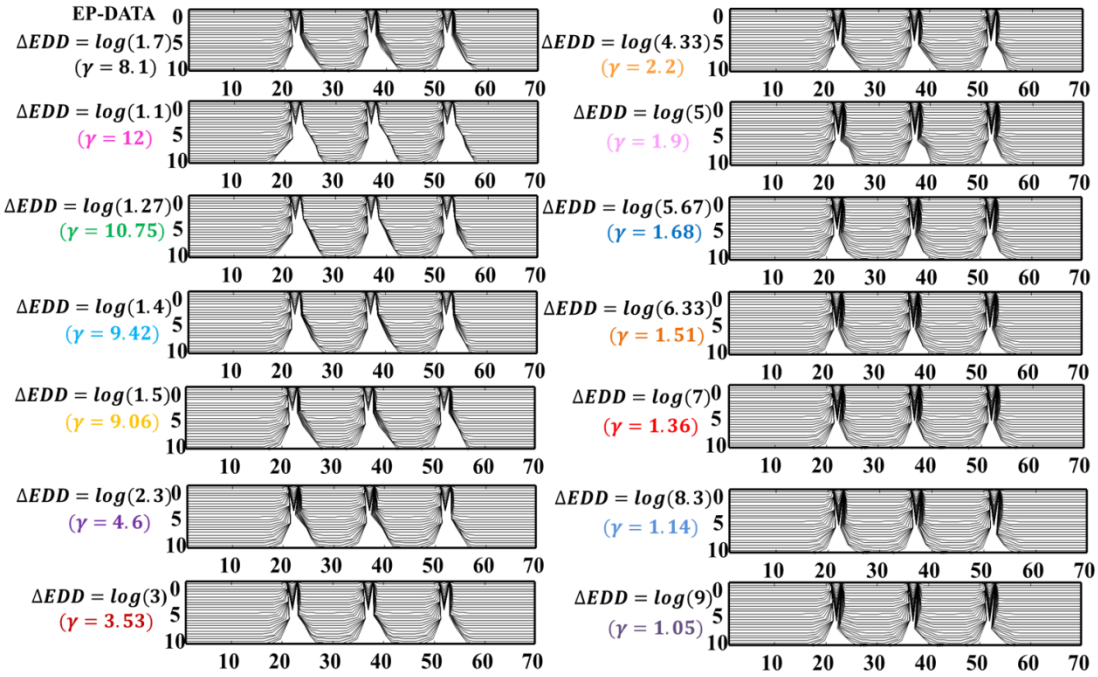

Fig.6.6 Resist profiles with various ΔEDD in each optimal exposure region.

Based on the analysis of above, we should develop the developer with small ΔEDD to enhance the resolution of the pattern. It means that EB drawing and its development needs a new developer with the small dose interval for high resolution patterning. The results show that ΔEDD is an indicator of the contrast of developer. On the other hand, I pointed out that the contrast parameter γ corresponds to $(\Delta EDD)^{-1}$ as described in section 6.1.1 and 6.1.2. I can suggest that the γ value in developer should be used with over $\left(log(3)\right)^{-1}$.

6.2 Relationship between Contrast and Allowance of Optimal Exposure for High contrast patterning

In this section, I investigate the relationship between high contrast and allowance for high resolution patterning. I put forward a hypothesis that the high contrast resist has a good allowance in fabrication of high resolution patterning at first. Then, I investigate the exposure regions in which very fine pattern can be formed with high and low contrast developers. And last, I try to prove our hypothesis by evaluating the resist profiles for various contrast developers. The method used here is the same as experiments that a series of exposure dosages were used to form dot arrays, and to

evaluate a SEM image of the resist pattern to judge whether the region of exposure dosage is suitable to form very fine pattern or not.

6.2.1 Method of calculating the exposure allowance

Allowance is an important characteristic for EB drawing and developing. [16] The allowance is defined as a region of exposure dosage with high resolution patterning. The allowance is dependent on resist, EB drawing and developer. Here, I measured the allowance with constant ΔEDD for calculating the resist profile by changing EDD regions. I use the mark to check whether the EDD region can form very fine dot arrays or not as shown in Fig.6.7. The mark of × shows that it cannot form dot arrays, the mark of Δ means that it can form dot arrays, but the dot arrays are not satisfied and mark of OK means that it can form fine dot arrays. From the Fig.6.7, I show that the exposure dosage between region 5 and 6 can form fine dot arrays. And I define the width of regions of 5 and 6 as the allowance. In the next section, we want to calculate the exposure allowance of high contrast resist and low contrast resist, respectively.

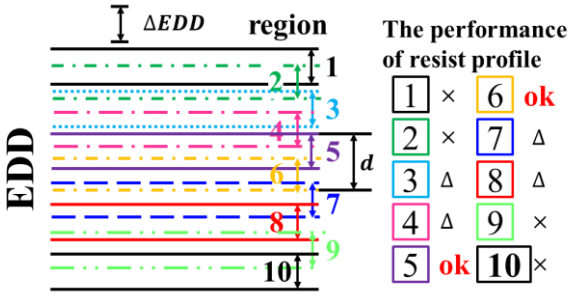

Fig.6.7 Schematic diagram of selecting EDD regions for high resolution patterning by evaluating whether resist dot profile is satisfied or not.

6.2.2 Calculating the allowance for high contrast resist patterning

Here, I use the high contrast with ΔEDD as log(1.1) and low contrast with ΔEDD as log(4.33) as example to investigate the exposure allowance.

6.2.2.1 The allowance of high contrast resist

ΔEDD of $\log(1.1)$ means that $\log(EDD_1/EDD_0) = \log(1.1)$. Using the same method as previous work, I could check a lot of EDD regions in the range of 10^{-5}-10^{-9} eV/nm^3 with a constant ΔEDD. The allowance of exposure dosage was selected by evaluating the profiles to judge whether the EDD region can form very fine pattern or not. For example, in the region 1 and region 2, it is difficult to form the complete and clear dots. The region n also has not ability to form very fine dot arrays. When the EDD moved into the range of 10^{-6}-10^{-7} eV/nm^3, it can form very fine dot arrays. Here, in order to show the results more clearly, many EDD regions for formation of nano dot arrays are calculated in the detail range of 10^{-6}-10^{-7} eV/nm^3.

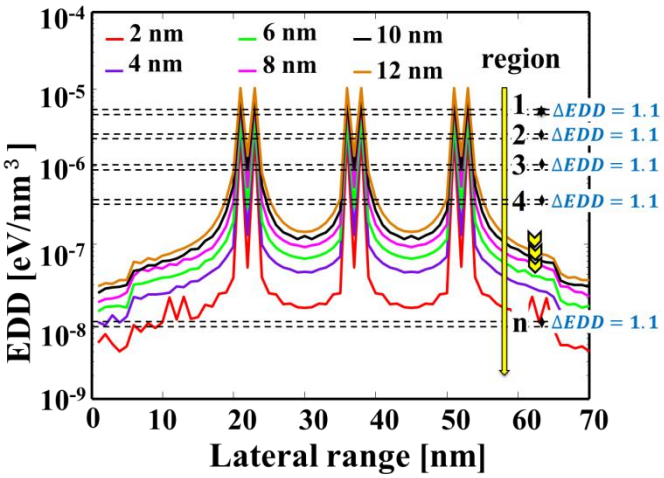

Fig.6.8 Selecting EDD regions with a constant ΔEDD from top to down in EDD range.

Based on the calculation, in the EDD range of $2.74 \times 10^{-7} - 1.58 \times 10^{-7}\ eV/cm^3$ with ΔEDD of $\log(1.1)$, complete and isolate pattern can formed as shown in Fig.6.9 and Fig. 6.10. And the allowance of width A_h of the range can be calculated as

$$A_h = 1.16 \times 10^{-7}(eV/nm^3) \tag{6.12}$$

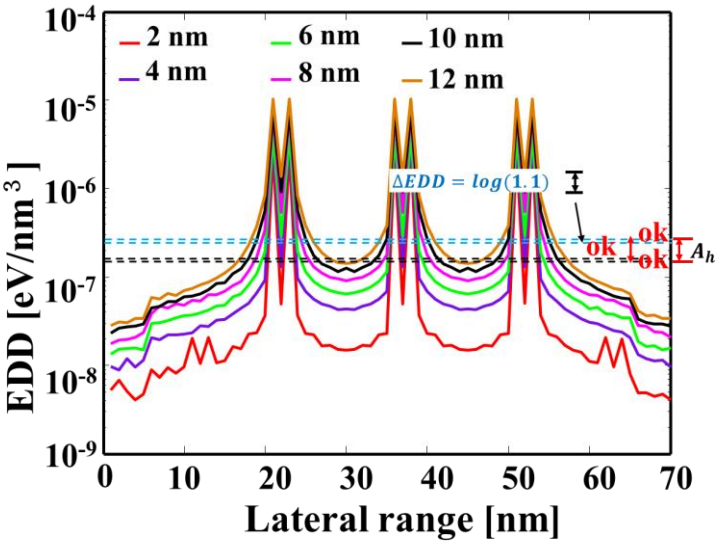

Fig.6.9 EDD ranges of forming very fine dot arrays with ΔEDD as log(1.1).

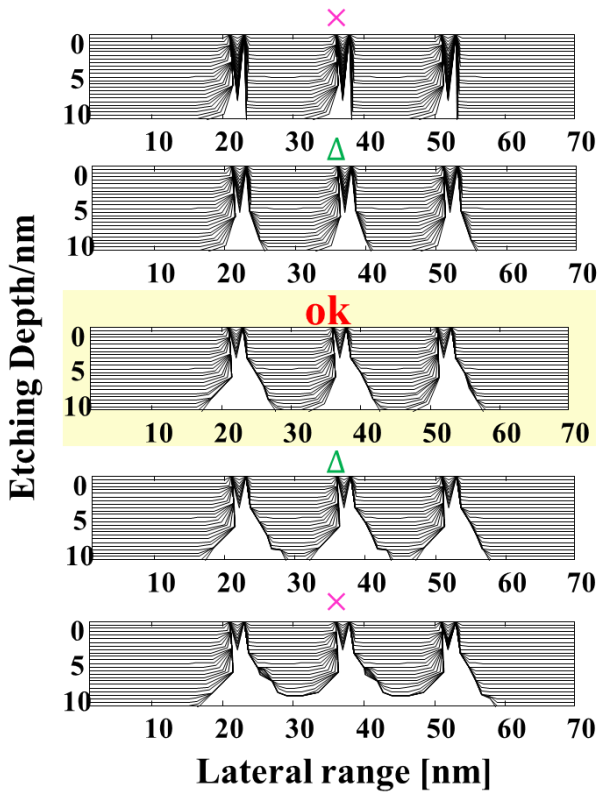

Fig.6.10 Resist profiles according to EDD ranges of with ΔEDD as $log(1.1)$.

6.2.2.2 Allowance in low contrast developing

Using the method as described above, it can obtain fine dot arrays in the EDD range of $6.84 \times 10^{-7} - 1.32 \times 10^{-7}\ eV/cm^3$ can be formed with constant ΔEDD

of $\log(4.33)$ as shown in Fig.6.11-6.12.

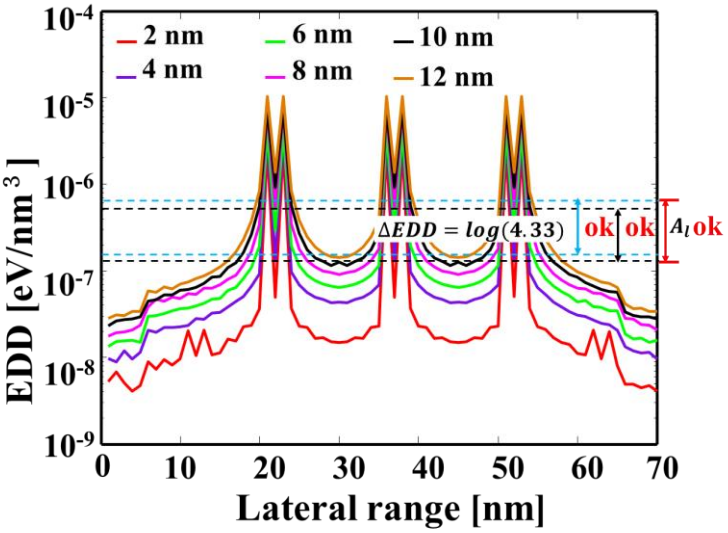

Fig.6.11 EDD range of forming very fine dot arrays with ΔEDD as log(4.33).

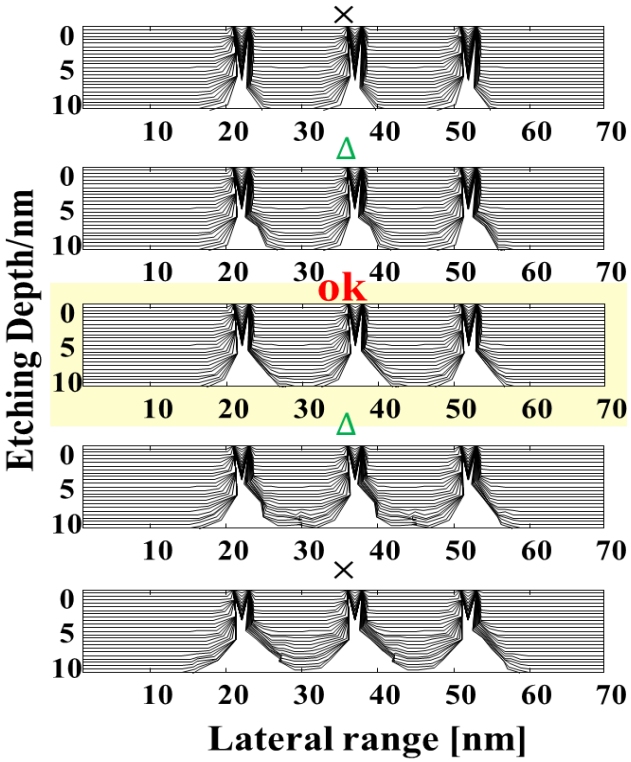

Fig.6.12 Resist profiles according to EDD ranges of with ΔEDD as log(4.33).

The allowance of width A_l of the EDD range can be calculated as

$$A_l = 5.52 \times 10^{-7}(eV/nm^3) \tag{6.13}$$

From calculating the allowance of high contrast and low contrast resist, it is clear that

see the allowance of high contrast developing is smaller than that using low contrast developing. We have to control the exposure dose severely when the high contrast developing in EB drawing is used for forming very fine dot arrays.

6.3 Calculating the Resist Profiles with Various Contrast Developers used in Experiments

6.3.1 Measurement of development contrast curve

Development contrast curves were obtained by measuring remained resist thickness of the HSQ resist for the dose in the following process. First, a 30-nm-thick HSQ resist layer was spin coated on a Si substrate at 4000 rpm for 30 s. The HSQ solution was made of Fox-15 (Dow corning) diluted as a 0.3% solution of methyl isobutyl ketone (MIBK). The 1×5 μm^2 rectangle patterns were fabricated by EB-drawing at an exposure dosage in the range of 0.5 – 15 mC/cm^2 after prebaking the sample for 40 min at 90 ^oC in an oven. The EB-drawn samples were developed in TMAH/NaCl solutions with different concentrations (2.3 wt% TMAH/4 wt% NaCl, 2.3 wt% TMAH/2 wt% NaCl and 2.3 wt% TMAH) for 1 min. Thicknesses of the drawn patterns were measured using atomic force microscopy (AFM; Hitachi WA0200).

6.3.2 Contrast curve

Figure 6.13 shows the contrast curves of the HSQ resist with various developers obtained by measuring the remaining thickness at various doses with each developer. From the contrast curves, development contrast values (γ-value) were obtained. The contrast values were defined as $\gamma = 0.8/\log_{10}(D_{0.8}/D_0)$, where 0.8 means 80% of normalized resist thickness and $D_{0.8}$ and D_0 are the exposure doses at the remaining resist thickness of 80% and 0% of original resist thickness, respectively. The data indicate that the γ-value increases from 1.9 to 8.1 as NaCl concentration increases. As shown in Fig.6.13, it is clear that we obtained the highest γ-value by using 2.3 wt% TMAH/4 wt% NaCl developer.

Then, the solubility rate was obtained by dividing the removed resist thickness in exposed area by the development time of 60 s. Using Fig.6.14, we can calculate the solubility rates with exposure dosages with various developers as shown in Fig.6.15.

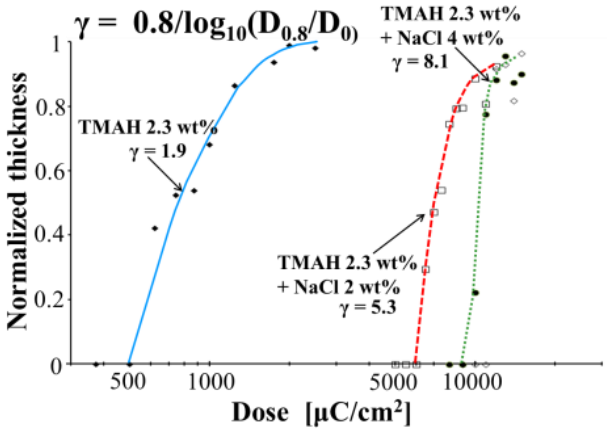

Fig. 6.13 Contrast curves of HSQ resist with various developers.

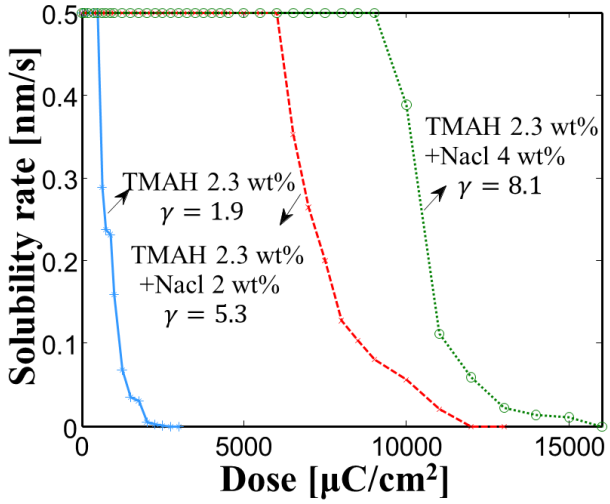

Fig.6.14 Solubility rates of HSQ resist with various developers.

6.3.3 Determining the suitable EDD regions

In order to calculate the resist profile, we have to select the suitable EDD region which corresponds to a region of the exposure dosage in experiments. In order to find optimal EDD region, at first we should determine the width of EDD region for different contrast developers. In previous section, we deduced the relationship function between EDD and *D* as follows:

$$\Delta D = \Delta EDD \tag{6.14}$$

$$\Delta D = log\frac{D_1}{D_0} \tag{6.15}$$

where D_0, D_1 are the initial exposure dose at a start of dissolubleness and the full dose at an end of complete dissolubleness. Using TMAH 2.3 wt%/NaCl 4 wt% developer, we observed that HSQ resist begins to be solved and becomes unsolved at exposure dosage of $9000\ \mu C/cm^2$ and $15000\ \mu C/cm^2$, respectively. The ΔEDD can be calculated as

$$\Delta \mathrm{EDD} = \log \frac{D_1}{D_0} = log\, \frac{5}{3} \tag{6.16}$$

Using the same method, the exposure dosage is in the range of 6000-12000 $\mu C/cm^2$ in TMAH 2.3wt%/NaCl 2wt% developer, the ΔEDD can be calculated as

$$\Delta D = log\, \frac{D_1}{D_0} = log\, \frac{EDD_1}{EDD_0}$$
$$= \log \frac{12000}{6000} = \log 2 \tag{6.17}$$

And in TMAH 2.3wt% developer, the exposure dosage is in the range of 500-2500 $\mu C/cm^2$, the ΔEDD can be calculated as

$$\Delta D = log\, \frac{D_1}{D_0} = log\, \frac{EDD_1}{EDD_0}$$
$$= \log \frac{2500}{500} = \log 5 \tag{6.18}$$

6.3.4 Calculating resist profiles with various developers

In this section, I will use the same method as above to find out the optimal EDD regions to fabricate very fine dot arrays with sufficient height using TMAH 2.3 wt%/NaCl 4 wt%, TMAH 2.3 wt%/NaCl 2 wt% and TMAH 2.3 wt% developers. Figure 6.15 presents the optimal resist profiles of three different contrast developers after development time as 60 s in simulation. From the results, I can consider that it can form isolate dot arrays using the three developers, however, the top of the resist profiles are very narrow and sharp just as 1-2 nm. In practical development, pattern collapse occurs to remove the narrow parts like needles.

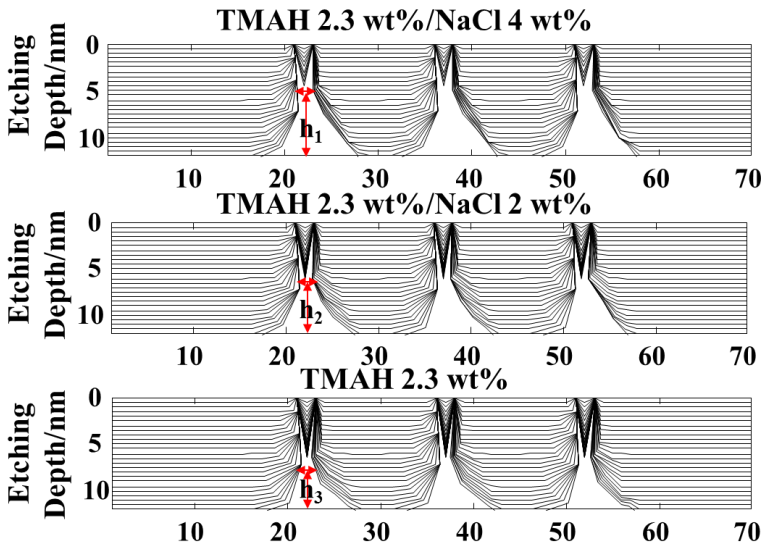

Fig.6.15 Calculated resist profile of HSQ resist using (a) TMAH 2.3 wt%/NaCl 4 wt% developer with γ of 8.1; (b) TMAH 2.3 wt%/NaCl 2 wt% developer with γ of 5.3; (c) TMAH 2.3 wt% developer with γ of 1.9.

From Fig.6.16, I can obtain the height of nano-resist-dot in TMAH 2.3 wt%/NaCl 2 wt% developer with height of 7 nm. In TMAH 2.3 wt%/NaCl 2 wt%, the height is 5.3 nm. The height of resist dot developed using TMAH 2.3 wt% developer is shortest just as 3.5 nm. It is difficult to remain on the substrate, even impossible to transfer the pattern to the underlying layer. It can be estimated that the TMAH 2.3 wt%/NaCl 4 wt% developer is more suitable to form very fine dot arrays than other developers.

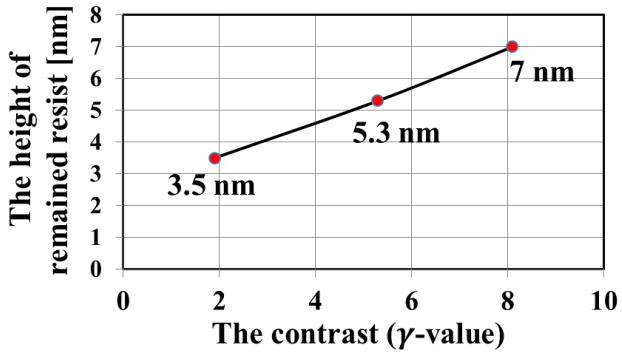

Fig.6.16 Variation of height of resist dots remained using TMAH 2.3 wt%/NaCl 4 wt% developer with contrast (γ=8.1), TMAH 2.3 wt%/NaCl 2 wt% developer with contrast (γ=5.3) and TMAH 2.3 wt% developer with contrast (γ=1.9) in EB drawing experiments.

6.4 Developers for 15×15 nm^2 Pitched Dot Arrays

Komori et al. have reported that the salty developer is suitable for 15×15 nm^2

pitched dot arrays. The process flow of the fabrication of nano dot arrays on a Si substrate has been described as follows. First, the HSQ resists (Fox-15 diluted as a 0.15 - 0.3% solution in MIBK) were spin-coated on a Si substrate at 8000 rpm for 30 s. The thicknesses of the HSQ resists were measured to be 12 – 22 nm. After prebaking the sample, EB-drawing was performed at an exposure dosage in the range of 10 – 70 mC/cm^2 with 4 shot/dot (dot size: 4×4 nm^2) to study the effects of developer concentrations on complete nano dot arrays formation with a pitch of 15×15 nm^2. Then, the samples were developed under the same conditions as that in contrast curves measurement. Finally, we observed the EB drawn patterns using high-resolution SEM.

Fig.6.17 shows the SEM images of 20×20 nm^2 and 15×15 nm^2 pitched HSQ resist dot arrays developed in various developers. Mean dot diameter was 9.7 nm in a pitch size of 15 nm at a dosage of 58 mC/cm^2 by using TMAH 2.3 wt%/NaCl 4 wt% developer. While, using the TMAH 2.3 wt%/NaCl 2 wt% developer, the dot arrays connected with each other. Using the lowest contrast TMAH 2.3 wt% developer, it even cannot form dot arrays with pitch size 20 nm. Comparing the results with simulated results (Fig.6.16 and 6.17), the simulation results agree well with the experimental results. Therefore, the simulation with EB-drawing and developing is very suitable for estimation of nano-dot arrays fabrication.

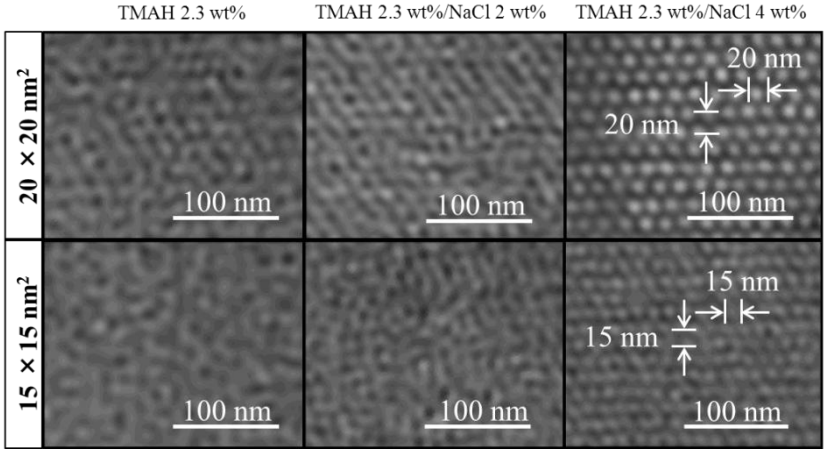

Fig.6.17 SEM images of 15×15 and 20×20 nm pitched HSQ resist dot arrays formed by 30-keV EB drawing in 12-nm-thick resist film on Si substrate and developed in various solutions.

6.5 Conclusions

I estimated the developed HSQ dot profiles with various intervals of EDD for investigating the effect of the dose interval (ΔEDD) on the contrast and patterning resolution. The γ-value was defined as contrast parameter that it can be changed by exposure dose interval (ΔD). Based on the relationship of ΔD (via experiment) and ΔEDD (via simulation), I used ΔEDD to instead of ΔD. Then the γ-value can be defined by ΔEDD. I changed ΔEDD to be larger and to be smaller to investigate the resist profiles and determine the suitable ΔEDD. Furthermore, I calculated the resist profiles based on $\Delta EDDs$ for 2.3 wt% TMAH/4 wt% NaCl, 2.3 wt% TMAH/2 wt% NaCl and 2.3 wt% TMAH developers. Comparing the simulation results with experimental results, the EB drawing and developing model agree well with experimental results. The following conclusions can be drawn on the basis of our simulations and experiments.

1) The high contrast developer in experiment has the small exposure interval ΔD which agrees with the simulation result.
2) ΔEDD is an indicator of contrast of resist patterning and for high resolution patterning.
3) It can form very fine dot arrays when ΔEDD is less than $\log(3)$.
4) The ΔEDD that corresponds to salty developer of 4 wt% TMAH and 2 wt% NaCl is small.
5) It is considered that TMAH 2.3 wt% and NaCl 4 wt% developer is more suitable to form very fine dot arrays.
6) It is necessary to investigate the developer with high contrast of resist pattern for nano-sized dot array formation.

References

1. J. K. W. Yang and K. K. Berggren, J. Vac. Sci. Technol. B **25(6)** 2025 (2007).
2. A. E. Grihorescu, M. C. Krogt, C. W. Hagen, and P. Kruit, Microelectron. Eng. **84** 822 (2007).
3. J. Kim, W. L. Chao, B. Griedel, X. G. Liang, M. Lewis, D. Hilken, and D. Olynick, J. Vac. Sci. Technol. B **27(6)** 2628 (2009).
4. S. W. Nam, M. J. Rooks, J. K. W. Yang, K. K. Berggren, H. M. Kim, M. H. Lee, K. B. Kim, J. H. Sim and D. Y. Yoon, J. Vac. Sci. Technol. B **27(6)** 2635 (2009).
5. J. K. W. Yang, B. Cord, H. G. Duan, K. K.Berggren, J. Klingfus, S. W. Nam, K. B. Kim,and M. J. Rooks, J. Vac. Sci. Technol. B **27(6)** 2622 (2009).
6. H. G. Duan, D. Winston, J. K. W. Yang, B. M. Cord, V. R. Manfrinato and K. K. Berggren, J. Vac. Sci. Technol. B **28(6)** (2010)
7. W. Henschel, Y. M. Georgiev, and H. Kurz, J. Vac. Sci. Technol. B **21** 2018 (2003).
8. D. L. Olynick, J. A. Liddle, A. V. Tivanski, M. K. Gilles, T. Tyliszczak, F. Salmassi, K. Liang, and S. R. Leone, J. Vac. Sci. Technol. B **24** 3048 (2006).
9. M. Haffner, A. Haug, A. Heeren, M. Fleischer, H. Peisert, T. Chasse and D. P. Kern, J. Vac. Sci. Technol. B **25** 2045 (2007).
10. X. Yang, S. Xiao, W. Wu, Y. Xu, K. Mountfield, R. Rottmayer, K. Lee, D. Kuo, and D. Weller: J. Vac. Sci. Technol. B **25** (2007) 2202.
11. J. Yang, and K. Berggren: J. Vac. Sci. Technol. B **25** (2007) 2025.
12. J. Kim, W. Chao, B. Griedel, X. Liang, M. Lewis, D. Hilken, and D. Olynick: J. Vac. Sci. Technol. B **27** (2009) 2628.
13. H. Zhang, T. Komori, Y. L. Zhang, Z. Mohamad, Y. Yin and S. Hosaka, submitted to JJAP.
14. K. Vutova, E. Koleva and G. Mladenov, ISBN 978-953-307-064-3 656 (2010).
15. P. Rai-Choudhury, Handbook of Microlithography, Micromachining, and Microfabrication, Technology & Engineering 423 (1997).
16. G. M. Schmid, L. E. Carpenter and J. A. Liddle, J. Vac. Sci. Technol. B **22** 3497 (2004).

17. S. D. Burns, G. M. Schmid, P. C. Tsiartas, C. G. Willson, and L. W. Flanagin, J. Vac. Sci. Technol. B **20** 537 (2002).
18. E. R. Nightingale, Jr., J. Phys. Chem. **63** 1381 (1959).

Chapter 7 Summary and Future Work

7.1 Summary

The high resolution requirements of EBL push the performance of both the lithographic tool and the resist materials to their limitations. Using the simulation tools, the limiting factors of resolution can be easily understood. In the thesis, I made the simulations based on the two main aspects (1) evaluating the dependence of exposure conditions in order to reduce the electron beam scattering range, and (2) calculating the resist profiles with solubility rates based on various EDDs in order to obtain optimal development contrast. Based on the simulation of the two aspects, I obtained the results as follows.

1. In chapter 3, the scattering behavior due to electron-atom interaction in negative and positive resists was investigated using Monte Carlo simulation. Energy deposition distribution in resist layer which reflect the energy deposition along the lateral and depth direction was calculated. Using rough developing simulation with critical energy deposition, it demonstrated that the negative resist is suitable to form small dot arrays.

2. In chapter 4, dependence of different exposure conditions such as Gaussian beam size, incident electron energy, the resist thickness and critical energy were analyzed. High resolution incident beam with diameter of 2 nm should be adopted for formation of very fine dot arrays. Using the thin resist of less than 20 nm can be effective suppress the effect of electron scattering. In addition, high critical energy was also demonstrated that it is benefit to form smaller pattern. Furthermore, we demonstrated that negative resist (calixarene) is more suitable than positive resist (PMMA and ZEP520) by simulation and experiments.

3. In chapter 5, a new model for calculating the resist pattern profile with a solubility rate based on EDD was proposed. By unifying the exposure dose (via experiment) and the EDD distributions (via calculations), three-dimensional solubility rates were determined for three-dimensional EDDs. The development simulation was

achieved by sequential calculation using the solubility rates. By determining a suitable EDD region as exposure dose to make well patterning, I obtained a sharpened nano-dot pattern of the resist. This simulation result agrees well with the experimental results obtained by using 2.3 wt% TMAH and 4 wt% NaCl developer. The model was demonstrated to be useful for predicting resist profile for different experimental solubility rates of developers.

4. In chapter 6, the exposure interval (ΔEDD) effect on the pattern contrast and resolution was discussed by evaluating the quality of resist profile. The high contrast developer was demonstrated that it has the small exposure interval ΔEDD. From the resist profiles with various ΔEDD, it was seen that the ΔEDD is an indicator of contrast of resist patterning. Furthermore, using the developer with contrast value γ that larger than $(\log(3))^{-1}$ should be adopted to form very fine dot arrays. However, the allowance of high contrast resist showed the small exposure allowance, which requires controlling the exposure dose severely when using the high contrast developing. In addition, TMAH 2.3 wt%/NaCl 4 wt% developer with the high contrast was demonstrated that it is suitable for formation of very fine dot arrays based on the simulation and experimental results.

7.2 Future Works

In this work, the dependence of exposure conditions and development conditions effect on the final resolution of pattern have been studied. However, in order to achieve a more accurate simulation of these process, there are several points that need to be considered in future works.

1. We demonstrated the high contrast resist has the good performance of exposure allowance in simulation. However, we did not have the experimental results by using a series exposure dosage and investigate the allowance. In future, we want to demonstrate that high contrast resist has large allowance in experiment.
2. We demonstrated the performance of development is related to the solubility rate and exposure dosage in this work. We calculated the resist profiles with different interval exposure dosage, but we did not consider the various solubility rates, especially the initial solubility rate. In the future work, we change the solubility rate and evaluate the resist profile. We try to demonstrate that a high initial development rate might be a more important parameter to consider than resist contrast.

List of Related Papers

1. **H. Zhang**, T. Tamura, Y. Yin, and S. Hosaka: "Estimation of Nanometer-sized EB patterning using Energy deposition distribution in Monte Carlo Simulation", Key Engineering Materials, **497** 127-132 (2012).
2. **H. Zhang**, T. Komori, Z. Mohamad, Y. Yin and S. Hosaka, "Comparison of Nano-sized Pattern of Calixarene and ZEP520 Resists by Using Energy Deposition Distribution", Key Engineering Materials, **534** 107-112 (2013).
3. **H. Zhang**, T. Komori, Y. L. Zhang, Z. Mohamad, Y. Yin and S. Hosaka, "Simulation of Fine Resist Profile Formation by Electron Beam Drawing and Development with Solubility Rate Based on Energy Deposition Distribution", submitted to JJAP.

List of Referred Papers

1. T. Komori, **H. Zhang**, T. Akahane, Z. Mohamad, Y. Yin and S. Hosaka, "Effect of Salty Development on Forming HSQ Resist Nanodot Arrays with a Pitch of 15×15 nm^2 by 30-keV Electron Beam lithography", Key Engineering Materials, **534** 113-117 (2013).
2. T. Komori, **H. Zhang**, T. Akahane, Z. Mohamad, Y. Yin and S. Hosaka, "Electron Beam Lithography of 15×15nm^2 Pitched Nanodot Arrays with a Size of Less than 10nm Using High Development Contrast Salty Developer", Japanese Journal of Applied Physics, **51** 06FB02 (2012).
3. Z. Mohamad, R. I. Alip, T. Komori, T. Akahane, **H. Zhang**, M. Huda, Y. Yin and S. Hosaka, "Fabrication of 30-nm-Pitched CoPt Magnetic Dot Arrays Using 30-keV-Electron Beam Lithography and Ion Milling for Patterned Media", Key Engineering Materials, **534** 118-121 (2013).

List of Presentations

1. **H. Zhang**, T. Komori, J. Liu, Y. L. Zhang, Y. Yin, S. Hosaka, "A new modeling of Calculating Resist Profile based on Energy Deposition Distribution in Electron beam Lithography", 4nd International Conference on Advanced Micro-Device Engineering (AMDE), Gunma, Japan (Dec.2012).

2. **H. Zhang**, T. Komori, Y. Yin, S. Hosaka, "The Simulation of Forming Fine Pitched Dot Array with a Dot Size of <10 nm Based on High Development Contrast Property in 30-keV lithography", The 9th International Symposium on Advancing the Chemical Sciences Challenges in Nanoscience", Xiamen, China, (Sep. 2012).

3. **H. Zhang**, T. Komori, Y. Yin, S. Hosaka, "Calculation of High-contrast HSQ resist using Energy Deposition Distribution in EB lithography", 3st International Conference on Advanced Micro-Device Engineering (AMDE), Gunma, Japan (Dec.2011).

4. T. Komori, **H. Zhang**, T. Akahane, Z. Mohamad, Y. Yin, and S. Hosaka:" The Effect of Salt Development for Forming HSQ Resist Nanodot Arrays with a Pitch of 15 × 15 nm^2 by 30-keV EB drawing", 3st International Conference on Advanced Micro-Device Engineering (AMDE), Gunma, Japan (Dec.2011).

5. Z. Mohamad, T. Komori, T. Akahane, R. I. Alip, **H. Zhang**, Y. Yin, S. Hosaka:" Fabrication of 30-nm-Pitched CoPt Magnetic Dot Arrays Using 30-keV-Electron Beam Lithography and Ion Milling for Patterned Media", 3st International Conference on Advanced Micro-Device Engineering (AMDE), Gunma, Japan (Dec.2011).

6. T. Komori, **H. Zhang**, T. Akahane, Z. Mohamad, Y.Yin, and S.Hosaka:" EB drawing of 15nm×15nm Pitched Nanodot Arrays with a Size of <10nm using High Contrast Developer", MNC2011, 24th International Micro-processes and Nanotechnology Conference, Kyoto, Japan (Oct. 2011).

7. 小森琢哉、**張慧**、赤羽隆志、"30 keV　電子線描画法を用いた 3 Tbit/in.^{2} (ピッチ 15 nm)超高密度磁気記録用ドット列を形成、第 72 回応用物理会学術講演会　(Oct.2011).

8. **H. Zhang**, Y. Yin, S. Hosaka:" Estimation of Nanometer-Scale Patterning of Calixarene Resist in Electron Beam Lithography", International Conference on Nanoscience and Technology, China (Sep.2011).

9. **H. Zhang**, T. Tamura, Y. Yin, and S. Hosaka:" Monte Carlo Simulation of Electron Scattering Processes for High-Resolution Electron Beam Lithography", 2Nd International Conference on Advanced Micro-Device Engineering (AMDE), Gunma, Japan (Dec.2010).

10. T. Tamura, **H. Zhang**, T. Akahane, M. Huda, T. Komori, Y. Yin, and S. Hosaka:"Fabrication of Nanometer Sized Si Dot Arrays Using Reactive Ion Etching with Metal Dot Arrays", 2Nd International Conference on Advanced Micro-Device Engineering (AMDE), Gunma, Japan (Dec.2010).